The role of the podoplanin-CLEC-2 pathway in stromal cell regulation of dendritic cell motility and lymph node architecture

HARVARD UNIVERSITY
Graduate School of Arts and Sciences

DISSERTATION ACCEPTANCE CERTIFICATE

The undersigned, appointed by the

Division of Medical Sciences

Committee on Immunology

have examined a dissertation entitled

The role of the podoplanin-CLEC-2 pathway in stromal cell regulation of dendritic cell motility and lymph node architecture

presented by Jillian Leigh Astarita

candidate for the degree of Doctor of Philosophy and hereby certify that it is worthy of acceptance.

Signature: _____

Typed Name: Dr. Charles Dimitroff

Signature: _____

Typed Name: Dr. Thorsten Mempel

Signature: _____

Typed Name: Dr. Theresa Lu

_____

Dr. Michael Carroll, Program Head

Date: August 29, 2014

_____

Dr. David Lopes Cardozo, Director of Graduate Studies

The role of the podoplanin-CLEC-2 pathway in stromal cell regulation of dendritic cell motility and lymph node architecture

A dissertation presented by

Jillian Leigh Astarita

to

The Division of Medical Sciences

In partial fulfillment of the requirements

for the degree of

Doctor of Philosophy

in the subject of

Immunology

Harvard University

Cambridge, Massachusetts

August 2014

Dissertation advisor: Dr. Shannon J. Turley Jillian Leigh Astarita

Podoplanin-CLEC-2 interactions in stromal cell regulation of DC motility and lymph node architecture

Abstract

In addition to leukocytes, secondary lymphoid organs are populated by non-hematopoietic stromal cells. This diverse group of cells supports lymphocyte migration and homing, facilitates antigen delivery, and promotes T cell survival. However, there is relatively little known about the specific molecules governing the roles that these cells play in regulating dendritic cell (DC) motility and lymph node architecture. Here, we examine the interaction between two molecules, CLEC-2 and podoplanin (PDPN), that are critical for DC migration and maintaining structural integrity of lymph nodes. Together, these studies identify novel functions of lymph node stromal cells and a unique function for PDPN in the immune system.

In response detecting an potentially harmful antigen, DCs in peripheral tissues mature and travel to downstream lymph nodes by following chemokine gradients secreted by lymphatic endothelial cells (LECs) and fibroblastic reticular cells (FRCs) present in the lymph node paracortex. We discovered that, in addition to chemokines, DC migration requires CLEC-2 on DCs, as engagement of CLEC-2 with PDPN, which is expressed by LECs and FRCs, incites DC motility and is required for DC entry into the lymphatics, efficient arrival in the lymph node, and migration along the FRC network within the lymph node.

Next, we examined the effect of this interaction with respect to the stromal cell. Through a combination approaches, we discovered that PDPN is a master regulator of

contractility in FRCs. The fact that FRCs are contractile cells was previously reported, but our study is the first to identify a function for this contractility: upon blockade of PDPN-mediated contractility, lymph nodes became enlarged, the FRC network became more sparse, and there were increased numbers of lymphocytes in the lymph node. Importantly, during an immune response, these changes resulted in more proliferation of antigen-specific T cells and impaired contraction of the lymph node upon resolution of inflammation. Finally, we found that CLEC-2 binding PDPN recapitulated the effect of PDPN deletion. Thus, during an immune response, CLEC-2^{+} DCs would use PDPN to efficiently migrate to the lymph node and simultaneously cause FRCs to relax and prepare the lymph node for expansion.

Table of Contents

Acknowledgements

There are many people that have provided me with invaluable support over the past several years while I have been working on this dissertation. First and foremost, I would like to thank my dissertation advisor, Dr. Shannon Turley. She has taught me an immense amount about immunology, doing scientific research with high integrity, and giving effective presentations. In addition, Shannon creates a wonderful, supportive lab environment that I have greatly enjoyed working in for the last four years. I am grateful that I will continue to benefit from Shannon's mentoring in the years to come.

Next, I want to thank all members of the Turley lab that I have had the opportunity to work with. Past lab members that helped me especially in my early years as a graduate student include Anne Fletcher, Veronika Lukacs-Kornek, Angelique Bellemare-Pelletier, Kutlu Elpek, and Sophie Acton. More recently, Viviana Cremasco has been a great friend in the lab, and we have had many productive conversations about our projects. My fellow graduate students Deepali Malhotra, Flavian Brown, and Jonathan Chang have also provided helpful suggestions and a great lab environment. Finally, I would like to thank my officemate for the past two years, Janice Nieves-Bonilla for her help in lab and her never-ending enthusiasm.

In addition to the Turley lab, the Cancer Immunology and AIDS department at Dana Farber has been a fun place to work. Everyone on the 14th floor of Dana provided a supportive environment and I always enjoyed our happy hours and conversations in the hallways.

I am very grateful to have been a part of the Harvard Immunology program. It was extremely helpful to have a small, welcoming community within the larger Harvard one. I especially want to thank Susan Perkins for her tireless efforts in calming frenzied graduate students and helping to organize the student data club and yearly program retreats. In addition,

I would like to thank my classmates for weathering the ups and downs of the first year of graduate school with me. It was fun to travel as a pack around Longwood and have sit-down dance parties between classes. In particular, Jonathan Sitrin and Daniel Dwyer, have become great friends.

Finally, I would like to thank my roommates, Lauren Barclay and Amy Emerman, for providing many hours of great conversations about the frustrations of graduate school and life in general. I am very grateful to my parents, Mark and Ellen Astarita, and my sisters, Erika and Alexa Astarita, for their continued love and support. Finally, I would like to thank my boyfriend, James Peck, for his calm patience and great friendship, and for ensuring that I always took time to escape the lab and spend some time outdoors.

for

James Peck,

who taught me to appreciate the importance of climbing mountains
and
long walks in the woods

Climb the mountains and get their good tidings
- John Muir

Chapter 1

Introduction

Attributions

Portions of this chapter were reproduced from the following publication (with permission from *Frontiers in Immunology*):

Astarita, J.L., Acton, S.E., Turley, S.J. Podoplanin: emerging functions in development, the immune system, and cancer. *Front Immunol* **3**, 283-293 (2012).

Overview

The immune system is composed of several diverse cell types that are scattered throughout the body. In order for this complicated system to function properly, its cells must be able to scan every part of the body for threats; however, at the same time, these cells need to be able to quickly communicate with one another upon detecting a pathogen. To accomplish these goals, the immune system has evolved an ingenious system whereby tissue-resident cells and circulating blood-borne cells encounter one another in lymph nodes that are present throughout the body. Lymph nodes are highly organized structures that continually filter lymph fluid carrying small antigens and cells. They contain distinct areas for B and T cells, which facilitates both antigen delivery to B cells and the chance that an entering dendritic cell (DC) carrying an antigen will find its cognate T cell. While several decades of research have been dedicated to elucidating how lymph nodes are organized and how leukocytes function within them, the molecular mechanisms delineating leukocyte migration and the changes lymph nodes undergo upon the induction of inflammatory responses are not fully understood. Furthermore, there is still very little known about the underlying backbone of lymph nodes – the endothelial cells and fibroblasts that make up the structural component of these specialized organs. This chapter will detail the current state of knowledge regarding the cellular and molecular mechanisms of the initiation of an inflammatory response, DC migration to draining lymph nodes, and the stromal cell compartment of lymph nodes.

Lymph node architecture

The lymph node is a highly organized tissue composed of several different areas. Lymph first flows into the lymph node through the afferent lymph vessels and then floods the subcapsular sinus before traveling around the periphery of the lymph node, through the

circuitous medullary region and draining out of the efferent lymph vessels (Figure 1.1)[1]. Lymph

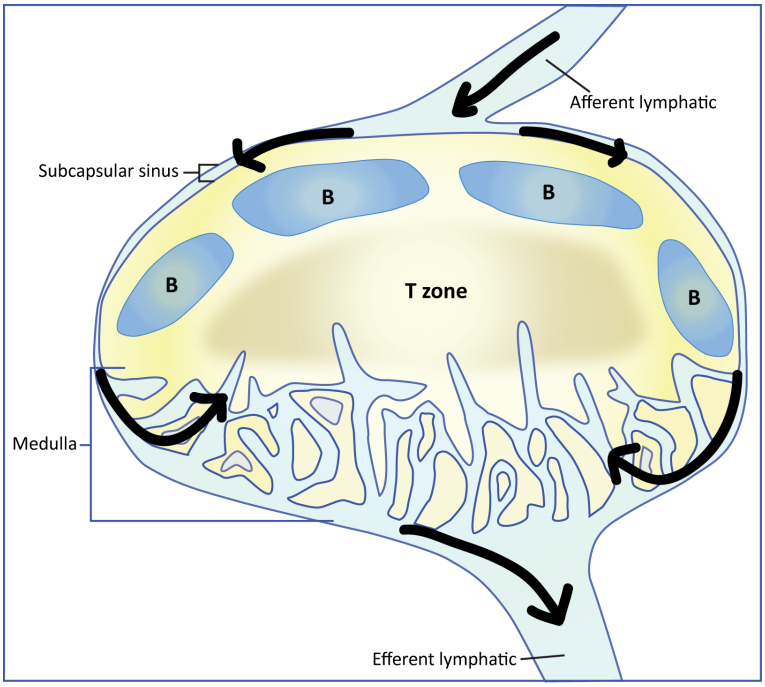

Figure 1.1. Lymph node architecture and lymph flow. Lymph and cells from peripheral tissues drain into a lymph node through the afferent lymphatic vessel. The fluid will then flood the subcapsular sinus and travel around the perimeter of the lymph node. Finally, the lymph will pool into the circuitous medullary vessels before draining out the efferent lymphatic vessel. T and B lymphocytes enter lymph nodes through specialized blood vessels called high endothelial venules (HEVs). Upon entry, B cells are directed towards follicles, which are located just beneath the subcapsular sinus. T cells are kept in the paracortex, which is in the center of the lymph node. Eventually, if they do not become activated, lymphocytes will exit through the efferent lymphatic vessel to travel to the next lymph node or return to circulation in the blood.

nodes are organized throughout the body such that they form chains along lymph vessels, and each successive lymph node receives antigens and some cells that have previously exited the upstream lymph node.

One of the major cell populations carried in the lymph, in the steady state but especially in times of inflammation, is the DC. In healthy animals, DCs from upstream peripheral tissues continually enter the lymphatics and travel to draining lymph nodes to present antigens and maintain peripheral tolerance. Following detection of a pathogen or inflammatory stimulus, this migration is greatly increased, and large numbers of DCs travel to the draining lymph node to present antigens and mount a T cell response. There are also lymph node-resident DCs that arise from immature monocytes that have traveled to lymph nodes[2,3]. These DCs perform a variety of functions, including both the maintenance of peripheral tolerance and initiation of immune responses in response to circulating antigens. Generally, DCs do not travel back out of lymph nodes; once they have performed their duties they will die in the draining lymph node.

Throughout their life, B and T cells continually circulate throughout the body through the bloodstream. Naïve lymphocytes express high levels of an L-selectin known as CD62L[4], which is an adhesion molecule that allows these cells to enter lymph nodes through specialized blood vessels called high endothelial venules (HEVs)[5,6]. Upon entering the lymph node, B cells follow a CXCL13 chemokine gradient to reach the B cell follicles, which are located just beneath the subcapsular sinus around the periphery of the lymph node. HEVs are located in the central part of the lymph node; thus, T cells find themselves in the paracortex immediately upon entry. They are kept from straying into the B cell follicles by a CCL19 and CCL21 gradient, which keeps them in the T zone.

Usually, after spending some time in a given lymph node, B and T cells do not see their cognate antigens and follow yet another chemokine gradient that leads them to exit the lymph

node through the draining efferent lymph vessel. From there, they can travel to the next lymph node in the chain or re-enter the blood stream to continue circulating. In rare instances, a given B or T cell will recognize their specific antigen and will receive signals to become activated, proliferate, and eventually travel to the site of inflammation to rid the body of an invading pathogen.

Dendritic cells: the critical link between innate and adaptive immunity

The DC is the cornerstone of the immune system; it provides an essential link between the innate and adaptive arms of the immune system. While there are several types of crosstalk between innate and adaptive immune cells, the DC is unequivocally involved in the most basic steps necessary for generating an effective, long-lasting adaptive immune response. DCs were first identified as interdigitating cells in the epidermis of the skin[7], but weren't fully characterized and named until a careful analysis was done by Steinman and Cohn in the 1970's[8-10]. Thereafter, it was quickly recognized that DCs are able to pick up antigens in peripheral tissues and migrate to draining lymph nodes. In the years since that discovery, a vast amount has been learned about each step a DC needs to take during this journey: detachment from surrounding tissues, entry into the draining lymphatics, entry into the lymph node through the subcapsular sinus, and travel to the T cell zone.

DCs are present in nearly every tissue in the body and are constantly sampling from their environment[2]. Along with other tissue-resident cells, they serve as sentinels guarding against invading pathogens. However, unlike other tissue-resident innate cells such as macrophages or mast cells, their primary aim is not to quickly react and immediately destroy the pathogen or alert neighboring cells. Instead, DCs respond to sensing a pathogen by undergoing maturation and migrating from the tissue to alert the adaptive immune system in the draining

lymph node. There are two main mechanisms by which DCs become activated: direct detection of conserved pathogen-associated patterns (PAMPs) and interactions with natural killer (NK) cells, NKT cells, and γδ T cells. DCs express a variety of pattern recognition receptors (PRRs), including Toll-like receptors (TLRs), Rig-I-like receptors (RLRs), and NOD-like receptors (NLRs), that recognize a range of substrates including bacterial lipopolysaccharide (LPS), viral RNA, and fungal components[11,12]. Detection of any of these PAMPs initiates a signaling cascade that increases DC production of cytokines and causes maturation.

During the process of maturation, DCs undergo many changes. Immature DCs are poorly immunogenic and mostly focus on uptake of particles from the surrounding tissue. However, upon sensing an inflammatory stimulus, DCs downregulate their phagocytosis and become highly immunogenic[13]. They contain endosomes full of major histocompatibility complex (MHC) II molecules that can be assembled at a moment's notice and upon maturation, these complexes become more stable on the cell surface and present peptides more effectively[14]. DCs also upregulate co-stimulatory molecules and cytokines that allow for the activation of T cells, including CD80 (B7.1), CD86 (B7.2), CD4, IL-12, and IL-4[15]. Finally, DCs downregulate chemokine receptors that attract them to sites of inflammation and upregulate CCR7, which directs them towards lymph nodes[16]. Upon reaching the T zone of a lymph node, DCs are competent to interact with their cognate T cell and initiate an adaptive immune response.

While signaling through PRRs is considered a strong stimulus for DC maturation, several studies have indicated that signals from LPS for example are not sufficient full DC maturation[17-21]. Thus, in addition to directly sensing danger through PRRs, DCs can be fully activated by interacting with other tissue-resident innate cells. Importantly, NK cells, γδ T cells, and NKT cells are specialized at recognizing lipids and other stressors that DCs cannot sense through PRRs, such as cancer cells. NKT and γδ T cells activate DCs in a CD1-depedendent manner and require

CD40-CD40L signaling[22-24]. NK cells are activated by cells that lack MHCI on their surface, and respond by producing IFNγ and TNFα, which allow a DC to effectively produce IL-12[25-27].

After these initial steps of maturation, DCs are mobilized to leave the peripheral tissue and migrate to a secondary lymphoid organ. In the late 1990's, it was discovered that chemokines play a major role in directing the migration of immune cells throughout the body[28] and shortly thereafter, CCL21 (formerly SLC and 6Ckine) and CCL19 (formerly ELC and M1P3-β) were identified as the key chemokines that direct DCs and lymphocytes to secondary lymphoid organs based on their expression of CCR7, the receptor for these chemokines[29-33]. The absolute requirement of these molecules was demonstrated by the *plt*/*plt* mouse, which lacks T cells and DCs in lymph nodes and was found to have a mutation in the *Ccl21* gene[34]. Conversely, CCR7-deficient mice also lack DCs and T cells in lymph nodes[29,35].

The final step in DC migration is entering the T cell paracortex. While there is less known about the precise factors governing the process, it has been demonstrated that DCs migrate through the floor of the SCS and move directly towards the T cell zone[36]. This movement requires CCR7. Interestingly, the proper migration of DCs is necessary for efficient T cell entry to the T zone due to DC-mediated modulation of the SCS and HEVs[37,38].

Although reorganization of the actin cytoskeleton is required for proper migration[39], the signaling pathways upstream of this cytoskeletal remodeling remain unclear. Integrins adhere to extracellular surfaces and are responsible for transducing migratory signals into cells[40]; however, DCs can migrate in an integrin-independent ameboid fashion[41,42]. Lammerman et al.[41] clearly demonstrated that DCs lacking integrins enter lymphatics and migrate to lymph nodes as efficiently as wild-type DCs. Therefore, there are likely other molecules besides integrins that mediate DC motility and specifically direct their motility toward draining lymph nodes.

DCs encounter stromal cells along every step of this journey – from epithelial cells in the

skin to LECs lining lymphatic vessels and FRCs in the T zone. It is highly likely that signals from stromal cells engage some receptor on the DC surface that would facilitate their motility and specific migration. Especially in the case of the intimate contact between DCs and FRCs in the paracortex, it seems likely that there are protein-protein interactions responsible for mediating this cell-cell contact.

Lymph node stromal cells

The existence of lymph node stromal cells (LNSCs) within lymph nodes has been recognized for several decades. Several early studies from the 1960's and 1970's describe the presence of dense reticular cords that formed a mesh-like network in the paracortex of lymph nodes[43-45]. Furthermore, these scientists defined fibroblastic reticular cells as cells that can synthesize and secrete the protein reticulin, which was later found to be collagen[44,45]. These studies greatly advanced the basic understanding of lymph node architecture, and in turn, a better understanding of how the immune system works, given that its functionality is tied to proper organization of the lymph node. However, until recently, these stromal cells were considered to be static structural elements of the lymph node. It is only in approximately the last decade that their active roles in immunity have been discovered, including their ability to direct the migration and support survival of lymphocytes and their roles in antigen delivery and presentation.

There are several major stromal subsets in residing in lymph nodes. Similar subsets exist in the spleen and Peyer's patches, and while these cells likely exhibit similar characteristics to their counterparts in the lymph node, their exact functions have not been well defined[46]. All stromal cells lack expression of the hematopoietic marker CD45 and constitute just 1-2% of the total cells in the lymph node, as it is mostly populated by B and T cells[47,48]. The stromal cell

subsets are largely distinguished by their expression of two key markers – podoplanin (PDPN; also known as gp38, Aggrus, and T1α) and CD31 (platelet endothelial adhesion molecule (PECAM)-1) – and their subanatomical location in lymph nodes (Figure 1.2). The populations include the following subsets: lymphatic endothelial cells (LECs; $PDPN^{+}CD31^{+}$), blood endothelial cells (BECs; $PDPN^{-}CD31^{+}$), follicular dendritic cells (FDCs; $PDPN^{+/-}CD31^{-}$), integrin alpha 7 (ITGA7)-positive pericytes (IAPs; $PDPN^{-}CD31^{-}$), and fibroblastic reticular cells (FRCs; $PDPN^{+}CD31^{-}$).

Endothelial cells

LECs line lymphatic vessels, which carry lymph that drains from peripheral tissues and filters through lymph nodes. This fluid carries small antigens and cells, particularly DCs, to lymph nodes, which allows for a critical surveillance of all the tissues in the body. In addition to forming these vessels, LECs play an active role in the homing of lymphocytes by secreting CCL21[46] to direct DCs and lymphocytes towards draining lymph nodes. They also secrete IL-7, which is critical for the reconstruction of a normal stromal network in lymph node recovering from infection[49].

BECs are responsible for lining blood vessels throughout the body. The majority of BECs in lymph nodes are part of specialized high endothelial venules (HEVs) through which lymphocytes enter the lymph node. These cells are readily identified by their expression of peripheral node addressin (PNAd), which is a glycoprotein that activated lymphocytes bind to with L-selectin[50,51].

Follicular dendritic cells

FDCs populate B cell zones in the lymph node. Their development and maintenance is highly dependent on TNF signals from B cells, such as lymphotoxin β (LTβ) and TNFα[52]. In turn,

Figure 1.2. Subanatomical location of lymph node stromal cells. *Subcapsular sinus and B cell follicle, red box.* Lymphatic endothelial cells (LECs) line the lymphatic vessels entering and surrounding the lymph vessels. They are also present throughout the floor of the subcapsular sinus. Just below this layer of LECs, there is a population of macrophages that are poised to quickly capture antigens and present them to the B cells below. DCs entering the lymph node in the lymph squeeze between LECs to enter directly through the subcapsular sinus. In the space between the B cell follicle and subcapsular sinus sits the marginal reticular cells, which secrete CXCL13 to help direct B cells to the follicle. The B cell follicle itself is populated by follicular dendritic cells (FDCs), which are extremely large cells with dendritic protrusions extending from the cell body. FDCs efficiently capture antigens through complement and Fc receptors and are instrumental in supporting B cell activation in germinal centers. *Paracortex, blue box*. The paracortex is populated by T cells and a dense network that is formed by fibroblastic reticular cells (FRCs) and the extracellular matrix components they secrete. DCs and lymphocytes crawl directly on this FRC highway, which facilitates interactions between antigen-bearing DCs and specific T cells. FRCs also wrap around high endothelial venules (HEVs), which are specialized blood vessels through which B and T lymphocytes enter the LN.

Figure 1.2 (continued)

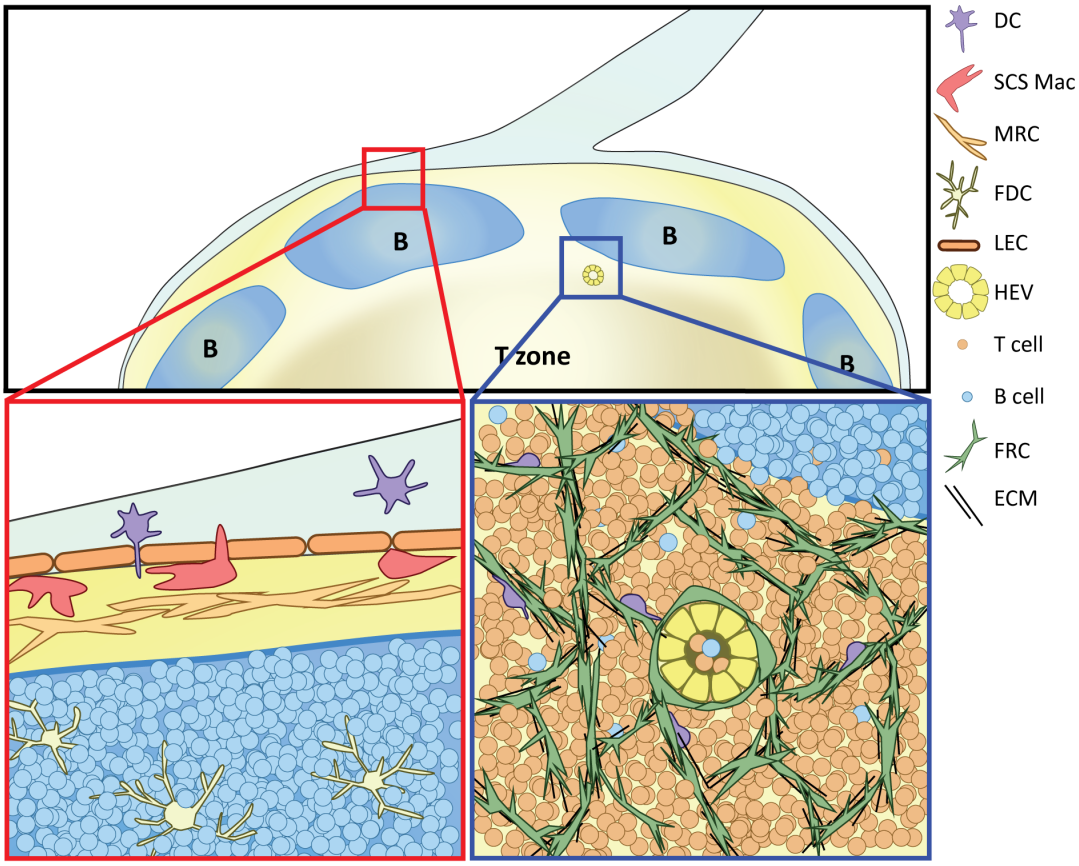

FDCs are believed to support B cell survival and homing to follicles through the secretion of BAFF and APRIL and CXCL13, respectively[53-55]. However, upon FDC depletion, CXCL13 and BAFF signals are still detectable[56,57], and in mice lacking FDCs and B cells, adoptively transferred wild-type B cells home to distinct areas on the edge of the paracortex[58], indicating that there is likely another stromal cell responsible for secretion of this cytokine. In fact, we recently identified that there are FRC-like cells present in B cell follicles that secrete CXCL13[46] and BAFF to support B cell homing and survival[59].

FDCs are critical for capturing and displaying antigen to B cells. As indicated by their name, FDCs are large cells with many dendrites extending from their cell body. They express high amounts of complement and Fc receptors[60,61], which allows them to capture and retain antigens and immune complexes on their surface for long periods of time. This function of FDCs is critical for developing germinal centers where maturing B cells undergo somatic hypermutation and class switch recombination to develop high affinity antibodies. However, recent evidence indicates that FDCs may only be required for later stages of germinal center maintenance and not the earliest steps[57].

Marginal reticular cells

A recently identified population of cells that are present just below the SCS on the outer edge of B cell follicles are called marginal reticular cells (MRCs). They secrete CXCL13 and express MadCAM1 in addition to PDPN and VCAM1. MRCs are thought to be related to lymphoid tissue organizer cells, which are required for the generation of lymph nodes during development[62]. However, further in vivo characterization of these cells is necessary to determine whether they are in fact a distinct subset of stromal cells.

Integrin α7-positive pericytes

IAPs were considered "double negative" cells (DNCs) for many years due to their lack of PDPN and CD31 expression. They are the only subset of LNSCs that expresses autoimmune regulatory element (AIRE) and they present a unique set of peripheral tissue antigens[63]. Malhotra et al.[46] recently sorted these cells to high purity and characterized them through in vitro cultivation and transcriptional profiling. These approaches revealed that about 50% of DNCs expressed integrin α7, which was not expressed by other stromal subsets in the lymph node. Interestingly, IAPs shared many characteristics with FRCs, including a myofibroblast phenotype with high contractility and expression of a multitude of extracellular matrix (ECM) components. They are largely localized in the medulla wrapped around medullary cords and blood vessels, which identified them as perictyes[46]. However, whether they are present on specific types of vessels has not yet been defined. A recent report indicates that some DNCs may be immature myofibroblast precursors for FRCs, as FRC-specific ablation of LTβR signals resulted in a loss of the expression of PDPN, CCL19, VCAM, and ICAM from FRCs[64]. More work is needed to determine which exact populations of the heterogeneous DNCs are in fact FRC precursors.

Fibroblastic reticular cells

FRCs reside in the T cell paracortex and are largely responsible for its organization. They secrete CCL19 and CCL21, two chemokines that are critical for proper homing of lymphocytes and dendritic cells (DCs)[34]. FRCs also produce IL-7 to support the survival of naïve T cells in the paracortex[65]. In addition, FRCs provide a structural scaffold upon which these immune cells crawl within the lymph node. Lymphocytes contact FRCs almost immediately upon entering the lymph node, as FRCs tightly wrap around HEVs and control B and T cell entry through discrete "exit ramps"[66]. Deeper in the paracortex, T cells and DCs travel along the FRC network, which

facilitates their interactions with one another and increases the possibility of a DC finding its cognate T cell[66,67]. In addition to providing this physical scaffold, FRCs secrete and enwrap large amounts of collagen and other ECM components to form a conduit system[68]. This system allows for fast delivery of small, soluble antigens deep into the lymph node.

In addition to these more structural functions, FRCs actively orchestrate immune responses by shaping T cell responses. FRCs play a role in maintaining peripheral tolerance through direct antigen presentation[63,69]. Interestingly, the ability of FRCs to stimulate antigen-specific T cell proliferation becomes altered upon exposure to viral stimuli[46,63]. Mueller et al.[70] found that FRCs could be directly infected by viruses, which led to an upregulation of PD-L1 on FRCs and persistent chronic infection. Furthermore, LTβR signaling in FRCs is necessary for proper T cell function during viral infections[64]. Another function of FRCs that is important for controlling T cell responses is their ability to dampen T cell responses in an antigen-independent manner[71-73]. This process requires IFNγ and TNFα production from the T cells, which in turn results in nitric oxide production by FRCs to inhibit T cell proliferation.

Overall, a vast amount of groundbreaking studies have emerged in recent years detailing the myriad functions of LNSCs. It is clear now that these cells are not a static, structural component forming lymph nodes and other lymphoid organs. Instead, they provide leukocytes with directional cues for migration, actively capture and present antigens to B and T cells, and shape immune responses.

Changes in stromal cells upon lymph node expansion and contraction

Upon inflammation, lymph nodes undergo vast amounts of swelling and increase to many times their original size and mass. These massive changes in organ size must be accompanied by changes in the underlying infrastructure of the organ, including the blood and

lymphatic vessels that feed the organ. Indeed, it has been known for many decades that any inflammatory response is accompanied by a large increase in the blood vasculature of lymph nodes upon treatment with an inflammatory stimulus[74]. These changes occur as early as two days after detection of a variety of inflammatory stimuli, indicating that the lymph node quickly begins to prepare for the impending influx of immune cells and the subsequent expansion it will undergo. After the inflammation has subsided, a resting vasculature structure within the lymph node is quickly re-established.

Both lymph node expansion and the subsequent lymph node contraction are tightly regulated by a variety of cell types and soluble mediators. First, there is a DC-dependent, B and T cell-independent phase of lymph node expansion occurring within one to two days of inflammation that is characterized by a rapid activation of the endothelium. HEVs, the specialized blood vessels through which lymphocytes enter the lymph nodes, increase in number and size proportionally with the increasing size of the whole lymph node[75,76]. Accordingly, endothelial cells begin proliferating at this time point and steadily increase in numbers. In the steady state, FRCs are normally tightly wrapped around $PNAd^+$ endothelial cells lining the HEVs; however, upon this initial stage of lymph node expansion, HEVs become disrupted and the FRCs become less closely-associated with these vessels[77]. Furthermore, the FRCs themselves begin to proliferate and increase in number. Thus, the stromal cells within the lymph nodes are able to sense and immediately being responding to a variety of inflammatory stimuli.

These changes require DCs, but not lymphocytes, and vascular endothelial growth factor (VEGF), a molecule that is critical in supporting angiogenesis and vascular growth. FRCs are the major producers of VEGF in lymph nodes, and its production is localized largely around lymphatic and blood vessels. Upon the initiation of lymph node expansion, VEGF levels increases

dramatically, presumably to support the rapidly expanding endothelial cell populations[75,78]. This increase in VEGF and stromal cell proliferation is abrogated upon depletion of DCs. This phenomenon specifically requires CD11c^{med} DCs, but not CCR7 or Langerhans cells[77]. Thus, a lymph node-resident DC population likely detects the presence of foreign material through innate signaling receptors and subsequently instructs the stromal cells to begin their proliferation. The exact signals governing these interactions have not been fully elucidated, but LTβ signaling is required for VEGF production. Thus, without DCs, LTβ signaling, and VEGF upregulation, there is dramatically reduced endothelial cell proliferation and expansion.

Another important event that occurs soon after exposure to an inflammatory stimulus is lymph node shutdown. It was first observed 50 years ago that upon inflammation, there is a sharp decrease in the number of circulating lymphocytes[79]. More recently, the mechanism underlying this shutdown has been described by Shiow et al.[80]. Normally, lymphocyte egress from lymph nodes is guided by a gradient of sphingosine 1-phosphate (S1P), which is detected by the S1P receptor-1 (S1PR1) on the surface of T and B cells[81,82]. However, upon inflammation, innate cells are activated to produce interferon (IFN)-γ, which is a strong inducer of CD69 on lymphocytes. Once CD69 is upregulated, it directly interacts with S1PR1 on the cell membrane to mediate S1PR1 downregulation. Therefore, immediately upon activation, B and T cells are temporarily unable to respond to the S1P gradient and remain in lymph nodes.

As immune cells continue to enter the lymph node and contribute to its swelling, there is a second phase where DCs are no longer necessary and B and T cells instead support the continued expansion and stabilization of increased endothelial cell and FRC numbers. In mice lacking either B cells or T cells, both endothelial cells and FRCs proliferated initially, but failed to accumulate as they do in wild-type mice. In addition to supporting the expansion of the stromal

cells, $CD4^+$ T cells interact with DCs to increase the diameter of the major arteriole feeding lymph nodes[76,83], which allows for the influx of more naïve lymphocytes.

After a period of lymph node expansion, the vasculature begins to stabilize and return to steady state levels of proliferation. Little is known about the signals governing lymph node contraction and return to homeostasis, but it is an active process that involves pro-resolution mediators such as lipotoxins and resolvins[84]. A return to quiescence in the vasculature also requires DCs, although in this phase, $CD11c^{hi}$ DCs play a role instead of the $CD11c^{med}$ DCs required in the initiation phase. When these DCs are depleted five days after CFA/OVA administration, endothelial cell proliferation remains high, and FRCs around HEVs continue to be disrupted and the HEVs remain leaky. Importantly, this continued stromal proliferation has detrimental effects on immune responses, as T cell-dependent B cell responses are attenuated upon $CD11c^{hi}$ depletion[77]. This may be due to competition for resources because lymph node trafficking into the lymph nodes remains high under these conditions.

All together, these studies indicate a progression of events whereby DCs, stromal cells, and lymphocytes engage in crosstalk with one another to generate a lymph node environment that is conducive to supporting the vast increase in cellularity and effective immune responses. First, lymph node-resident DCs detect a harmful antigen and give signals to the FRCs to increase production of VEGF, possibly through increased LTβ signaling. This results in increased endothelial cell proliferation and an increase in HEVs, which is followed by increased numbers of naïve lymphocytes entering into the lymph node. These lymphocytes, specifically the T cells, interact with the DCs to increase blood flow to the lymph node. Then, after several days have elapsed and the adaptive response is initiated, different signals regulate a return to homeostasis and baseline proliferation of the stromal cells.

Conduits, antigen delivery, and fluid flow

As lymph enters a lymph node through the afferent lymphatic vessel, it floods the SCS, flows through the cortical sinuses, drains into the medullary sinuses, and finally exits through the efferent lymphatic vessel[85-87]. Thus, sensing flow rates may be another important mechanism by which FRCs and other stromal cells can prepare for an imminent immune response.

The first immune cells that encounter lymph-borne antigens are the macrophages that line the floor of the SCS. These macrophages capture debris, antigens, and pathogens from the lymph and present them to B cells in the underlying follicles, who in turn present the antigens to T cells at the B-T border[88,89]. Additionally, B cells can directly capture antigens bound by complement and deliver them to FDCs for prolonged display to other B cells[90]. As the lymph flows out through the medulla, macrophages and DCs that reside there can also capture antigen. For example, a recent study demonstrates that while SCS macrophages are necessary for the initial control of viral spread, SIGNR1^{+} DCs in the medulla are required for the initiation of an effective humoral response against the influenza virus[91].

Several years ago, it was observed that, in addition to the lymph that flows through the major lymphatic vessels, there must be another, faster delivery system for antigens. Several groups noted that DCs were able to capture antigens and present them to T cells in a time frame that did not allow for migration of DCs from peripheral tissues to the lymph node[92-95]. While earlier scientists had speculated that the reticular network might play a role in antigen transport, this idea was not substantiated until Gretz et al.[96] demonstrated that antigens below a 70 kDa cutoff were able to quickly access many areas of the lymph node that larger antigens were precluded from. Since then, it has been elucidated that FRCs generate the conduits by encircling the ECM components they secrete[68,97]. The specific components of the conduit

network and its roles in antigen delivery have been defined by detailed imaging and transcriptional analyses, but there is still surprisingly little known about how FRCs might modify conduits to regulate the size of antigens entering or the rate of the lymph flowing through them.

In developing lymph nodes, FRCs and a dense conduit network is present throughout the entire node. As B cells begin to populate the lymph node and defined follicles are formed, this network is greatly thinned out within the B cell zones. However, this sparse network is still functional and able to support the transport of antigens into the B cell follicles[98]. Interestingly, as FRCs become increasingly restricted to the T cell zone, FDCs populating the follicles are able to embrace the collagen fibers left behind and appear to maintain these B cell conduits[58]. Furthermore, a recent study by Cremasco et al.[59] indicates that there are functional FRCs that remain in B cell follicles; thus, they may play a role in maintaining the function of these conduits.

Conduits present in the T cell area are much more extensive and dense than those in the B cell follicles, and the components of these conduits are relatively well characterized. FRCs synthesize a large variety of ECM components, including many collagens, fibronectin, laminin, vitronectin, and the ERTR7 antigen, which they secrete and wrap around to generate a lumen through which lymph flows[46,68]. Conduits are composed of an inner collagen core that is surrounded by a microfibrillar zone containing ERTR7 and fibrillins. Then there is a basement membrane layer that is enwrapped by the FRCs (Fig 1.3).

In addition to generating these components, FRCs must be able to remodel them as changing conditions arise, such as during an immune response when the lymph node must swell. Fittingly, FRCs produce many matrix metalloproteases (MMPs) and matrix assembly proteins, which would allow them to change the composition of the conduits[46].

The signals that would instruct FRC remodeling of the conduits are largely unknown; however, given that lymphocytes are continually trafficking along the network, it is likely that

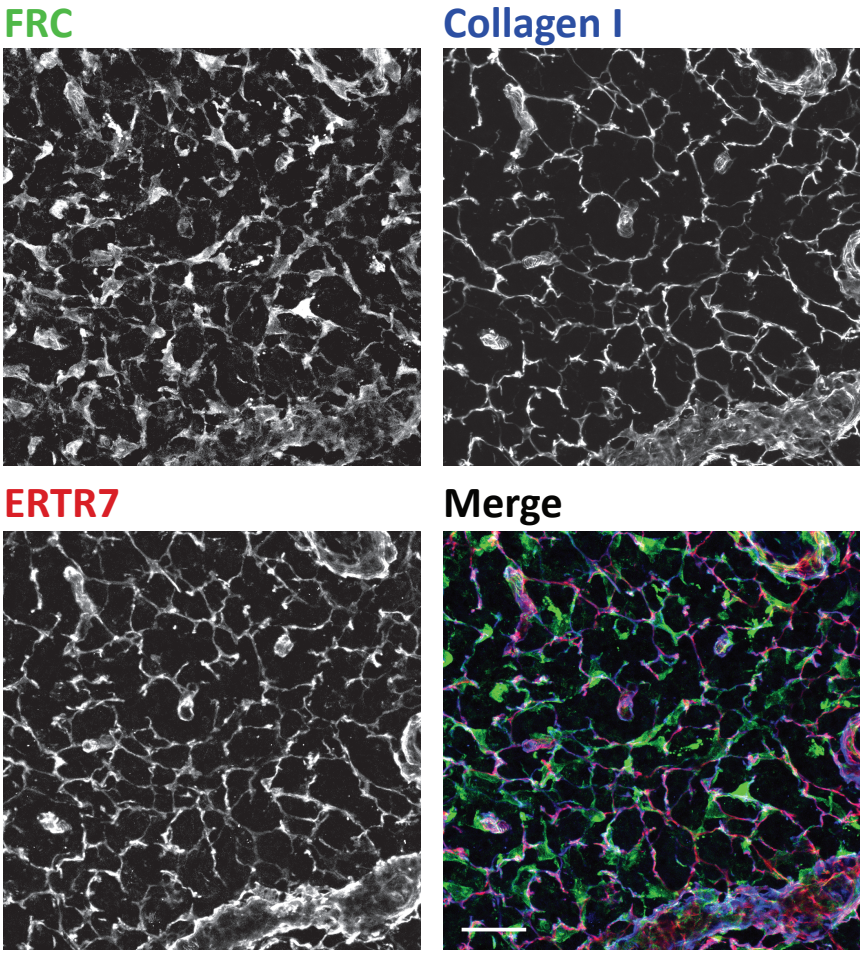

Figure 1.3. The FRC conduit network. Confocal image of FRCs (green), collagen I (blue), and ERTR7 (red). Note how the FRC cell bodies are closely associated with the ERTR7 and collagen components of the conduits. This dense network is present throughout the T cell paracortex. A similar, but much less dense, network is also present in B cell follicles. Scale bar, 30 μm.

signals from these cells might influence FRC control of the conduits. Indeed, Katakai et al.[99] discovered that T cell interactions with the network are important for its production *in vitro*. Upon *in vitro* culture of FRCs, they produce some ECM components, but when co-cultured with $CD4^+$ T cells or the supernatant from activated T cells, the $ERTR7^+$ network becomes much

denser. The T-cell mediated ECM production is dependent on signaling through the TNFR and LTβR on FRCs[99]. The TNF and LTαβ signaling pathways have been extensively studied with regard to their critical role in the development of lymph nodes[52,100]. Thus, this study reveals another area in which these signaling pathways are involved. Additionally, this T cell instruction of the conduit network may be critical during the extensive remodeling that occurs upon T cell activation and lymph node expansion.

Besides the delivery of antigens, the lymph flow into lymph nodes provides important signals to FRCs due to the pressure of fluid flow itself. Fibroblasts are sensitive to the stiffness of their surrounding environment and can sense changes in stiffness or fluid flow through mechanotransduction[101,102]. In terms of the lymph node, there is a constant, slow rate of flow, but this rate can be drastically increased in response to inflammation or edema in the body[103-105]. Thus, it is highly likely that FRCs would be able to sense changes in lymph flow through the conduits, or pressure changes within the lymph node, and respond accordingly. In fact, Tomei et al.[106] discovered that fluid flow was critical for the production of CCL21 and an FRC network in vitro. Providing even a low amount of fluid flow resulted in a dramatic reorganization of cultured FRCs into tube-like structures surrounding bundles of collagen that resembled conduits formed in vivo. Increased fluid flow also caused increased proliferation of FRCs[106].

Thus, conduits are a unique system of lymph transport that serve many important functions in the immune system, including the fast delivery of antigens and influencing FRC secretion and remodeling of the ECM network.

PDPN and CLEC-2: a putative link between immune cells and lymph node stromal cells

To date, no molecules mediating specific cell-to-cell interactions between DCs and stromal cells have been elucidated. However, it is well known that DCs interact with stromal

cells at every part of their lives and especially during migration to draining lymph nodes following exposure to inflammatory stimuli. We have identified PDPN and a c-type lectin, CLEC-2 (*Clec1b*), as candidates for mediators of this interaction. Platelets, DCs, and other immune cells have been reported to express CLEC-2, but no function has been elucidated for it in DCs. Furthermore, while PDPN has been used extensively as a marker for FRCs and LECs in a variety of tissues, there have not been any specific functions ascribed to this molecule.

CLEC-2-PDPN interactions are required for blood-lymph separation

During embryonic development, the lymphatic system forms when the lymph sac begins to bud from the developing circulatory system[107]. On day E11.5, PDPN first appears in the developing circulatory system on Prox-1^{+} lymphatic cells[108]. It was first reported by Schacht et al.[108] that *Pdpn*$^{-/-}$ mice have abnormal lymphatic vessels that cannot properly regulate lymph flow and that this defect did not appear in blood vessels. These findings were further supported by Fu et al.[109], who reported that endothelial cell expression of PDPN was responsible for a blood-lymphatic misconnection. Furthermore, continued expression of PDPN into adulthood is required to maintain proper vascular architecture, as an inducible deletion of T-synthase, a major glycosyltransferase required for O-glycan synthesis and normal levels of PDPN expression, showed similar blood-lymph mixing[109].

Interactions between PDPN on LECs and CLEC-2 on platelets are critical for the development and maintenance of normal lymphatic vessels[110,111]. Accordingly, the blood-lymphatic mixing phenotype observed in PDPN-deficient mice is also observed in mice where hematopoietic cells lack Syk, SLP-76, PLCγ2, or CLEC-2[111-113]. It was initially believed that platelets could not be involved in this phenotype because mice lacking nearly all platelets had normal lymphatic vasculature[114]. However, elegant studies have proven that CLEC-2 expression and

downstream signaling through SLP-76 are required specifically in platelets[110,115]. The interaction of platelet CLEC-2 and PDPN on LECs induces platelet aggregation and prevents blood from flowing into new lymphatic vessels budding from the cardinal vein. Furthermore, injecting a PDPN-blocking antibody or otherwise inhibiting platelet aggregation is sufficient to disrupt lymphatic development[116]. Overall, the model that has emerged indicates that during the budding of the lymph sac from the cardinal vein, PDPN becomes upregulated on Prox-1^{+}Lyve-1^{+} LECs and binds to CLEC-2 on platelets. This interaction activates downstream signaling in platelets, which results in platelet aggregation. This aggregation then allows for a complete separation of the budding lymphatic vessels from the developing blood vessels.

Interestingly, recent studies indicate that the continued interactions between CLEC-2 and PDPN are required for the maintenance of blood-lymph separation in adult animals. Hess et al.[117] revealed that platelets normally form thrombi at the lymphovenous junction to prevent backflow of blood into lymph vessels. In mice lacking CLEC-2, platelets failed to aggregate and form these thrombi, which led to bleeding in both neonates and adult mice. Benezech et al.[118] expanded these findings by demonstrating that the bleeding and disrupted lymph nodes in mice with a platelet-specific deletion of CLEC-2 was due to a profound defect in lymphatic endothelial cell proliferation. Finally, Herzog et al.[119] found that an interaction between platelets and FRCs around HEVs is critical for maintaining vascular integrity and preventing bleeding in mucosal lymph nodes.

CLEC-2: molecular characteristic and roles in platelets

The only known receptor for PDPN is CLEC-2, a C-type lectin that is expressed by platelets, neutrophils, and DCs[120-122]. Glycosylation of threonine 34 on PDPN is required for CLEC-2 binding of PDPN. This amino acid resides in the platelet-aggregation stimulating (PLAG)

domain, which is highly conserved between PDPN homologues[123]. Engagement of CLEC-2 on platelets by PDPN or rhodocytin, a snake venom toxin, leads to platelet aggregation and activation. Upon binding to its ligand, CLEC-2 dimerizes and the hemi-immunoreceptor tyrosine-based activation motif (YxxL) in its cytoplasmic tail is phosphorylated by Syk, which results in phosphorylation of PLCγ2 and further downstream signaling, leading to actin reorganization[124,125].

The effect of CLEC-2 engagement by PDPN has been extensively studied in platelets; however, the effect of this interaction in PDPN-expressing cells has not been addressed. This is an area that warrants further exploration, given that in vivo, many $PDPN^+$ cells will be exposed to CLEC-2 signals, whether they are tumor cells interacting with $CLEC\text{-}2^+$ platelets or FRCs interacting with $CLEC\text{-}2^+$ DCs.

Furthermore, ITAM signaling plays several important roles in DC biology. Most of these studies have focused on the role of DAP12 and FcRγ, two adaptor proteins containing ITAM domains[126]. One area where these molecules play a role is in integrating signals from integrins to affect TLR signaling and subsequent DC activation[127,128]. However, it is likely that there are other ITAM-containing proteins that may be involved in some of these functions that have yet to be discovered.

PDPN: molecular characteristics and functions

PDPN is a 36-43 kDa mucin-type transmembrane protein. It has homologues in humans, mice, rats, dogs, and hamsters and is relatively well conserved between species. PDPN has a wide variety of functions including regulation of organ development, cell motility, and tumorigenesis and metastasis[125,129]. PDPN has been identified and studied in many different contexts; thus, it has been given several names. PDPN was first described on LECs as the E11

antigen[130] and on FRCs of lymphoid organs and thymic epithelial cells as gp38[131,132]. PDPN is also homologous to T1α/rTI$_{40}$, one of the first molecular markers of alveolar type I epithelial cells[133,134], PA2.26, which is upregulated in skin keratinocytes upon injury[135], OTS-8, a molecule induced in osteoblasts upon phorbol ester treatment[136], and Aggrus, a platelet-aggregating factor[137]. Finally, this molecule was given the name podoplanin due to its expression on kidney podocytes and possible involvement in the flattening of podocyte foot processes[138].

While PDPN expression patterns in many of these cells have been well characterized, there is still little known about the physiological functions of this protein. PDPN binds to the C-type lectin receptor CLEC-2, which is highly expressed by platelets and immune cells. However, this interaction has only been extensively studied with regard to platelets, as discussed above. PDPN has also been used as a marker for FRCs in the lymph node and spleen and lymphatic vessels in tumors, but there is limited data on whether PDPN expression is required for the function of these cells or influences their interactions with leukocytes.

The majority of data examining the function and signaling pathways of PDPN are from studies of PDPN overexpression in tumor cells. While these studies certainly provide critical insight into cellular and molecular aspects of PDPN biology, it is important to understand whether PDPN functions similarly in non-pathological settings and in cell types where it is naturally expressed.

PDPN in development

PDPN is first expressed in the developing mouse embryo on day E9 in the foregut, proepicardial organ, and central nervous system[134,139]. Throughout development, it is also expressed in the fetal rat kidney, choroid plexus, intestine, and esophagus[134]. Over time, PDPN expression is increasingly restricted such that in an adult animal, PDPN is predominantly

expressed in alveolar type I cells, mature osteoblasts, LECs, and FRCs[108,130,134]. PDPN is critical for normal development of some of these organs and has been well studied in PDPN-deficient animals. *Pdpn*$^{-/-}$ mice develop normally until around day E10, which coincides with the appearance of PDPN protein. From days E10-16, approximately 40% of *Pdpn*$^{-/-}$ embryos die; the ones that survive to birth die within a few days[140]. However, interestingly, when the mice are crossed onto a C57Bl/6 background, many more embryos survive to birth, and although 50% die in the first week, approximately 20% of the mice do survive to adulthood[116]. The reason why the genetic background affects the severity of the defects suffered by the *Pdpn*$^{-/-}$ mice is intriguing and warrants further study. Furthermore, it would be of great use to the field to have a conditional knockout of PDPN to avoid these survival defects.

In addition to its role in lymphatic vessel development, PDPN may play a role in the development or maintenance of lymphoid organ architecture. In the spleens of mice lacking lymphocytes, no PDPN expression is observed, although FRCs are still present as indicated by VCAM-1 and ERTR7 staining[141,142]. It appears that this lack of expression is due to a lack of lymphotoxin, but it remains unclear exactly which cell type provides that signal during development of the spleen. A more striking phenotype has been observed by Peters et al.[143] in that *Pdpn*$^{-/-}$ mice lack nearly all lymph nodes, and the ones that develop are extremely disorganized. The spleens of these mice were present, but were also disorganized. It is interesting to speculate whether this phenotype indicates an important function for PDPN on FRCs; however, it is also possible that the lack of lymph nodes is due to impaired lymph flow caused by the malformed lymphatic vessels. Thus, further work is needed to dissect this phenotype.

The first defects described in *Pdpn*$^{-/-}$ mice were in the lung, as these mice die shortly after birth due to an inability to inflate the lungs[144]. This defect stems from an impairment in the

development of alveolar type I cells. These cells cover the majority of the lung surface and play a key role in the proper development of the alveoli, which are the major gas exchange centers of the lung[145]. In normal lung development, alveolar type I cells exhibit a high proliferation rate during early and mid-gestation periods, but this high growth rate slows a few days before birth[144]. However, when alveolar type I cells lack PDPN, they continue proliferating in later stages of embryonic development, which is partially explained by a decrease in the negative cell cycle regulator, p21, at birth[146].

PDPN is also necessary for proper development of the heart. PDPN is first expressed in the proepicardial organ on day E9.5 and by day E12.5, it is expressed in most of the heart. Without PDPN expression, the hearts of developing mice exhibit hypoplasia in the pulmonary vein, left atrium dorsal wall, and the atrial septum[147]. In this setting, the lack of PDPN leads to a dysregulation of epithelial-mesenchymal transition (EMT), a process that involves the transition of sessile epithelial cells into more motile mesenchymal cells through the downregulation of epithelial markers, such as adhesion molecules like E-cadherin[148]. In PDPN-deficient mice, the epicardium-derived cells responsible for cardiac development show increased levels of E-cadherin and decreased levels of RhoA compared with their wild-type counterparts, which is indicative of impaired EMT[139,140]. These studies are the first evidence that PDPN may play a role in physiological instances of EMT in non-transformed cells.

Overall, PDPN is crucial for the development of multiple organs, including the lymphatic system, lungs, and heart. Interestingly, PDPN serves diverse functions in these organs. In some instances it is required for CLEC-2-dependent platelet aggregation, but in others it seems to have an intrinsic effect on proliferation or differentiation in a specific cell type. This raises the question of whether PDPN function could to some degree be tissue specific. The range of

physiological effects downstream of PDPN expression may be due to different protein interactions and binding partners in diverse cell types.

Molecular interactions and signaling of PDPN

PDPN contains a single transmembrane domain, a short, nine amino acid cytoplasmic tail, and a heavily glycosylated extracellular domain[149]. While there are no obvious conserved protein domains in PDPN, several studies have identified specific residues on PDPN that mediate interactions with other proteins (Figure 1.4).

The first hints at the cellular function of PDPN came from Scholl et al.[135], who discovered that PDPN was upregulated in keratinocytes from induced epidermal carcinogenesis and was localized to membrane protrusions such as filopodia and lamellipodia. PDPN co-localized with ezrin, radixin, and moesin (ERM) family proteins, and was later found to directly bind ezrin and moesin. This interaction requires a conserved motif of three basic residues in the cytoplasmic tail (see Figure 1.4) and overexpression of PDPN resulted in increased phosphorylation of ERM proteins[150,151]. The ERM proteins function as connectors between integral membrane proteins and the actin cytoskeleton. Phosphorylation causes a conformational change that exposes binding sites for actin and other proteins[152]. Thus, this interaction likely underlies many of the effects that PDPN has on cytoskeleton. A closer examination of the effects of PDPN upregulation revealed that overexpression of PDPN in epithelial cell lines caused them to become more mesenchymal in appearance, with decreased stress fibers and increased filopodia[150,151]. These changes, in addition to a downregulation of E-cadherin and other epithelial markers, are indicative of cells undergoing EMT, which is indeed what Martin-Villar et al.[150] observed. However, Wicki et al.[151] demonstrated that while PDPN overexpression resulted in increased motility, it did not result in an E-cadherin switch or EMT. Discrepancies were also found when

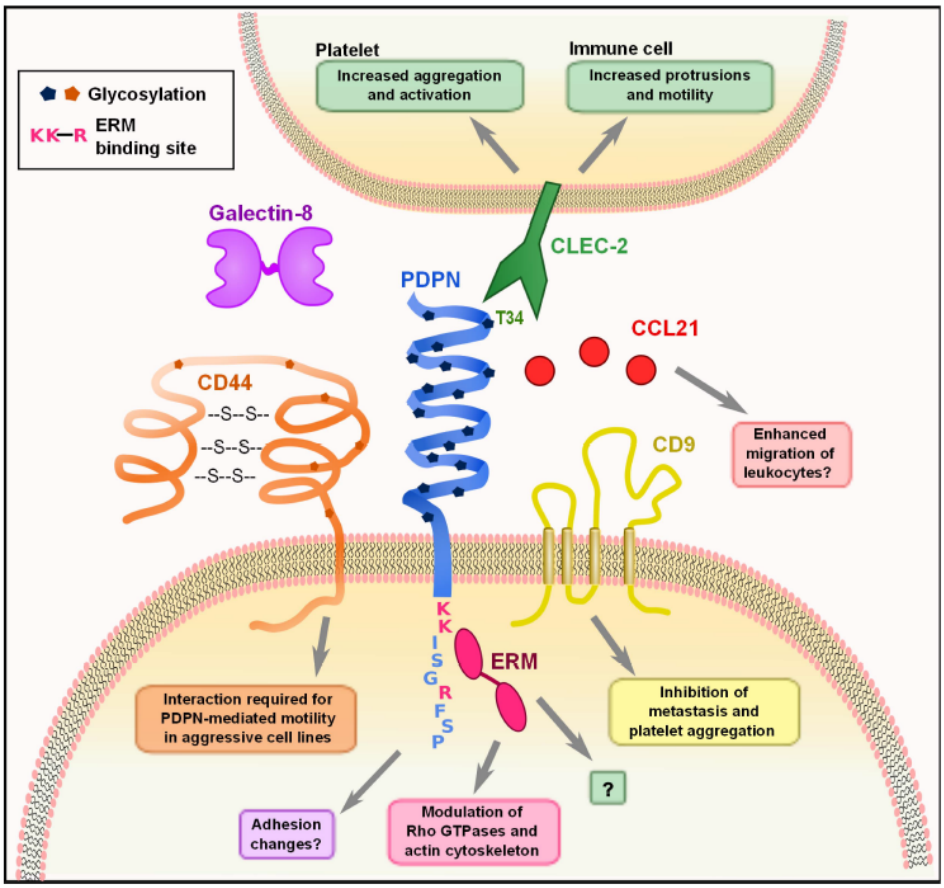

Figure 1.4. Molecular interactions of PDPN. PDPN interacts with a variety of intracellular and transmembrane proteins to mediate effects on cell migration and adhesion. The binding of PDPN to CD44 or ezrin, radixin, moesin family proteins results in increased cell migration and rearrangement of the actin cytoskeleton to generate actin-rich protrusions of the membrane. The three amino acids colored in pink (K,K,R) are the basic residues required for ERM protein binding. Interactions between PDPN and CD9 affect metastasis and platelet aggregation. The engagement of PDPN by CLEC-2 causes increased motility in DCs and aggregation and activation of platelets. PDPN binds with high affinity to the chemokine CCL21 and while the consequences of this effect have not been examined, it may play a role in facilitating leukocyte migration. Finally, PDPN binding to galectin-8 may modulate adhesion of LECs.

the involvement of Rho family small G proteins was examined. Martin-Villar et al.[150] reported that PDPN overexpression resulted in an increase in RhoA and no change in Rac-1 or Cdc42, while Wicki et al.[151] found a downregulation in RhoA, Rac-1, and Cdc42. In addition, Navarro et al.[153] found that knocking down PDPN in LECs resulted in decreased levels of activated RhoA and increased levels in Cdc42. While it is clear that the expression of PDPN has an effect on the activity levels of these proteins, more work must be done to fully elucidate the mechanism. As described above, it is possible that PDPN exerts different effects and utilizes distinct signaling cascades in various cell types, which could partially explain the observed discrepancies.

Recently, it was discovered that PDPN resides in lipid rafts in the plasma membrane. Barth et al.[154] found that PDPN resides in detergent-insoluble fractions of alveolar type I epithelial cells, but its function within these rafts remains unknown. It was subsequently reported that human PDPN expressed in Madin-Darby Canine Kidney (MDCK) type II cells is localized to lipid rafts[155]. In these cells, the transmembrane and cytoplasmic domains of PDPN were necessary for association with lipid rafts. Furthermore, manipulation of this localization by substituting the transmembrane domain with that of other proteins inhibited PDPN-mediated increases in EMT, migration, and phosphorylation of ERMs[155]. Interestingly, cytoskeletal interactions are not required for PDPN to get into lipid rafts[154]; however, the cytosolic domain is necessary[155] and one way this might be explained is via interactions with ERMs, given that ezrin is also raft-associated.

Given that the cytoplasmic tail of PDPN is extremely short, it is difficult to imagine that there is much direct signaling downstream of PDPN other than through the ERM proteins, simply due to spatial restrictions. Interestingly, however, PDPN also interacts with two integral membrane proteins that could help to further explain how it affects cell motility and metastasis. CD44, which is widely expressed, affects many cellular functions such as migration and adhesion,

and the expression of some isoforms is linked to more invasive cancers. Martín-Villar et al.[156] noted that CD44 and PDPN were coordinately upregulated in aggressive cancer cell lines and subsequently found that they directly bind to one another. This interaction is dependent on correct glycosylation of the extracellular domain of PDPN, and CD44 expression is required for PDPN-induced cell migration[156]. Additionally, Nakazawa et al.[157] found that PDPN directly interacts with the tetraspanin CD9 through transmembrane domains 1 and 2 of CD9. CD9 acts as a tumor suppressor in many cancers[158], and co-expression of CD9 and PDPN resulted in a CD9-mediated decrease of PDPN-induced metastasis. CD9 also inhibited PDPN-mediated platelet aggregation without directly interfering with CLEC-2 binding of PDPN[157]. This finding indicates that CD9 potentially disrupts CLEC-2 multimerization, which is required for downstream signaling. These interactions provide some insight into how PDPN can exert striking effects on actin cytoskeleton rearrangement, cell motility, and metastasis. Still however, much remains to be elucidated such as the downstream signaling changes that occur upon PDPN binding to CD9 or CD44, how PDPN overexpression results in an increase of ERM phosphorylation, and how that in turn modulates the activity of the Rho family small G proteins.

LECs and FRCs, the two major subsets of lymphoid stromal cells, express high levels of PDPN[65], but only a few studies have examined the molecular function of PDPN in these cells. PDPN interacts with galectin-8 on LECs, and this interaction is also dependent on PDPN glycosylation[159]. Galectin-8 can have varying effects on adhesion depending on whether it is secreted or membrane-bound[160]; it seems that PDPN binding to galectin-8 may affect LEC adhesion, but additional studies are needed to fully elucidate the consequences of this interaction. PDPN also binds CCL21 with high affinity, and this interaction is also dependent on glycosylation of PDPN[161]. This interaction has interesting implications for lymphocyte trafficking,

as both LECs and FRCs express CCL21 to direct lymphocyte and DC trafficking to the T zone of lymph nodes[3,31,66].

It has yet to be examined whether the above binding partners of PDPN are cell-type specific or how interaction with one protein affects the binding of PDPN to another interacting molecule. With the exception of the ERMs and CD44, it remains unclear whether PDPN can bind to several of these proteins at one time or whether such interactions might be mutually exclusive. A more global understanding of these various interactions is critical to our overall understanding of PDPN's molecular functions and downstream signaling.

Transcriptional control of PDPN expression

Information about the transcriptional control of PDPN first came from the early studies of the role of PDPN in the development of the lymphatic system. The fact that PDPN was specifically expressed on differentiating LECs but not nearby BECs led to the discovery that Prox-1, the major regulator of LEC differentiation, controlled the induction of PDPN[162]. In fact, forced expression of Prox-1 was sufficient to induce a LEC-like phenotype in differentiated BECs, including the upregulation of PDPN[162]. Furthermore, it was later found that IL-3, which is involved controlling the differentiation of a variety of hematopoietic cells and is produced by LECs but not BECs, was capable of upregulating Prox-1 and PDPN[163]. However, Prox-1 is not expressed in FRCs or in many of the other cells types expressing PDPN. Therefore alternative pathways must be involved in PDPN expression in tissues other than lymphatics. This may be another reason why the physiological functions of PDPN are so varied between different systems.

In skin cancers, osteosarcomas, and gliomas, PDPN is regulated by the AP-1 transcription factor[164-166]. AP-1 is a heterodimeric complex comprised of Fos and Jun proteins. Both Fos and

Jun are critical for progression of many carcinomas, including models of skin carcinogenesis[167]. Durchdewald et al.[164] compared genetic profiles of skin tumors from mice that had either WILD-TYPE Fos expression or Fos specifically deleted in keratinocytes and found that PDPN was one of the most highly upregulated genes in the Fos-sufficient samples. Furthermore, they demonstrated that Fos directly binds to the PDPN promoter. This interaction was further characterized in gliomas, and it was found that PTEN expression, a negative regulator of the PI3K-AKT-AP-1 pathway, was inversely correlated with PDPN expression (Figure 1.5)[166]. Furthermore, the PDPN promoter is heavily methylated, which keeps it repressed[166]. Thus, it appears that a major pathway of PDPN upregulation in malignant conditions depends on the activity of Fos and Jun (AP-1) transcription factors.

Finally, there have been two reports of pro-inflammatory cytokines resulting in PDPN upregulation in disease. In rheumatoid arthritis (RA), fibroblast-like synoviocytes are the main mediators of inflammation and tissue destruction and undergo a process resembling EMT during RA progression[168]. Ekwall et al.[169] recently reported that while PDPN is absent from the synovium of healthy subjects and patients with osteoarthritis, it is highly upregulated in RA patients. Furthermore, expression of PDPN in cultured synoviocytes is increased upon treatment with IL-1β, TNF-α, or TGF-β1[169]. Similarly, PDPN upregulation was observed in keratinocytes treated in vitro with TGF-β1, IL-6, IL-22, or IFN-γ [170]. The TGF-β1-mediated PDPN upregulation required Smad2/3 and 4 signaling, while STAT1 and STAT3 were necessary for IFN-γ signaling and STAT1 was required for IL-6 and IL-22 signaling[170].

Overall, it appears that a multitude of stimuli can drive PDPN expression, including normal differentiation factors such as Prox-1 and potentially malignant factors such as pro-tumorigenic signaling pathways and pro-inflammatory cytokines. It is possible that the different pathways controlling PDPN upregulation could result in the activation of distinct downstream

signaling pathways and therefore different cellular outcomes. For instance, a tumor cell and a LEC compose two distinct environments with different signaling pathways and molecules active; upregulating PDPN in these distinct signaling milieus would likely have diverse outcomes.

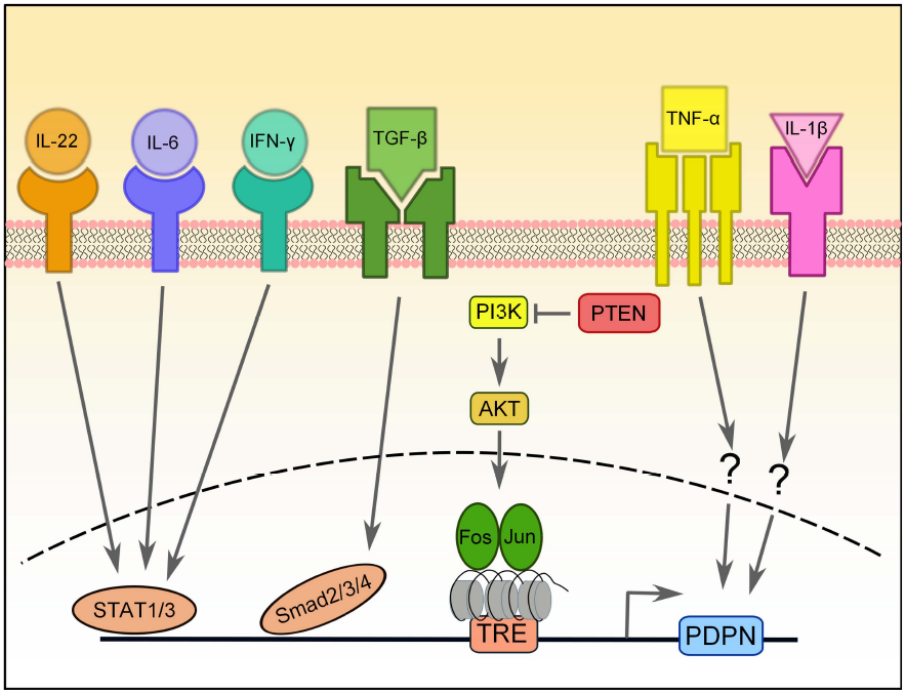

Figure 1.5. Transcriptional regulation of PDPN expression. PDPN expression can be upregulated by a number of pro-inflammatory cytokines, including IL-22, IL-6, IFN-γ, TGF-β, IL-1β, and TNF-α, but the signaling pathways involved are largely unknown. PDPN upregulation induced by TGF-β requires Smad2/3 and 4activity, while upregulation induced by IFN-γ depends on STAT1 and STAT3 and that of IL-6 and IL-22 depends on STAT3. The PI3K-AKT-AP-1 pathway can also induce PDPN expression in brain tumors that have lost the negative regulation normally provided by PTEN. AP-1, a transcription factor comprised of Fos and Jun proteins, binds to the tetradecanoylphorbolacetate-responsive element (TRE) in the promoter of PDPN, which is heavily methylated.

PDPN functions in the immune system

While PDPN is a well-established marker for LECs[130], FRCs[132], and follicular dendritic cells of lymphoid organs, until very recently, no particular function had been ascribed to PDPN in these immune cell populations.

PDPN signaling has intrinsic effects on the proliferation, migration, and tube formation of LECs. Navarro et al.[153,171] demonstrated that knocking down PDPN expression in vitro inhibited the ability of LECs to properly polarize towards a wound and migrate to close the wound. Reduced PDPN levels also decreased capillary formation when the cells were plated in a deformable 3D matrix[171]. These effects were mediated by decreased RhoA activity and increased Cdc42 activity in cells lacking PDPN[153]. The mechanism underlying this effect was further investigated by Osada et al.[115], who found that when LECs were incubated with WILD-TYPE but not *Clec-2*$^{-/-}$ platelets, the migration, proliferation, and in vitro tube formation of LECs was inhibited. This inhibition was mediated at least in part by BMP9 released in granules from the platelets upon contact with the LECs[115]. In contrast, Bertozzi et al.[110] found that co-culture of platelets with LECs did not affect their viability or proliferation. More work is necessary to determine whether CLEC-2 signals from platelets or other cells provide important signals to LECs in vivo.

In addition to its high expression on stromal cells, several recent reports have described PDPN expression on hematopoietic cells, including subsets of T cells and macrophages[122,143,172]. Interestingly, in these cases, as in those from cancer studies, PDPN expression is usually correlated with inflammatory or disease settings. In experimental autoimmune encephalomyelitis (EAE), ectopic germinal centers form in the central nervous system (CNS) and are believed to accelerate inflammation and disease progression[173]. Th17 cells are particularly important for the formation of these ectopic germinal centers and EAE progression[174]. PDPN

expression has been reported in ectopic lymphoid tissues in instances of chronic inflammation and cancer[175-177], but only on FRC-like stromal cells. Recently, Peters et al.[143] found that Th17 cells generated in vitro and those found in inflamed CNS tissue of mice with EAE express PDPN. Administration of a PDPN blocking antibody to mice with EAE did not attenuate disease severity, but significantly reduced the number of ectopic germinal centers induced by Th17-mediated disease. While the mechanism of PDPN function in T cells is not yet clear, it likely plays an important role in regulating T cell physiology in inflamed tissues.

PDPN expression has been observed on some macrophage subsets. It was first found on $F4/80^+$ macrophages in the red pulp of the spleen. These $PDPN^+$ macrophages exhibited marked phagocytic potential and elevated numbers in mice following systemic zymosan treatment[172]. PDPN is also expressed by inflammatory macrophages such as thioglycollate-elicited peritoneal macrophages and LPS-treated RAW264.7 cells[178]. These studies showed that expression of PDPN by macrophages was sufficient to induce CLEC-2-mediated aggregation of platelets in vitro. While the in vivo functions of PDPN expression by hematopoietic cells have not been fully elucidated, interesting implications abound given what is known about PDPN function in cancer and autoimmunity.

Conclusions

The major goal of this dissertation was to explore the roles that CLEC-2 and PDPN have in the immune system. We first focused on determining whether CLEC-2 played a role in DC migration from peripheral tissues to draining lymph nodes. Our results indicated that CLEC-2-deficient DCs were profoundly impaired in every step of their migration: leaving the skin and entering draining lymphatics, migrating through lymph vessels, entering into lymph nodes through the SCS, and finally, crawling along the FRC network. As a consequence, *Clec-2*$^{-/-}$ DCs

were unable to fully initiate T cell responses. CLEC-2 mediated these effects by inducing the formation of actin-rich protrusions that caused upregulated DC motility upon engagement with its ligands PDPN or rhodocytin.

Following this study, we next examined the role that PDPN played in controlling FRC biology. We found that normal expression of PDPN was critical for the maintenance of FRC contractility. Upon PDPN deletion or blockade, FRCs were unable to contract collagen matrices and, as a result, exhibited increased survival and uncontrolled proliferation. These cellular defects had striking effects on the in vivo FRC network: upon PDPN blockade, lymph nodes became enlarged and less stiff, presumably to the relaxation of the FRC network. These effects resulted in dysregulated immune responses, with increased T cell proliferation and impaired contraction of lymph nodes upon resolution of inflammation. Finally, we discovered that CLEC-2 engagement of PDPN delivered an inhibitory signal that recapitulated genetic deletion of PDPN. Taken together, the work conducted in this dissertation indicates that upon CLEC-2 engagement of PDPN, DCs receive signals that enhance their motility and, in turn, FRCs are instructed to relax and prepare lymph nodes for an impending expansion and immune response.

References

1. Bajénoff, M. *et al.* Highways, byways and breadcrumbs: directing lymphocyte traffic in the lymph node. *Trends Immunol.* **28,** 346–352 (2007).

2. Banchereau, J. & Steinman, R. M. Dendritic cells and the control of immunity. *Nature* **392,** 245–252 (1998).

3. Turley, S. J., Fletcher, A. L. & Elpek, K. G. The stromal and haematopoietic antigen-presenting cells that reside in secondary lymphoid organs. *Nature Publishing Group* **10,** 813–825 (2010).

4. Andrian, von, U. H. & Mempel, T. R. Homing and cellular traffic in lymph nodes. *Nat Rev Immunol* **3,** 867–878 (2003).

5. Mueller, S. N. & Germain, R. N. Stromal cell contributions to the homeostasis and functionality of the immune system. *Nature Publishing Group* **9,** 618–629 (2009).

6. Lämmermann, T. & Sixt, M. The microanatomy of T-cell responses. *Immunol. Rev.* **221,** 26–43 (2008).

7. Tapia, F. J., Cáceres-Dittmar, G., Acuña, L. & Mosca, W. Epidermal Langerhans cells in infectious diseases. *Histol. Histopathol.* **4,** 499–508 (1989).

8. Steinman, R. M., Lustig, D. S. & Cohn, Z. A. Identification of a novel cell type in peripheral lymphoid organs of mice. 3. Functional properties in vivo. *J. Exp. Med.* **139,** 1431–1445 (1974).

9. Steinman, R. M. & Cohn, Z. A. Identification of a novel cell type in peripheral lymphoid organs of mice. I. Morphology, quantitation, tissue distribution. *J. Exp. Med.* **137,** 1142–1162 (1973).

10. Steinman, R. M. & Cohn, Z. A. Identification of a novel cell type in peripheral lymphoid organs of mice. II. Functional properties in vitro. *J. Exp. Med.* **139,** 380–397 (1974).

11. Medzhitov, R. Toll-like receptors and innate immunity. *Nat Rev Immunol* **1,** 135–145 (2001).

12. Broz, P. & Monack, D. M. Newly described pattern recognition receptors team up against intracellular pathogens. *Nature Publishing Group* **13,** 551–565 (2013).

13. Savina, A. & Amigorena, S. Phagocytosis and antigen presentation in dendritic cells. *Immunol. Rev.* **219,** 143–156 (2007).

14. Turley, S. J. *et al.* Transport of peptide-MHC class II complexes in developing dendritic cells. *Science* **288,** 522–527 (2000).

15. Iwasaki, A. & Medzhitov, R. Toll-like receptor control of the adaptive immune responses. *Nat Immunol* **5,** 987–995 (2004).

16. Sallusto, F. *et al.* Rapid and coordinated switch in chemokine receptor expression during dendritic cell maturation. *Eur. J. Immunol.* **28,** 2760–2769 (1998).

17. Fujii, S.-I., Liu, K., Smith, C., Bonito, A. J. & Steinman, R. M. The linkage of innate to adaptive immunity via maturing dendritic cells in vivo requires CD40 ligation in addition to antigen presentation and CD80/86 costimulation. *J. Exp. Med.* **199,** 1607–1618 (2004).

18. Spörri, R. & Reis e Sousa, C. Inflammatory mediators are insufficient for full dendritic cell activation and promote expansion of CD4+ T cell populations lacking helper function. *Nat Immunol* **6,** 163–170 (2005).

19. Bonneville, M., O'Brien, R. L. & Born, W. K. Gammadelta T cell effector functions: a blend of innate programming and acquired plasticity. *Nature Publishing Group* **10,** 467–478 (2010).

20. Münz, C., Steinman, R. M. & Fujii, S.-I. Dendritic cell maturation by innate lymphocytes: coordinated stimulation of innate and adaptive immunity. *J. Exp. Med.* **202,** 203–207 (2005).

21. Cella, M. *et al.* Ligation of CD40 on dendritic cells triggers production of high levels of interleukin-12 and enhances T cell stimulatory capacity: T-T help via APC activation. *J. Exp. Med.* **184,** 747–752 (1996).

22. Leslie, D. S. *et al.* CD1-mediated gamma/delta T cell maturation of dendritic cells. *J. Exp. Med.* **196,** 1575–1584 (2002).

23. Vincent, M. S. *et al.* CD1-dependent dendritic cell instruction. *Nat Immunol* **3,** 1163–1168 (2002).

24. Hermans, I. F. *et al.* NKT cells enhance CD4+ and CD8+ T cell responses to soluble antigen in vivo through direct interaction with dendritic cells. *The Journal of Immunology* **171,** 5140–5147 (2003).

25. Zitvogel, L. Dendritic and natural killer cells cooperate in the control/switch of innate immunity. *J. Exp. Med.* **195,** F9–14 (2002).

26. Mocikat, R. *et al.* Natural killer cells activated by MHC class I(low) targets prime dendritic cells to induce protective CD8 T cell responses. *Immunity* **19,** 561–569 (2003).

27. Gerosa, F. *et al.* Reciprocal activating interaction between natural killer cells and dendritic cells. *J. Exp. Med.* **195,** 327–333 (2002).

28. Baggiolini, M. Chemokines and leukocyte traffic. *Nature* **392,** 565–568 (1998).

29. Kellermann, S. A., Hudak, S., Oldham, E. R., Liu, Y. J. & McEvoy, L. M. The CC chemokine receptor-7 ligands 6Ckine and macrophage inflammatory protein-3 beta are potent chemoattractants for in vitro- and in vivo-derived dendritic cells. *The Journal of Immunology* **162,** 3859–3864 (1999).

30. Robbiani, D. F. *et al.* The leukotriene C(4) transporter MRP1 regulates CCL19 (MIP-3beta, ELC)-dependent mobilization of dendritic cells to lymph nodes. *Cell* **103,** 757–768 (2000).

31. Luther, S. A., Tang, H. L., Hyman, P. L., Farr, A. G. & Cyster, J. G. Coexpression of the chemokines ELC and SLC by T zone stromal cells and deletion of the ELC gene in the plt/plt mouse. *Proceedings of the National Academy of Sciences* **97,** 12694–12699 (2000).

32. Lin, C. L., Suri, R. M., Rahdon, R. A., Austyn, J. M. & Roake, J. A. Dendritic cell chemotaxis and transendothelial migration are induced by distinct chemokines and are regulated on maturation. *Eur. J. Immunol.* **28,** 4114–4122 (1998).

33. Dieu, M. C. *et al.* Selective recruitment of immature and mature dendritic cells by distinct chemokines expressed in different anatomic sites. *J. Exp. Med.* **188,** 373–386 (1998).

34. Gunn, M. D. *et al.* Mice lacking expression of secondary lymphoid organ chemokine have defects in lymphocyte homing and dendritic cell localization. *J. Exp. Med.* **189,** 451–460 (1999).

35. Förster, R. *et al.* CCR7 coordinates the primary immune response by establishing functional microenvironments in secondary lymphoid organs. *Cell* **99,** 23–33 (1999).

36. Braun, A. *et al.* Afferent lymph–derived T cells and DCs use different chemokine receptor CCR7–dependent routes for entry into the lymph node and intranodal migration. *Nat Immunol* **12,** 879–887 (2011).

37. Moussion, C. & Girard, J.-P. Dendritic cells control lymphocyte entry to lymph nodes through high endothelial venules. *Nature* **479,** 542–546 (2011).

38. Wendland, M. *et al.* Lymph node T cell homeostasis relies on steady state homing of dendritic cells. *Immunity* **35,** 945–957 (2011).

39. Benvenuti, F. *et al.* Requirement of Rac1 and Rac2 expression by mature dendritic cells for T cell priming. *Science* **305,** 1150–1153 (2004).

40. Hynes, R. O. Integrins: bidirectional, allosteric signaling machines. *Cell* **110,** 673–687 (2002).

41. Lämmermann, T. *et al.* Rapid leukocyte migration by integrin-independent flowing and squeezing. *Nature* **453,** 51–55 (2008).

42. Frittoli, E. *et al.* The signaling adaptor Eps8 is an essential actin capping protein for dendritic cell migration. *Immunity* **35,** 388–399 (2011).

43. Kelly, R. H. Functional anatomy of lymph nodes. I. The paracortical cords. *Int. Arch. Allergy Appl. Immunol.* **48,** 836–849 (1975).

44. Weiss, L. The white pulp of the spleen. *Bulletin Johns Hopkins Hospital* **15,** (1964).

45. Pictet, R., Orchi, L., Forssmann, W. G. & Girardier, L. An electron microscopic study of the perfusion-fixed spleen. I. The splenic circulation and the RES concept. *Z. Zellforsch. Mikrosk. Anat.* **96,** (1969).

46. Malhotra, D. *et al.* Transcriptional profiling of stroma from inflamed and resting lymph nodes defines immunological hallmarks. *Nat Immunol* **13,** 499–510 (2012).

47. Malhotra, D., Fletcher, A. L. & Turley, S. J. Stromal and hematopoietic cells in secondary lymphoid organs: partners in immunity. *Immunol. Rev.* **251,** 160–176 (2013).

48. Fletcher, A. L. *et al.* Reproducible isolation of lymph node stromal cells reveals site-dependent differences in fibroblastic reticular cells. *Front Immunol* **2,** 35 (2011).

49. Onder, L. *et al.* IL-7-producing stromal cells are critical for lymph node remodeling. *Blood* **120,** 4675–4683 (2012).

50. Streeter, P. R., Rouse, B. T. & Butcher, E. C. Immunohistologic and functional characterization of a vascular addressin involved in lymphocyte homing into peripheral lymph nodes. *The Journal of Cell Biology* **107,** 1853–1862 (1988).

51. Streeter, P. R., Berg, E. L., Rouse, B. T., Bargatze, R. F. & Butcher, E. C. A tissue-specific endothelial cell molecule involved in lymphocyte homing. *Nature* **331,** 41–46 (1988).

52. Gommerman, J. L. & Browning, J. L. Lymphotoxin/light, lymphoid microenvironments and autoimmune disease. *Nat Rev Immunol* **3,** 642–655 (2003).

53. Hase, H. *et al.* BAFF/BLyS can potentiate B-cell selection with the B-cell coreceptor complex. *Blood* **103,** 2257–2265 (2004).

54. Fu, Y. X., Huang, G., Wang, Y. & Chaplin, D. D. B lymphocytes induce the formation of follicular dendritic cell clusters in a lymphotoxin alpha-dependent fashion. *J. Exp. Med.* **187,** 1009–1018 (1998).

55. Balogh, P., Aydar, Y., Tew, J. G. & Szakal, A. K. Ontogeny of the follicular dendritic cell phenotype and function in the postnatal murine spleen. *Cell. Immunol.* **214,** 45–53 (2001).

56. Wang, X. *et al.* Follicular dendritic cells help establish follicle identity and promote B cell retention in germinal centers. *J. Exp. Med.* **208,** 2497–2510 (2011).

57. Boulianne, B. *et al.* AID-Expressing Germinal Center B Cells Cluster Normally within Lymph Node Follicles in the Absence of FDC-M1+ CD35+ Follicular Dendritic Cells but Dissipate Prematurely. *The Journal of Immunology* **191,** 4521–4530 (2013).

58. Bajénoff, M. & Germain, R. N. B-cell follicle development remodels the conduit system and allows soluble antigen delivery to follicular dendritic cells. *Blood* **114,** 4989–4997 (2009).

59. Cremasco, V. *et al.* B cell homeostasis and follicle confines are governed by fibroblastic reticular cells. *Nat Immunol*

60. Roozendaal, R. & Carroll, M. C. Complement receptors CD21 and CD35 in humoral immunity. *Immunol. Rev.* **219,** 157–166 (2007).

61. Allen, C. D. C. & Cyster, J. G. Follicular dendritic cell networks of primary follicles and germinal centers: phenotype and function. *Seminars in Immunology* **20,** 14–25 (2008).

62. Katakai, T. *et al.* Organizer-like reticular stromal cell layer common to adult secondary lymphoid organs. *J. Immunol.* **181,** 6189–6200 (2008).

63. Fletcher, A. L. *et al.* Lymph node fibroblastic reticular cells directly present peripheral tissue antigen under steady-state and inflammatory conditions. *J. Exp. Med.* **207,** 689–697 (2010).

64. Chai, Q. *et al.* Maturation of Lymph Node Fibroblastic Reticular Cells from Myofibroblastic Precursors Is Critical for Antiviral Immunity. *Immunity* 1–12 (2013). doi:10.1016/j.immuni.2013.03.012

65. Link, A. *et al.* Fibroblastic reticular cells in lymph nodes regulate the homeostasis of naive T cells. *Nat Immunol* **8,** 1255–1265 (2007).

66. Bajénoff, M. *et al.* Stromal Cell Networks Regulate Lymphocyte Entry, Migration, and Territoriality in Lymph Nodes. *Immunity* **25,** 989–1001 (2006).

67. Katakai, T. *et al.* A novel reticular stromal structure in lymph node cortex: an immuno-platform for interactions among dendritic cells, T cells and B cells. *Int. Immunol.* **16,** 1133–1142 (2004).

68. Sixt, M. *et al.* The conduit system transports soluble antigens from the afferent lymph to resident dendritic cells in the T cell area of the lymph node. *Immunity* **22,** 19–29 (2005).

69. Lee, J.-W. *et al.* Peripheral antigen display by lymph node stroma promotes T cell tolerance to intestinal self. *Nat Immunol* **8,** 181–190 (2007).

70. Mueller, S. N. *et al.* Viral targeting of fibroblastic reticular cells contributes to immunosuppression and persistence during chronic infection. *Proceedings of the National Academy of Sciences* **104,** 15430–15435 (2007).

71. Lukacs-Kornek, V. *et al.* Regulated release of nitric oxide by nonhematopoietic stroma controls expansion of the activated T cell pool in lymph nodes. *Nat Immunol* **12,** 1096–1104 (2011).

72. Siegert, S. *et al.* Fibroblastic reticular cells from lymph nodes attenuate T cell expansion by producing nitric oxide. *PLoS ONE* **6,** e27618 (2011).

73. Khan, O. *et al.* Regulation of T cell priming by lymphoid stroma. *PLoS ONE* **6,** e26138 (2011).

74. Anderson, N. D., Anderson, A. O. & Wyllie, R. G. Microvascular changes in lymph nodes draining skin allografts. *The American Journal of Pathology* **81,** 131–160 (1975).

75. Webster, B. *et al.* Regulation of lymph node vascular growth by dendritic cells. *J. Exp. Med.* **203,** 1903–1913 (2006).

76. Soderberg, K. A. *et al.* Innate control of adaptive immunity via remodeling of lymph node feed arteriole. *Proceedings of the National Academy of Sciences* **102,** 16315–16320 (2005).

77. Tzeng, T. C. *et al.* CD11chi Dendritic Cells Regulate the Re-establishment of Vascular Quiescence and Stabilization after Immune Stimulation of Lymph Nodes. *The Journal of Immunology* **184,** 4247–4257 (2010).

78. Chyou, S. *et al.* Fibroblast-type reticular stromal cells regulate the lymph node vasculature. *J. Immunol.* **181,** 3887–3896 (2008).

79. Hall, J. G. & Morris, B. The immediate effect of antigens on the cell output of a lymph node. *Br J Exp Pathol* **46,** 450–454 (1965).

80. Shiow, L. R. *et al.* CD69 acts downstream of interferon-alpha/beta to inhibit S1P1 and lymphocyte egress from lymphoid organs. *Nature* **440,** 540–544 (2006).

81. Matloubian, M. *et al.* Lymphocyte egress from thymus and peripheral lymphoid organs is dependent on S1P receptor 1. *Nature* **427,** 355–360 (2004).

82. Allende, M. L., Dreier, J. L., Mandala, S. & Proia, R. L. Expression of the sphingosine 1-phosphate receptor, S1P1, on T-cells controls thymic emigration. *Journal of Biological Chemistry* **279,** 15396–15401 (2004).

83. Kumamoto, Y., Mattei, L. M., Sellers, S., Payne, G. W. & Iwasaki, A. CD4+ T cells support cytotoxic T lymphocyte priming by controlling lymph node input. *Proc. Natl. Acad. Sci. U.S.A.* **108,** 8749–8754 (2011).

84. Serhan, C. N., Chiang, N. & Van Dyke, T. E. Resolving inflammation: dual anti-inflammatory and pro-resolution lipid mediators. *Nature Publishing Group* **8,** 349–361 (2008).

85. Girard, J.-P., Moussion, C. & Förster, R. HEVs, lymphatics and homeostatic immune cell trafficking in lymph nodes. *Nature Publishing Group* **12,** 762–773 (2012).

86. Sinha, R. K., Park, C., Hwang, I.-Y., Davis, M. D. & Kehrl, J. H. B lymphocytes exit lymph nodes through cortical lymphatic sinusoids by a mechanism independent of sphingosine-1-phosphate-mediated chemotaxis. *Immunity* **30,** 434–446 (2009).

87. Grigorova, I. L. *et al.* Cortical sinus probing, S1P1-dependent entry and flow-based capture of egressing T cells. *Nat Immunol* **10,** 58–65 (2009).

88. Carrasco, Y. R. & Batista, F. D. B cells acquire particulate antigen in a macrophage-rich area at the boundary between the follicle and the subcapsular sinus of the lymph node. *Immunity* **27,** 160–171 (2007).

89. Junt, T. *et al.* Subcapsular sinus macrophages in lymph nodes clear lymph-borne viruses

and present them to antiviral B cells. *Nature* **450,** 110–114 (2007).

90. Phan, T. G., Grigorova, I., Okada, T. & Cyster, J. G. Subcapsular encounter and complement-dependent transport of immune complexes by lymph node B cells. *Nat Immunol* **8,** 992–1000 (2007).

91. Gonzalez, S. F. *et al.* Capture of influenza by medullary dendritic cells via SIGN-R1 is essential for humoral immunity in draining lymph nodes. *Nat Immunol* **11,** 427–434 (2010).

92. Ingulli, E., Ulman, D. R., Lucido, M. M. & Jenkins, M. K. In situ analysis reveals physical interactions between CD11b+ dendritic cells and antigen-specific CD4 T cells after subcutaneous injection of antigen. *The Journal of Immunology* **169,** 2247–2252 (2002).

93. Itano, A. A. & Jenkins, M. K. Antigen presentation to naive CD4 T cells in the lymph node. *Nat Immunol* **4,** 733–739 (2003).

94. Maurer, T. *et al.* CpG-DNA aided cross-presentation of soluble antigens by dendritic cells. *Eur. J. Immunol.* **32,** 2356–2364 (2002).

95. Pior, J., Vogl, T., Sorg, C. & MacHer, E. Free hapten molecules are dispersed by way of the bloodstream during contact sensitization to fluorescein isothiocyanate. *J. Invest. Dermatol.* **113,** 888–893 (1999).

96. Gretz, J. E., Anderson, A. O. & Shaw, S. Cords, channels, corridors and conduits: critical architectural elements facilitating cell interactions in the lymph node cortex. *Immunol. Rev.* **156,** 11–24 (1997).

97. Kaldjian, E. P., Gretz, J. E., Anderson, A. O., Shi, Y. & Shaw, S. Spatial and molecular organization of lymph node T cell cortex: a labyrinthine cavity bounded by an epithelium-like monolayer of fibroblastic reticular cells anchored to basement membrane-like extracellular matrix. *Int. Immunol.* **13,** 1243–1253 (2001).

98. Roozendaal, R. *et al.* Conduits Mediate Transport of Low-Molecular-Weight Antigen to Lymph Node Follicles. *Immunity* **30,** 264–276 (2009).

99. Katakai, T. Lymph Node Fibroblastic Reticular Cells Construct the Stromal Reticulum via Contact with Lymphocytes. *J. Exp. Med.* **200,** 783–795 (2004).

100. Mebius, R. E. Organogenesis of lymphoid tissues. *Nat Rev Immunol* **3,** 292–303 (2003).

101. Provenzano, P. P. & Keely, P. J. Mechanical signaling through the cytoskeleton regulates cell proliferation by coordinated focal adhesion and Rho GTPase signaling. *Journal of Cell Science* **124,** 1195–1205 (2011).

102. Wozniak, M. A. & Chen, C. S. Mechanotransduction in development: a growing role for contractility. *Nat Rev Mol Cell Biol* **10,** 34–43 (2009).

103. Mullins, R. J. & Hudgens, R. W. Increased skin lymph protein clearance after a 6-h arterial bradykinin infusion. *Am. J. Physiol.* **253,** H1462–9 (1987).

104. Harrell, M. I., Iritani, B. M. & Ruddell, A. Tumor-induced sentinel lymph node lymphangiogenesis and increased lymph flow precede melanoma metastasis. *The American Journal of Pathology* **170,** 774–786 (2007).

105. Staberg, B., Klemp, P., Aasted, M., Worm, A. M. & Lund, P. Lymphatic albumin clearance from psoriatic skin. *J. Am. Acad. Dermatol.* **9,** 857–861 (1983).

106. Tomei, A. A., Siegert, S., Britschgi, M. R., Luther, S. A. & Swartz, M. A. Fluid flow regulates stromal cell organization and CCL21 expression in a tissue-engineered lymph node microenvironment. *J. Immunol.* **183,** 4273–4283 (2009).

107. Oliver, G. Lymphatic vasculature development. *Nat Rev Immunol* **4,** 35–45 (2004).

108. Schacht, V. *et al.* T1alpha/podoplanin deficiency disrupts normal lymphatic vasculature formation and causes lymphedema. *EMBO J.* **22,** 3546–3556 (2003).

109. Fu, J. *et al.* Endothelial cell O-glycan deficiency causes blood/lymphatic misconnections and consequent fatty liver disease in mice. *J. Clin. Invest.* **118,** 3725–3737 (2008).

110. Bertozzi, C. C. *et al.* Platelets regulate lymphatic vascular development through CLEC-2-SLP-76 signaling. *Blood* **116,** 661–670 (2010).

111. Suzuki-Inoue, K. *et al.* Essential in Vivo Roles of the C-type Lectin Receptor CLEC-2: EMBRYONIC/NEONATAL LETHALITY OF CLEC-2-DEFICIENT MICE BY BLOOD/LYMPHATIC MISCONNECTIONS AND IMPAIRED THROMBUS FORMATION OF CLEC-2-DEFICIENT PLATELETS. *Journal of Biological Chemistry* **285,** 24494–24507 (2010).

112. Abtahian, F. *et al.* Regulation of blood and lymphatic vascular separation by signaling proteins SLP-76 and Syk. *Science* **299,** 247–251 (2003).

113. Sebzda, E. *et al.* Syk and Slp-76 mutant mice reveal a cell-autonomous hematopoietic cell contribution to vascular development. *Developmental Cell* **11,** 349–361 (2006).

114. Shivdasani, R. A. *et al.* Transcription factor NF-E2 is required for platelet formation independent of the actions of thrombopoietin/MGDF in megakaryocyte development. *Cell* **81,** 695–704 (1995).

115. Osada, M. *et al.* Platelet Activation Receptor CLEC-2 Regulates Blood/Lymphatic Vessel Separation by Inhibiting Proliferation, Migration, and Tube Formation of Lymphatic Endothelial Cells. *Journal of Biological Chemistry* **287,** 22241–22252 (2012).

116. Uhrin, P. *et al.* Novel function for blood platelets and podoplanin in developmental separation of blood and lymphatic circulation. *Blood* **115,** 3997–4005 (2010).

117. Hess, P. R. *et al.* Platelets mediate lymphovenous hemostasis to maintain blood-lymphatic separation throughout life. *J. Clin. Invest.* **124,** 273–284 (2014).

118. Benezech, C. *et al.* CLEC-2 is required for development and maintenance of lymph nodes. *Blood* **123,** 3200–3207 (2014).

119. Herzog, B. H. *et al.* Podoplanin maintains high endothelial venule integrity by interacting with platelet CLEC-2. *Nature* **502,** 105–109 (2014).

120. Colonna, M., Samaridis, J. & Angman, L. Molecular characterization of two novel C-type lectin-like receptors, one of which is selectively expressed in human dendritic cells. *Eur. J. Immunol.* **30,** 697–704 (2000).

121. Sobanov, Y. *et al.* A novel cluster of lectin-like receptor genes expressed in monocytic, dendritic and endothelial cells maps close to the NK receptor genes in the human NK gene complex. *Eur. J. Immunol.* **31,** 3493–3503 (2001).

122. Kerrigan, A. M. *et al.* CLEC-2 is a phagocytic activation receptor expressed on murine peripheral blood neutrophils. *J. Immunol.* **182,** 4150–4157 (2009).

123. Kaneko, M. K., Kato, Y., Kitano, T. & Osawa, M. Conservation of a platelet activating domain of Aggrus/podoplanin as a platelet aggregation-inducing factor. *Gene* **378,** 52–57 (2006).

124. Hughes, C. E. *et al.* CLEC-2 activates Syk through dimerization. *Blood* **115,** 2947–2955 (2010).

125. Suzuki-Inoue, K., Inoue, O. & Ozaki, Y. Novel platelet activation receptor CLEC-2: from discovery to prospects. *J. Thromb. Haemost.* **9 Suppl 1,** 44–55 (2011).

126. Ivashkiv, L. B. Cross-regulation of signaling by ITAM-associated receptors. *Nat Immunol* **10,** 340–347 (2009).

127. Gerold, G. *et al.* A Toll-like receptor 2-integrin beta3 complex senses bacterial lipopeptides via vitronectin. *Nat Immunol* **9,** 761–768 (2008).

128. Kagan, J. C. & Medzhitov, R. Phosphoinositide-mediated adaptor recruitment controls Toll-like receptor signaling. *Cell* **125,** 943–955 (2006).

129. Wicki, A. & Christofori, G. The potential role of podoplanin in tumour invasion. *Br J Cancer* **96,** 1–5 (2006).

130. Wetterwald, A. *et al.* Characterization and cloning of the E11 antigen, a marker expressed by rat osteoblasts and osteocytes. *Bone* **18,** 125–132 (1996).

131. Farr, A. G. *et al.* Characterization and cloning of a novel glycoprotein expressed by stromal cells in T-dependent areas of peripheral lymphoid tissues. *J. Exp. Med.* **176,** 1477–1482 (1992).

132. Farr, A., Nelson, A. & Hosier, S. Characterization of an antigenic determinant preferentially expressed by type I epithelial cells in the murine thymus. *Journal of Histochemistry & Cytochemistry* **40,** 651–664 (1992).

133. Rishi, A. K. *et al.* Cloning, characterization, and development expression of a rat lung alveolar type I cell gene in embryonic endodermal and neural derivatives. *Developmental Biology* **167,** 294–306 (1995).

134. Williams, M. C., Cao, Y., Hinds, A., Rishi, A. K. & Wetterwald, A. T1 alpha protein is developmentally regulated and expressed by alveolar type I cells, choroid plexus, and ciliary epithelia of adult rats. *Am. J. Respir. Cell Mol. Biol.* **14,** 577–585 (1996).

135. Scholl, F. G., Gamallo, C., Vilaro, S. & Quintanilla, M. Identification of PA2.26 antigen as a novel cell-surface mucin-type glycoprotein that induces plasma membrane extensions and increased motility in keratinocytes. *Journal of Cell Science* **112 (Pt 24),** 4601–4613 (1999).

136. Nose, K., Saito, H. & Kuroki, T. Isolation of a gene sequence induced later by tumor-promoting 12-O-tetradecanoylphorbol-13-acetate in mouse osteoblastic cells (MC3T3-E1) and expressed constitutively in ras-transformed cells. *Cell Growth Differ.* **1,** 511–518 (1990).

137. Kato, Y. *et al.* Molecular Identification of Aggrus/T1 as a Platelet Aggregation-inducing Factor Expressed in Colorectal Tumors. *Journal of Biological Chemistry* **278,** 51599–51605 (2003).

138. Breiteneder-Geleff, S. *et al.* Podoplanin, novel 43-kd membrane protein of glomerular epithelial cells, is down-regulated in puromycin nephrosis. *The American Journal of Pathology* **151,** 1141–1152 (1997).

139. Mahtab, E. A. F. *et al.* Podoplanin deficient mice show a RhoA-related hypoplasia of the sinus venosus myocardium including the sinoatrial node. *Dev. Dyn.* **238,** 183–193 (2009).

140. Mahtab, E. A. F. *et al.* Cardiac malformations and myocardial abnormalities inpodoplanin knockout mouse embryos: Correlation with abnormal epicardial development. *Dev. Dyn.* **237,** 847–857 (2008).

141. Ngo, V. N., Cornall, R. J. & Cyster, J. G. Splenic T zone development is B cell dependent. *J. Exp. Med.* **194,** 1649–1660 (2001).

142. Bekiaris, V. *et al.* Role of CD30 in B/T segregation in the spleen. *The Journal of Immunology* **179,** 7535–7543 (2007).

143. Peters, A. *et al.* Th17 Cells Induce Ectopic Lymphoid Follicles in Central Nervous System Tissue Inflammation. *Immunity* **35,** 986–996 (2011).

144. Ramirez, M. I. *et al.* T1α, a lung type I cell differentiation gene, is required for normal lung cell proliferation and alveolus formation at birth. *Developmental Biology* **256,** 62–73 (2003).

145. Williams, M. C. A LVEOLART YPEI C ELLS: Molecular Phenotype and Development. *Annu. Rev. Physiol.* **65,** 669–695 (2003).

146. Millien, G. *et al.* Alterations in gene expression in T1 alpha null lung: a model of deficient alveolar sac development. *BMC Dev. Biol.* **6,** 35 (2006).

147. Douglas, Y. L. *et al.* Pulmonary vein, dorsal atrial wall and atrial septum abnormalities in

podoplanin knockout mice with disturbed posterior heart field contribution. *Pediatr. Res.* **65,** 27–32 (2009).

148. Thiery, J. P. Epithelial-mesenchymal transitions in tumour progression. *Nat Rev Cancer* **2,** 442–454 (2002).

149. Martín-Villar, E. *et al.* Characterization of human PA2.26 antigen (T1alpha-2, podoplanin), a small membrane mucin induced in oral squamous cell carcinomas. *Int. J. Cancer* **113,** 899–910 (2005).

150. Martin-Villar, E. *et al.* Podoplanin binds ERM proteins to activate RhoA and promote epithelial-mesenchymal transition. *Journal of Cell Science* **119,** 4541–4553 (2006).

151. Wicki, A. *et al.* Tumor invasion in the absence of epithelial-mesenchymal transition: Podoplanin-mediated remodeling of the actin cytoskeleton. *Cancer Cell* **9,** 261–272 (2006).

152. Fehon, R. G., McClatchey, A. I. & Bretscher, A. Organizing the cell cortex: the role of ERM proteins. 1–12 (2010). doi:10.1038/nrm2866

153. Navarro, A., Perez, R. E., Rezaiekhaligh, M. H., Mabry, S. M. & Ekekezie, I. I. Polarized migration of lymphatic endothelial cells is critically dependent on podoplanin regulation of Cdc42. *AJP: Lung Cellular and Molecular Physiology* **300,** L32–L42 (2010).

154. Barth, K., Bläsche, R. & Kasper, M. T1alpha/podoplanin shows raft-associated distribution in mouse lung alveolar epithelial E10 cells. *Cell. Physiol. Biochem.* **25,** 103–112 (2010).

155. Fernández-Muñoz, B. *et al.* The transmembrane domain of podoplanin is required for its association with lipid rafts and the induction of epithelial-mesenchymal transition. *The International Journal of Biochemistry & Cell Biology* **43,** 886–896 (2011).

156. Martín-Villar, E. *et al.* Podoplanin associates with CD44 to promote directional cell migration. *Mol. Biol. Cell* **21,** 4387–4399 (2010).

157. Nakazawa, Y. *et al.* Tetraspanin family member CD9 inhibits Aggrus/podoplanin-induced platelet aggregation and suppresses pulmonary metastasis. *Blood* **112,** 1730–1739 (2008).

158. Zöller, M. Tetraspanins: push and pull in suppressing and promoting metastasis. *Nat Rev Cancer* **9,** 40–55 (2009).

159. Cueni, L. N. & Detmar, M. Galectin-8 interacts with podoplanin and modulates lymphatic endothelial cell functions. *Experimental Cell Research* **315,** 1715–1723 (2009).

160. Zick, Y. *et al.* Role of galectin-8 as a modulator of cell adhesion and cell growth. *Glycoconj. J.* **19,** 517–526 (2004).

161. Kerjaschki, D. Lymphatic Neoangiogenesis in Human Kidney Transplants Is Associated

with Immunologically Active Lymphocytic Infiltrates. *Journal of the American Society of Nephrology* **15,** 603–612 (2004).

162. Hong, Y.-K. *et al.* Prox1 is a master control gene in the program specifying lymphatic endothelial cell fate. *Dev. Dyn.* **225,** 351–357 (2002).

163. Gröger, M. *et al.* IL-3 induces expression of lymphatic markers Prox-1 and podoplanin in human endothelial cells. *The Journal of Immunology* **173,** 7161–7169 (2004).

164. Durchdewald, M. *et al.* Podoplanin is a novel fos target gene in skin carcinogenesis. *Cancer Research* **68,** 6877–6883 (2008).

165. Kunita, A., Kashima, T. G., Ohazama, A., Grigoriadis, A. E. & Fukayama, M. Podoplanin Is Regulated by AP-1 and Promotes Platelet Aggregation and Cell Migration in Osteosarcoma. *The American Journal of Pathology* **179,** 1041–1049 (2011).

166. Peterziel, H. *et al.* Expression of podoplanin in human astrocytic brain tumors is controlled by the PI3K-AKT-AP-1 signaling pathway and promoter methylation. *Neuro-Oncology* **14,** 426–439 (2012).

167. Eferl, R. & Wagner, E. F. AP-1: a double-edged sword in tumorigenesis. *Nat Rev Cancer* **3,** 859–868 (2003).

168. Huber, L. C. *et al.* Synovial fibroblasts: key players in rheumatoid arthritis. *Rheumatology (Oxford)* **45,** 669–675 (2006).

169. Ekwall, A.-K. H. *et al.* The tumour-associated glycoprotein podoplanin is expressed in fibroblast-like synoviocytes of the hyperplastic synovial lining layer in rheumatoid arthritis. *Arthritis Research & Therapy* **13,** R40 (2011).

170. Honma, M., Minami-Hori, M., Takahashi, H. & Iizuka, H. Podoplanin expression in wound and hyperproliferative psoriatic epidermis: Regulation by TGF-β and STAT-3 activating cytokines, IFN-γ, IL-6, and IL-22. *Journal of Dermatological Science* **65,** 134–140 (2012).

171. Navarro, A., Perez, R. E., Rezaiekhaligh, M., Mabry, S. M. & Ekekezie, I. I. T1 /podoplanin is essential for capillary morphogenesis in lymphatic endothelial cells. *AJP: Lung Cellular and Molecular Physiology* **295,** L543–L551 (2008).

172. Hou, T. Z. *et al.* A distinct subset of podoplanin (gp38) expressing F4/80+ macrophages mediate phagocytosis and are induced following zymosan peritonitis. *FEBS Letters* **584,** 3955–3961 (2010).

173. Weyand, C. M., Kurtin, P. J. & Goronzy, J. J. Ectopic lymphoid organogenesis: a fast track for autoimmunity. *The American Journal of Pathology* **159,** 787–793 (2001).

174. Jäger, A., Dardalhon, V., Sobel, R. A., Bettelli, E. & Kuchroo, V. K. Th1, Th17, and Th9 effector cells induce experimental autoimmune encephalomyelitis with different pathological phenotypes. *J. Immunol.* **183,** 7169–7177 (2009).

175. Peduto, L. *et al.* Inflammation Recapitulates the Ontogeny of Lymphoid Stromal Cells. *The Journal of Immunology* **182,** 5789–5799 (2009).

176. Shields, J. D., Kourtis, I. C., Tomei, A. A., Roberts, J. M. & Swartz, M. A. Induction of lymphoidlike stroma and immune escape by tumors that express the chemokine CCL21. *Science* **328,** 749–752 (2010).

177. Link, A. *et al.* Association of T-Zone Reticular Networks and Conduits with Ectopic Lymphoid Tissues in Mice and Humans. *The American Journal of Pathology* **178,** 1662–1675 (2011).

178. Kerrigan, A. M. *et al.* Podoplanin-expressing inflammatory macrophages activate murine platelets via CLEC-2. *J. Thromb. Haemost.* **10,** 484–486 (2012).

Chapter 2

Podoplanin-rich stromal networks induce DC motility via activation of CLEC-2

Attributions

Reference (reproduced with permission from *Immunity*):

Acton, S.E.*, Astarita, J.L.*, Malhotra, D., Lukacs-Kornek, V., Franz, B., Hess, P.R., Zoltan, J., Kuligowski, M., Fletcher, A.L., Elpek, K.G., Bellemare-Pelletier, A., Sceats, L., Reynoso, E.D., Gonzalez, S.F., Graham, D.B., Chang, J., Peters, A., Woodruff, M., Swat, W., Morita, T., Kuchroo, V., Carroll, M.C., Kahn, M.L., Wucherpfennig, K.W., Turley, S.J. Podoplanin-rich stromal networks induce DC motility via activation of CLEC-2. *Immunity* **37**, 276-289 (2012).

*these authors contributed equally to this work.

S.E.A. convinced of the study, performed experiments, analyzed data, and wrote the manuscript. J.L.A performed experiments, analyzed data, and aided in writing the manuscript. B.F. generated key reagents. D.M., V.L-K., A.L.F., K.G.E., A.B-P., L.S., E.D.R, S.F.G, D.B.G., J.C., and M.W. performed individual experiments. P.R.H, Z.J.K., and M.L.K provided *Clec-2*$^{-/-}$ mice and key reagents. W.S., T.M., V.K., M.C.C., M.L.K., and K.W.W. provided critical comments on the manuscript. S.J.T. supervised the study and aided in writing the manuscript.

Introduction

Cell motility is crucial for leukocytes to traffic between tissues and to interact with one another and their microenvironment. As the quintessential antigen-presenting cell, dendritic cells (DCs) are dependent on migration via stromal networks to carry antigens long distances from parenchymal tissues to lymph nodes, where they initiate adaptive immunity and tolerance[1]. DCs generally reside in parenchymal tissues as immature antigen-capturing cells. Upon encountering pathogens or tissue damage, DCs undergo maturation, which promotes the processing and presentation of MHC-peptide complexes, upregulation of co-stimulatory molecules, and DC migration to lymph nodes[2]. Migratory DCs utilize the lymphatics as a highway to move to regional lymph nodes where they have the highest chance of interacting with the appropriate antigen-specific T cell.

To reach lymph nodes, tissue-resident DCs must first crawl to and enter afferent lymphatics, which begin as blind-ended vessels within most parenchymal tissues and convey lymph toward the thoracic duct[2]. Upon arrival at lymph nodes, DCs traverse the floor of the lymph-draining subcapsular sinus, penetrate the parenchyma, and then crawl along fibroblastic reticular cells (FRCs) in the T cell-rich paracortex. To date, the only well-established directional cues guiding tissue-derived DCs to the lymph node paracortex are the chemokines CCL19 and CCL21[3,4], two CCR7 ligands expressed by lymphatic endothelial cells (LECs) and fibroblastic reticular cells (FRCs)[5]. However, how these chemokines act as functional gradients across such vast distances has not been adequately explained, which raises the question of whether additional hitherto undiscovered migration mechanisms may also be involved. Recent studies demonstrated that tissue-derived DCs can migrate from tissues to lymph nodes using amoeboid, integrin-independent mechanisms[6,7]. However, the specific molecules that support amoeboid

movement and initiate cytoskeletal rearrangements to cause spreading and translocation of DCs along stromal scaffolds remain elusive.

We identified the transmembrane glycoprotein podoplanin (PDPN, gp38, T1α) as a candidate molecule that migratory DCs encounter en route to lymph nodes due to its high expression by both LECs and FRCs[8,9]. Interestingly, a steady state function of PDPN in mature lymphatic vessels and on FRCs has not been defined. It is known that PDPN is required for separation of blood and lymphatic vessels during development because PDPN on lymphatics is engaged by CLEC-2 on platelets and leads to platelet aggregation and vessel separation. Thus, on most backgrounds, *Pdpn*$^{-/-}$ mice die shortly after birth due to severe defects in lymphatic vessel formation leading to fatal edema[10,11]. PDPN has been reported to be upregulated by dermal fibroblasts exposed to inflammatory mediators. PDPN expression is also increased on tumor cells, believed to promote tumor cell invasion and metastatic spread, and correlated with poor prognosis[12].

CLEC-2 (encoded by *Clec1b*) is a member of the dectin-1 sub-family of C-type lectin receptors (CLRs) and the receptor for PDPN[13,14]. CLEC-2 expression by leukocytes, including human DCs, was reported over a decade ago[15] but its function in these cells has remained enigmatic. CLEC-2 was first discovered on platelets as the receptor that induces aggregation following exposure to the snake toxin rhodocytin. Similar to *Pdpn*$^{-/-}$ mice, *Clec1b*$^{-/-}$ mice are embryonic lethal due to profound defects in vascular development[16]. *In vitro* studies have shown that CLEC-2 plays a role in endocytosis by neutrophils[17] and may mediate engulfment of human immunodeficiency virus type 1[13]. CLEC-2 binds to PDPN via its extracellular C-type lectin-like domain, which promotes CLEC-2 multimerization at the plasma membrane[14]. CLEC-2 contains a hem-immunoreceptor tyrosine-based activation motif (hemITAM), with a single YXXL sequence in its cytoplasmic tail. CLEC-2 activation in platelets initiates a tyrosine

phosphorylation signaling cascade mediated by Src, Syk, Vav, SLP-76, and PLCγ family members[14,16]. Syk has recently been reported to mediate phosphorylation of CLEC-2 in myeloid cells as well[18]. Vav phosphorylation is required for PLCγ activation in platelets, and CLEC-2-induced platelet aggregation is attenuated in the absence of Vav1 and Vav3[19]. Our results described below reveal a role for CLEC-2 in the migratory behavior of DCs, whereby CLEC-2-mediated rearrangement of the actin cytoskeleton is induced by interactions with the PDPN-rich stromal scaffold.

Results

DCs interact closely with the PDPN-rich lymphatic vessels and FRC scaffold

Stromal cells provide three-dimensional (3D) scaffolds and molecular cues that coordinate leukocyte migration and compartmentalization within lymphoid organs[20]. En route to lymph nodes, DCs migrate through lymphatics and along the FRC network to reach the T cell zone. Previous studies have shown that DCs make contact with LECs upon emigrating from peripheral tissues[21,22]; however, it has not been previously demonstrated whether DCs make direct contact with LECs or FRCs *in vivo*. Using multi-photon intravital microscopy, we observed that DCs migrating into the lymph node interacted closely with afferent lymphatic vessels (Figure 2.1a), often for many minutes, before squeezing between collagen fibers and entering the lymph node (Figure 2.1b and Supplementary Movie 1). Electron microscopy further revealed close contact between DCs and FRCs within the subcapsular sinus (Figure 2.1c).

LECs and FRCs, which line the structures that DCs utilize during migration to the T cell zone, express PDPN at their surfaces[23]. However, the precise distribution, localization, and abundance of this glycoprotein under steady state and inflammatory conditions have not been previously described. Using whole-mount staining of ear skin, PDPN was found to be expressed

Figure 2.1. **Migrating DCs make direct contact with lymphatic endothelial cells and FRCs upon lymph node entry**. a, Multiphoton imaging showing migratory DCs interacting with afferent lymphatic vessels. *Far left,* Overview of whole popliteal lymph node (CFSE-labeled DCs [green], second harmonic (collagen fibers) [red]. White box indicates region shown at higher magnification. *Far right,* schematic showing DC [white] in relation to lymphatic vessels [dotted lines]. b, Multi-photon imaging showing migratory DCs entering lymph node. *Left,* Overview of whole popliteal lymph node (CFSE-labeled DCs [green], second harmonic (collagen fibers) [red]. *Right,* Motion analysis showing path of migratory DC. Sequential time points are overlaid in red, green and blue. Static objects are shown in white, motile objects are shown by the separation of red, green and blue. c, *Left,* Schematic showing positions of subcapsular sinus fibroblasts, DCs, lymphocytes (L), and tip of FRC. *Right*, transmission electron microscopy of subcapsular sinus; box indicates region shown at higher magnification.

Figure 2.1 (continued)

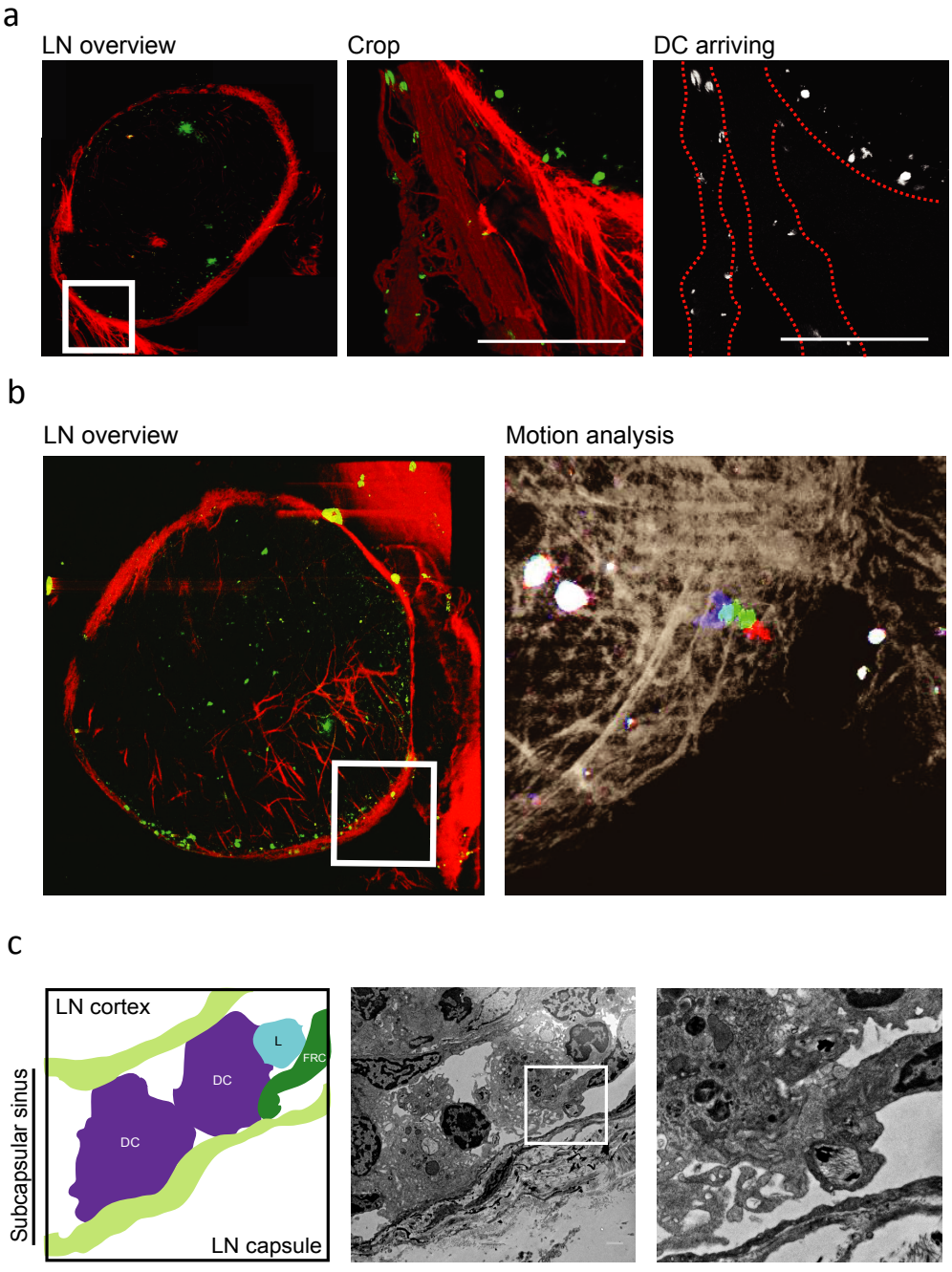

Figure 2.2. *Pdpn* mRNA and protein expression by LECs and FRCs. a, Fluorescence microscopy of tissue whole mounts and schematics of ear skin at resting state. Scale bar, 100 μm. b, Representative dot plots showing *Left*, proportion of stromal cells ($CD45^-$), and *Right*, subsets of lymphoid stromal cells (FRCs, $CD31^-PDPN^+$; LECs, $CD31^+PDPN^+$; blood endothelial cells (BECs) $CD31^+PDPN^-$) in draining Lymph nodes at rest. c, Graph representing the expression value (EV) of *Pdpn* mRNA from microarray analysis of sorted BECs, LECs, and FRCs from resting or inflamed LNs. d, Graph showing mean fluorescence intensity (MFI) of surface PDPN on BECs, LECs, and FRCs isolated from draining Lymph nodes 24 hours after intradermal injection of PBS (resting) or LPS (inflamed) into ear skin. Data represent mean values and standard deviation from 4 independent experiments. e, Fluorescence microscopy of ear skin whole mounts at 0 (resting) and 24 hours (inflamed) after intradermal LPS injection. Fluorescence images show overlays of PDPN (red) and Lyve-1 (green) antibody staining in the tips and along the lengths of afferent lymphatic vessels. Representative black and white images from 3 independent experiments show individual PDPN and Lyve-1 stains. Scale bar, 20 μm.

Figure 2.2 (continued)

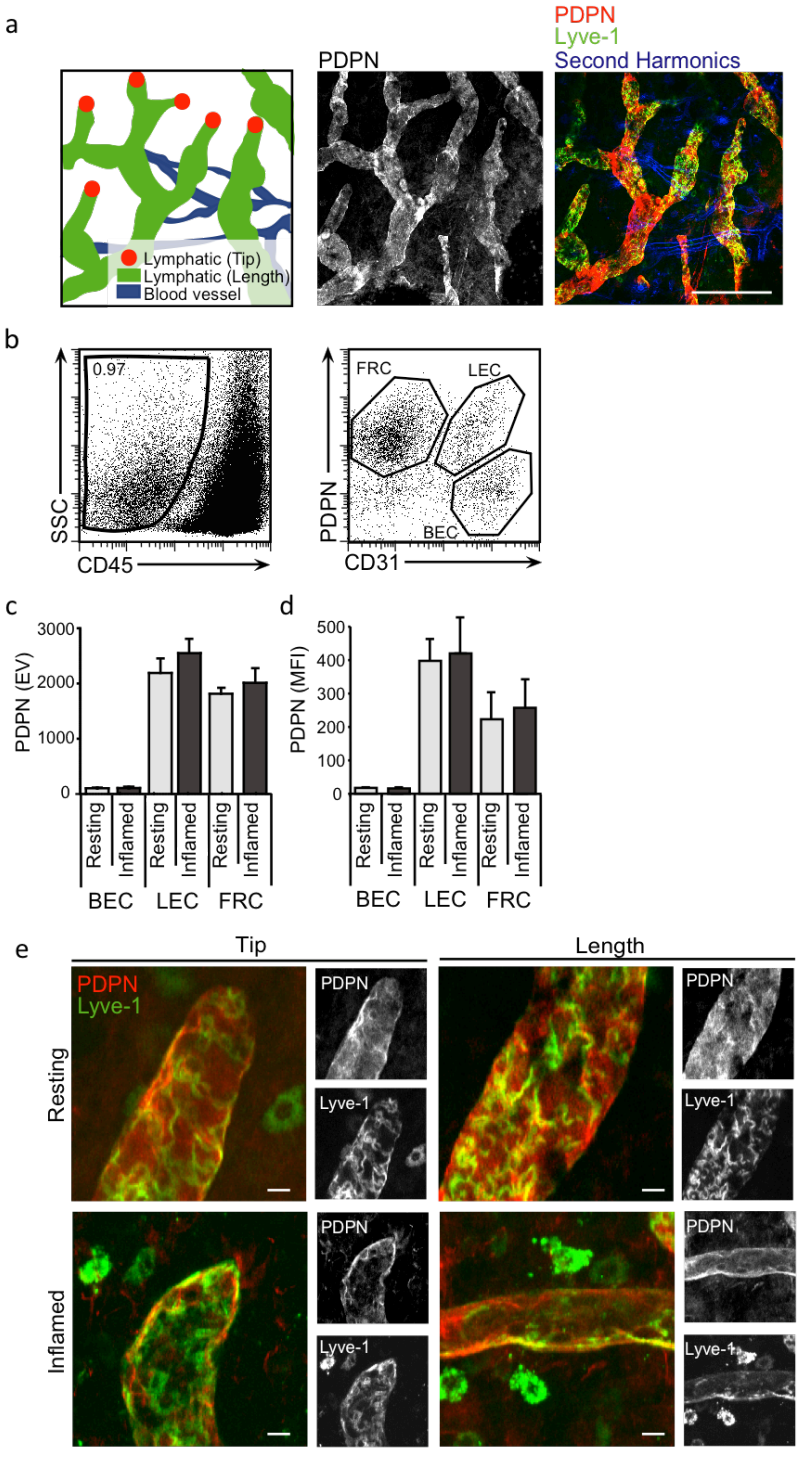

both at the tips and along the length of lymphatic vessels with a mostly uniform distribution (Figure 2.2a). Using microarray and cytometric analysis of lymph node stromal cell subsets, we found that that PDPN was expressed at the mRNA and protein levels by LECs and FRCs but not by blood endothelial cells (Figures 2.2b-d). Furthermore, we found that the amounts of *Pdpn* mRNA and protein, and the localization of PDPN on lymphatics, were unchanged during inflammation (Figures 2.2c-e). These results suggest that PDPN is constitutively expressed by stromal structures in skin, lymphatics, and lymph nodes under resting and inflammatory conditions.

CLEC-2 expression by DCs

Next we sought to determine whether the DCs express the PDPN receptor, CLEC-2. CLEC-2 is reportedly expressed by human and mouse platelets and various myeloid cell types, including blood neutrophils, splenic DCs, bone marrow-derived DCs (BMDCs), and peritoneal macrophages[10,15,17,18]. Consistent with those reports, we found that *Clec1b* mRNA was expressed by BMDCs (Figure 2.3a). We also found that *Clec1b* mRNA was expressed by DCs freshly isolated from skin and lymph nodes (Figure 2.3a). Lymph node and skin DCs expressed ~750-fold and ~1200-fold higher amounts of *Clec1b* mRNA, respectively, than FRCs, which served as a negative control. BMDCs expressed ~100-fold higher amounts of *Clec1b* mRNA than the negative control. Using flow cytometry with recombinant PDPN-Fc (rPDPN-Fc), which specifically binds to CLEC-2, we confirmed surface expression of CLEC-2 on BMDCs (Figure 2.3b) and lymph node DCs (Figure 2.3c). Thus, DCs from skin, lymph node, and bone marrow cultures express CLEC-2 at the mRNA and protein levels.

Next we examined whether CLEC-2 surface expression by DCs changed upon exposure to an inflammatory mediator. We found that exposure to LPS caused CLEC-2 surface expression

to increase ~2-fold (Figure 2.3d). However, in studies where we monitored the subcellular localization of CLEC-2 using A375 cells transfected with a CLEC-2-GFP fusion protein, we found that this molecule rapidly clustered at the plasma membrane and then partially internalized in a dynamin-dependent manner into vesicular structures (Figure 2.3e and data not shown). Thus, CLEC-2 may be upregulated on the DC surface following exposure to an inflammatory stimulus but in a stromal cell niche where PDPN is constitutively present, some portion of CLEC-2 may be quickly internalized following ligand engagement.

CLEC-2 expression is required for efficient DC migration to lymph nodes

Given that PDPN is expressed along the entire migratory route from skin to lymph nodes and that DCs in these sites express the PDPN receptor, CLEC-2, we tested whether the CLEC-2 pathway contributed to their migration using several approaches. First FITC skin painting was employed to examine migration of skin-resident DCs to lymph nodes in mice lacking CLEC-2. Because *Clec1b*$^{-/-}$ mice exhibit neonatal lethality, fetal liver chimeras (FLCs) were generated from WT and *Clec1b*$^{-/-}$ embryos to evaluate CLEC-2 function. Six weeks after reconstitution, CLEC-2 expression was analyzed in CD11c^{+} and CD11c^{-} lymph node cells from WT or *Clec1b*$^{-/-}$ FLCs. As expected, *Clec1b*$^{-/-}$ mRNA signal was detected in CD11c^{+} cells from WT but not *Clec1b*$^{-/-}$ FLCs (Figure 2.4a). Notably, the *Clec1b* mRNA in WT FLCs tracked with CD11c^{+} cells (Figure 2.4a), suggesting that CLEC-2 is not highly expressed by CD11c^{-} cells in lymph nodes. Ears of WT and *Clec1b*$^{-/-}$ FLCs were painted with FITC, and draining lymph nodes were analyzed by flow cytometry 24-72 hours later. WT migratory DCs (FITC^{+}CD11c^{+}MHCII^{hi}) entered the draining lymph nodes at 24 hours; however, the percentage and total numbers of *Clec1b*$^{-/-}$ DCs were significantly reduced compared with WT DCs (30% and 50%, respectively; Figures 2.4b-d). By 72 hours, the numbers of FITC^{+}CD11c^{+}MHCII^{hi} DCs present in draining lymph nodes had decreased

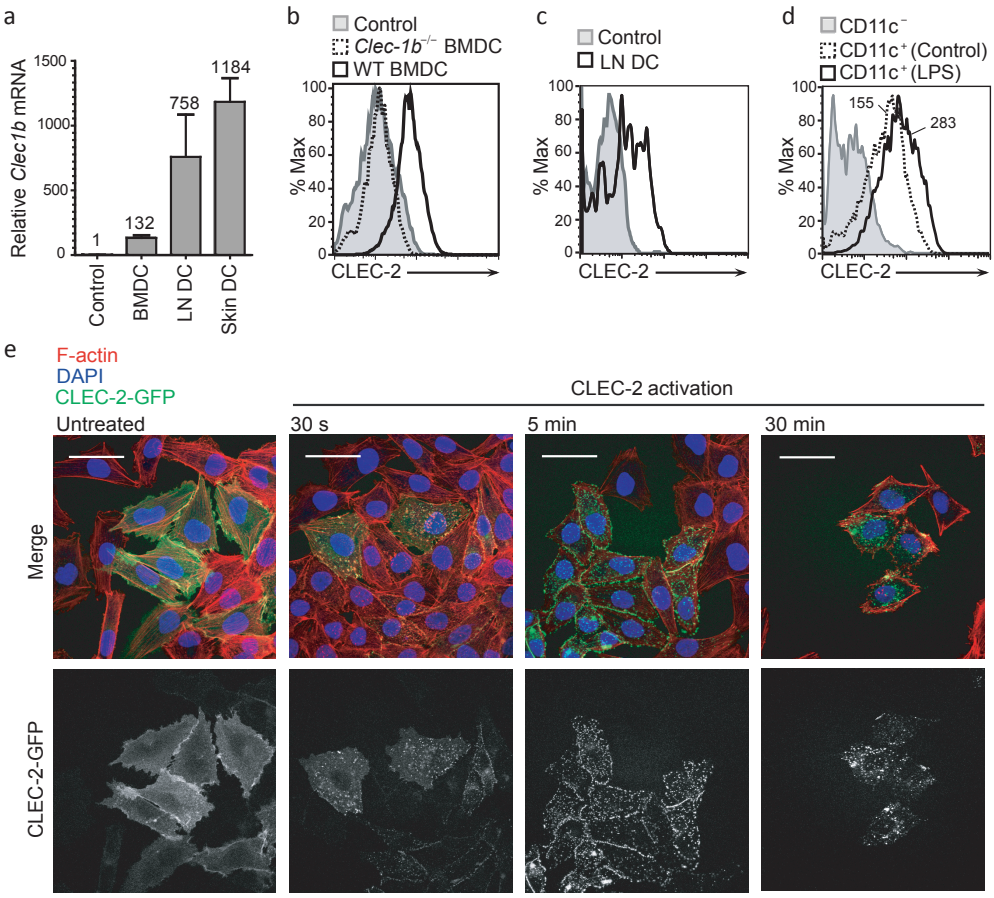

Figure 2.3 *Clec1b* mRNA and protein expression by DCs. a, Quantitative PCR analysis of *Clec1b* mRNA levels in FRCs (negative control), BMDCs, LN DCs, and skin DCs. LN and skin DCs were sorted from primary tissues by flow cytometry. Values above bars depict the mRNA level relative to the negative control. b, flow cytometry analysis of surface CLEC-2 protein using rPDPN-Fc on WT (solid line) and *Clec1b*$^{-/-}$ (dashed line) BMDCs. Gray line (filled histogram), secondary control. c, FACS analysis of surface CLEC-2 protein using rPDPN-Fc on freshly isolated WT LN DCs (solid line). Gray line (filled histogram), secondary control. d, Flow cytometry analysis of surface CLEC-2 protein using rPDPN-Fc on BMDCs treated for 12 hours with LPS (solid line) or left untreated (dashed line). Gray line (filled histogram), secondary control. e, Representative fluorescence microscopic images from 3 independent experiments of

Figure 2.3 (continued). A375 cells transfected with CLEC-2-GFP that were either stimulated with rhodocytin or left untreated. *Top*, overlay of F-actin (red), DAPI (blue), and CLEC-2-GFP (green). *Bottom*, CLEC-2-GFP fluorescence alone. Scale bars, 50 μm.

compared with the 24 hour time point, and no differences were observed between the conditions (Figures 2.4b, d). That no significant difference was measured at this time point could reflect a more important function for CLEC-2 in dermal DCs, which migrate to lymph nodes more rapidly than Langerhans cells. However, the dependence of Langerhans cells, which arrive in peak numbers at 72 hours, on CLEC-2 could not be directly evaluated in our FLCs due to their radioresistant nature[2]. Consistent with the decrease in *Clec1b*$^{-/-}$ DC migration at 24 hours, lymph node cellularity was reduced 30% at 72 hours in *Clec1b*$^{-/-}$ compared with WT FLCs (Figure 2.4e). This difference likely reflects an impaired adaptive immune response due to a combination of reduced numbers of migratory DCs arriving at earlier time points and the inability of the *Clec1b*$^{-/-}$ DCs to efficiently enter the T zone and crawl along the FRC scaffold (see below).

As a second test, competitive *in situ* migration assays with WT and *Clec1b*$^{-/-}$ BMDCs were performed. WT and *Clec1b*$^{-/-}$ DCs were labeled with CFSE and Far Red dyes, respectively, mixed in equal numbers ($2x10^5$ of each), and co-injected into the same footpad. Donor DCs arriving in the draining (popliteal) and distal lymph nodes were enumerated 24 hours later by flow cytometry. The numbers of *Clec1b*$^{-/-}$ DCs were significantly reduced compared with their WT counterparts, with WT DCs migrating 3-fold more efficiently from skin to lymph node (Figures 2.4f, g). Similar results were obtained in experiments in which Far Red-labeled WT and CFSE-labeled *Clec1b*$^{-/-}$ DCs were used, thereby ruling out any specific effect of the fluorescent dyes on migration (data not shown). Using a third approach to confirm the role of CLEC-2 in migration,

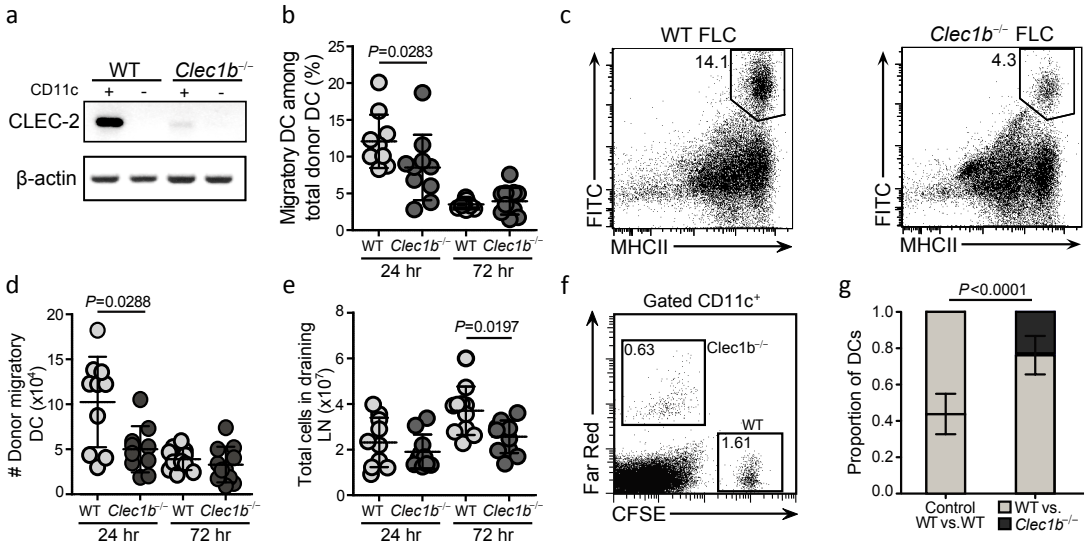

Figure 2.4. DCs utilize CLEC-2 for efficient migration from skin to draining Lymph nodes. a, RT-PCR analysis of *Clec1b* mRNA in $CD11c^+$ and $CD11c^-$ cells that were MACS purified from WT or *Clec1b*$^{-/-}$ FLCs. b, Percentages of migratory ($MHCII^{hi}FITC^+$) DCs among total donor ($CD45.2^+$) DCs in draining LNs of WT and *Clec1b*$^{-/-}$ FLC mice at 24 and 72 hours post-FITC painting. c, Representative dot plots (gated on $CD45.2^+CD11c^+$ cells) showing $MHCII^{hi}FITC^+$ DCs in WT and *Clec1b*$^{-/-}$ FLCs 24 hours after FITC painting. d, Total numbers of migratory donor ($CD45.2^+CD11c^+MHCII^{hi}FITC^+$) DCs in draining LNs of WT and *Clec1b*$^{-/-}$ FLCs at 24 and 72 hours post-FITC painting. e, Total cellularity in draining LNs collected from WT and *Clec1b*$^{-/-}$ FLCs 24 and 72 hours after FITC painting. For b, d, and e, data represent 10 mice per experimental condition from 3 independent experiments. f, FACS analysis of popliteal (draining) and axillary (distal) LN 24 hours following injection of wild-type ($CFSE^+$) and *Clec1b*$^{-/-}$ ($Far\ red^+$) DCs mixed in equal numbers ($2x10^5$ of each) prior to injection into the footpad. g, Quantification of labeled DCs arriving in the draining LN.

DCs were treated with rPDPN-Fc protein prior to injection to occupy surface CLEC-2 and thereby out-compete its capacity to bind endogenous PDPN on stroma. Enumeration of migratory DCs in the draining lymph node revealed that engagement of CLEC-2 with rPDPN-Fc prior to injection significantly reduced their capacity to reach lymph nodes (Figure 2.5a). Finally, we tested the role of PDPN in DC migration from skin to lymph node following local injection of siRNA. When PDPN expression was reduced on stromal cells, DC migration to the draining lymph node was reduced by 50% (Figures 2.5b-d).

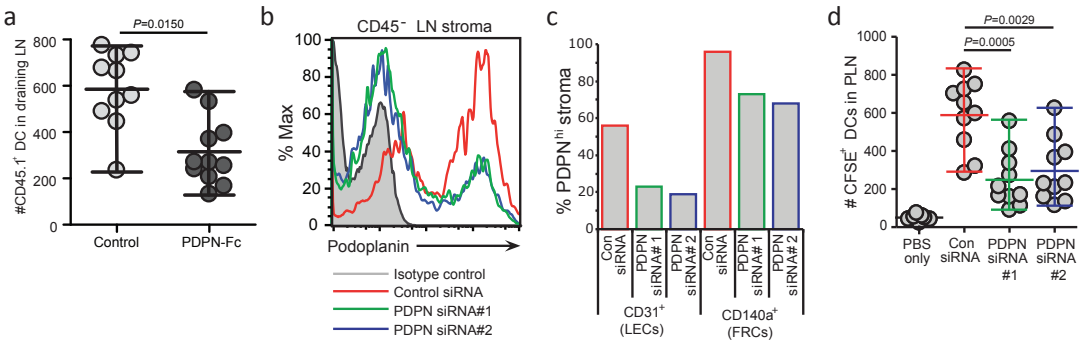

Figure 2.5 Inhibiting the CLEC-2-PDPN interaction impairs DC migration. a, Numbers of control and rPDPN-Fc-coated ($CD45.1^+$) DCs arriving in popliteal lymph node 24 hours following footpad injection. Data represent 25 mice per experimental condition collated from 3 independent experiments. b, PDPN expression in stromal cells ($CD45^-$) from popliteal LNs 72 hours following footpad injection of PDPN siRNA. c, Quantification of PDPN knockdown in endothelial cells and FRCs in popliteal LNs. d, Quantification of reduction in numbers of CFSE-labeled DCs arriving in popliteal LN from footpad following PDPN siRNA injection.

Our results thus far suggested that efficient migration by DCs requires CLEC-2 binding to PDPN on the surface of stromal cells lining their migratory path. However, another possible explanation was that *Clec1b*$^{-/-}$ DCs displayed intrinsic defects in responsiveness to motility cues such as CCR7 ligands or to maturation stimuli. To address this possibility, we first compared the ability of WT and *Clec1b*$^{-/-}$ DCs to migrate towards a CCL21 gradient in a transwell plate. Importantly, both sets of DCs migrated efficiently into the lower chamber in response to the chemokine, and no significant differences were observed (Figure 2.6a). These data demonstrate that responsiveness to CCR7 ligands is not impaired in *Clec1b*$^{-/-}$ DCs, leading us to conclude that the migration defect observed in *Clec1b*$^{-/-}$ DCs was due to a CCR7-independent signaling pathway directly downstream of CLEC-2. Next we evaluated the ability of WT and *Clec1b*$^{-/-}$ DCs to mature in response to a pro-inflammatory stimulus. *Clec1b*$^{-/-}$ BMDCs exhibited the same phenotype as their WT counterparts (Figure 2.6b) and responded normally to LPS by upregulating surface MHC class II and B7-2 (CD86) (Figure 2.6c). Thus, the impaired migratory potential of *Clec1b*$^{-/-}$ DCs was not due to intrinsic defects in chemotaxis or maturation.

To determine the functional significance of migratory defects observed in *Clec1b*$^{-/-}$ DCs, the ability of migratory DCs to stimulate naïve T cells was assessed in vivo. First, mice received OVA peptide-loaded DCs from WT or *Clec1b*$^{-/-}$ donor mice via footpad injection followed by intravenously administered naïve, CFSE-labeled OT-I T cells one day later. OT-I T cell proliferation was significantly impaired in mice that received *Clec1b*$^{-/-}$ DCs compared with their WT counterparts (Figures 2.7a, b). Similar results were also observed when WT DCs were pre-incubated with rPDPN-Fc prior to injection (Figures 2.7c, d).

Next we evaluated whether the impaired T cell responses with *Clec1b*$^{-/-}$ DCs was due to a difference in their capacity to capture or present antigen. First, an in vitro T cell activation assay was used to compare the ability of WT and *Clec1b*$^{-/-}$ DCs to stimulate antigen-specific T cells. DCs

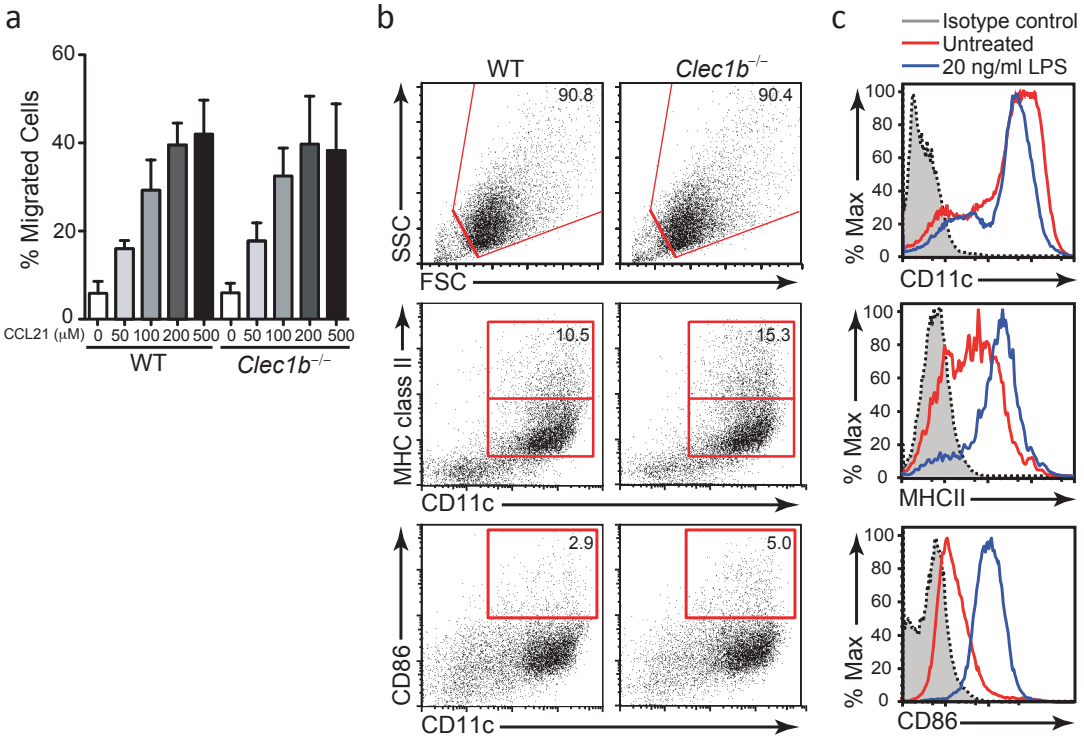

Figure 2.6 *Clec1b*$^{-/-}$ DCs respond normally to chemokine gradients and maturation stimuli. a, Quantification of DC migration in response to CCL21 concentrations (50-500 μM) using a transwell assay. Data represent mean and standard deviation from 3 independent experiments. b, FACS plots showing FSC vs. SSC profiles and surface CD11c, MHC class II, and CD86 (B7-2) on untreated WT and *Clec1b*$^{-/-}$ DCs from day 5 GM-CSF bone marrow cultures. c, Histograms showing surface CD11c, MHC class II and CD86 on untreated and LPS-treated DCs from *Clec1b*$^{-/-}$ bone marrow cultures.

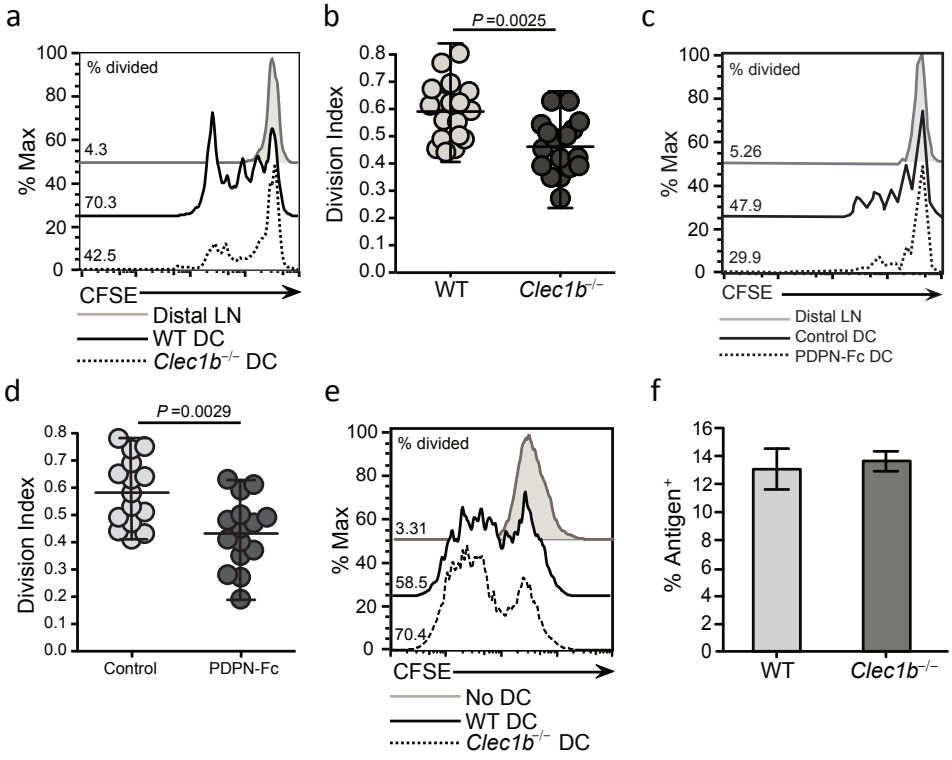

Figure 2.7 T cell division is impaired due to decreased migration of *Clec1b*$^{-/-}$ DCs. a, Histograms showing OT-1 T cell proliferation (CFSE dilution) in popliteal LN following footpad injection of OVA-peptide loaded WT and *Clec1b*$^{-/-}$ DCs. Numbers show the percentage of divided cells among donor OT-1 T cells. b, Summary of data in a. c, Histograms showing OT-1 T cell proliferation (CFSE dilution) in popliteal lymph node following footpad injection of OVA-loaded DCs with or without pre-incubation with rPDPN-Fc. Numbers show the percentage of divided cells among donor OT-1 T cells. d, Summary of data in b. Data are from 15 individual mice per experimental condition and 2 independent experiments. e, Histograms showing proliferation of OT-1 T cells upon co-culture of naïve, CFSE-labeled OT-1 T cells with OVA peptide-loaded WT and *Clec1b*$^{-/-}$ DCs for 48 hours. Numbers indicate the percentage of divided cells among donor OT-1 T cells. Data are representative of 3 independent experiments. f, Percentage of WT or *Clec1b*$^{-/-}$ DCs that captured particulate antigen (fluorescently-labeled latex beads).

were pulsed with OVA peptide (SIINFEKL) and then co-cultured with naïve CFSE-labeled OT-I T cells. As shown in Figure 2.7e, OT-I T cells divided to the same extent whether WT or *Clec1b*$^{-/-}$ DCs served as antigen presenting cells. We then examined whether endocytic activity might explain the different abilities of WT and *Clec1b*$^{-/-}$ DCs to stimulate T cell responses in vivo and found that WT and *Clec1b*$^{-/-}$ DCs exhibited equal antigen uptake activity (Figure 2.7f). Thus, *Clec1b*$^{-/-}$ DCs exhibit alterations in migration but appear to capture and present soluble antigens normally. Collectively, these data suggest that CLEC-2 contributes to adaptive immunity by fostering migration of antigen-bearing DCs from tissues to lymph nodes.

Migratory DCs use CLEC-2 at multiple junctures en route to lymph nodes

Having shown that migratory DCs likely encounter PDPN at various points along their migration to lymph nodes, we next determined precisely where the CLEC-2-PDPN interaction played a role. First, intravital microscopy of ear skin was employed to evaluate whether CLEC-2 was important for DC entry into afferent lymphatics. WT DCs rapidly associated with and were able to enter lymphatic vessels (Figures 2.8a, c). In contrast, the majority of *Clec1b*$^{-/-}$ DCs remained in the dermis and failed to interact with lymphatic structures (Figures 2.8b, c). Overall, there was a 30% decrease in the amount of *Clec1b*$^{-/-}$ DCs that entered lymphatics. Furthermore, WT DCs were able to migrate from the subcapsular sinus deep into the lymph node parenchyma, whereas *Clec1b*$^{-/-}$ DCs were impaired in accessing the paracortex and remained relatively close to the capsule, resulting in a 40% reduction in the distance migrated (Figure 2.8d, e). Finally we evaluated the motile behavior of WT and *Clec1b*$^{-/-}$ DCs within lymph nodes. Both WT and *Clec1b*$^{-/-}$ DCs penetrated agarose-embedded lymph nodes and showed motile behavior therein (Figure 2.8f, Movie S2); however, fewer *Clec1b*$^{-/-}$ DCs infiltrated the tissue compared with their WT counterparts, despite equal starting numbers of WT and *Clec1b*$^{-/-}$ DCs.

Figure 2.8. *Clec1b*$^{-/-}$ DCs exhibit impaired migration *in vivo*. a, i, Z-projection of ear dermis incubated with WT BMDCs. Lymphatic vessels are shown in green and infiltrating DCs are shown in red. Scale bar indicates 100 μm. ii, zoomed image showing DCs interacting with lymphatic vessel. b, i, Z-projection of ear dermis incubated with *Clec1b*$^{-/-}$ BMDCS. Scale bar indicates 100 μm ii, zoomed image showing DCs interacting with lymphatic vessel. c, Quantification of localization of WT and *Clec1b*$^{-/-}$ DCs within ear sheets. Data are collated from 3 independent experiments. d, i, Z-projection of LN from a Ub-GFP BM chimeric mouse (WT BM>Ub-GFP host) injected with WT and *Clec1b*$^{-/-}$ DCs 24 hours prior to dissection and fixation. GFP^{+} stroma is shown in white, WT DCs are shown in red, *Clec1b*$^{-/-}$ DCs are shown in green. Scale bar indicates 100 μm. ii, location of WT DCs relative to LN capsule (dotted line). iii, location of *Clec1b*$^{-/-}$ DCs relative to LN capsule (dotted line). e, Quantification of distance from LN capsule. f, i, Z-projection of vibratome cut GFP-ubiquitin LN slice showing position of WT (red) and *Clec1b*$^{-/-}$ (green) infiltrated DCs. GFP^{+} LNSCs are shown in white. Scale bar indicates 100 μm. ii, Overlay showing tracks of WT (red) and *Clec1b*$^{-/-}$ (green) DCs on GFP^{+} LN (white) over 2 hour period of time lapse imaging. iii, tracks of WT (red) and *Clec1b*$^{-/-}$ (green) DCs within LN slice. g, Representative plots showing directionality of migrating WT and *Clec1b*$^{-/-}$ DCs within LN slices of Ub-GFP BM chimeric mouse with GFP^{+} stroma. Tracks were adjusted to begin at origin (0.0) and overlaid. Axes span 150 μm. h, Displacement and i, Velocity of WT and *Clec1b*$^{-/-}$ DCs within LN slices of Ub-GFP BM chimeric mouse. Data are collated from 8 LN slices from 4 different donors from 3 independent experiments.

Figure 2.8 (continued)

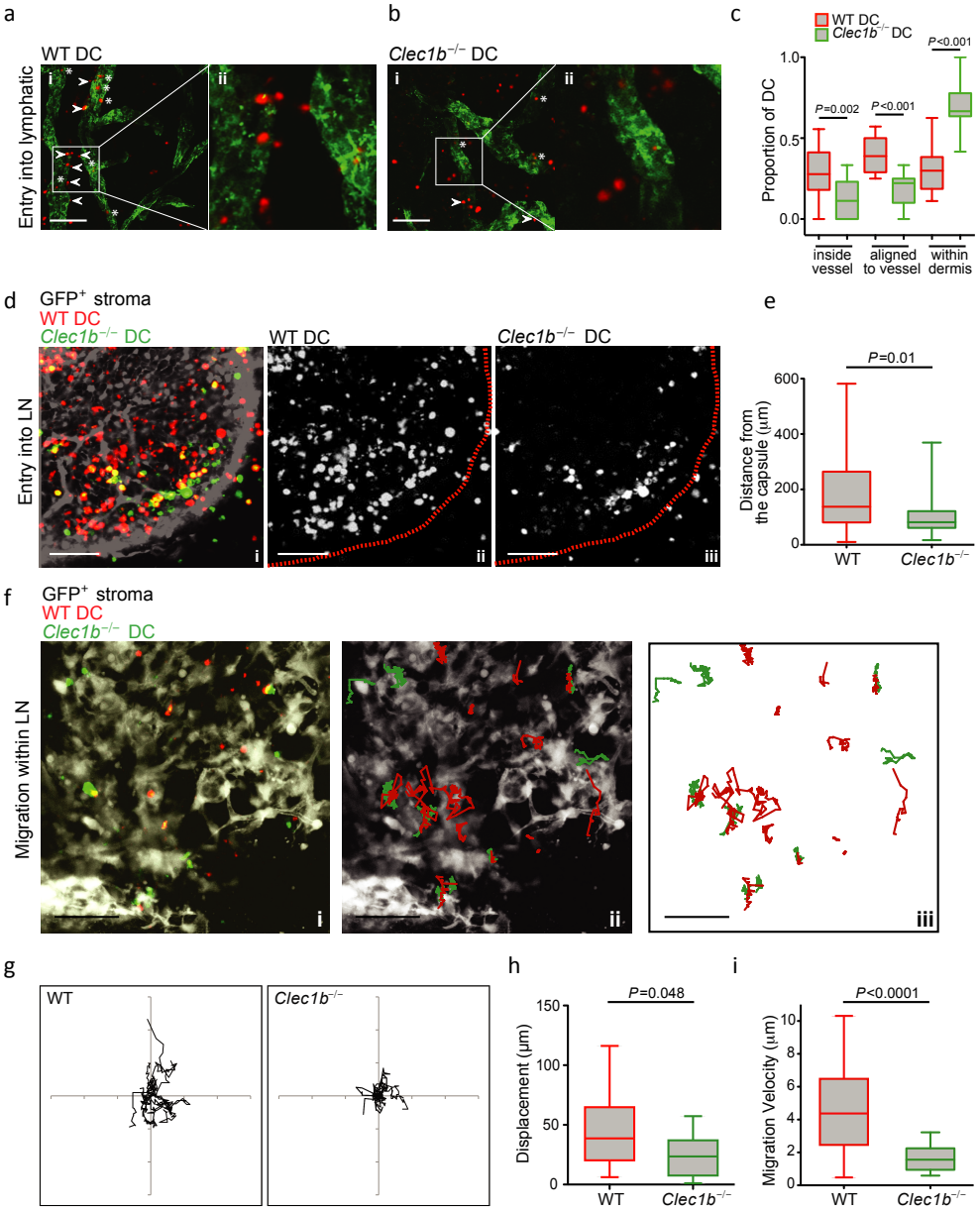

The directionality, displacement, and velocity of DCs that penetrated the tissue were determined over a 120 minute period. WT DCs exhibited greater displacement (Figures 2.8g, h) and higher velocity (Figure 2.8i) compared with *Clec1b*$^{-/-}$ cells, whereas directionality was equivalent between the two DC populations (Figure 2.8g). Thus, CLEC-2 expression by DCs supports their motility at multiple points along the journey to lymph nodes: from the entry of dermal lymphatics to migration into the lymph node paracortex.

CLEC-2 activation leads to protrusion formation and stabilization in DCs

Next we sought to investigate the mechanism by which CLEC-2 promotes DC migration. Initially we asked whether CLEC-2 activation might trigger DC maturation, which is known to promote migratory potential, but no activation was observed upon rhodocytin treatment (Figure 2.9). Time-lapse imaging was then employed to examine the morphodynamic behavior

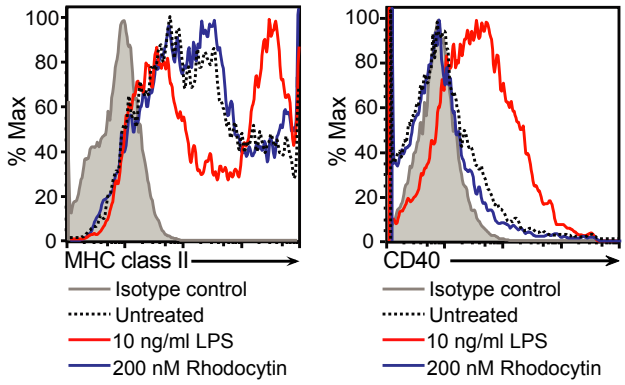

Figure 2.9 CLEC-2 activation does not affect maturation in DCs. FACS analysis of surface MHC class II and CD40 levels on DCs 24 hours following treatment with LPS or rhodocytin.

of DCs following CLEC-2 activation. DCs were cultured in three-dimensional (3D) collagen matrices[24] following treatment with either PDPN or rhodocytin. Notably, CLEC-2 activation triggered vigorous protrusive activity in WT DCs with multiple, highly-branched protrusions extending simultaneously from the cell body (Figure 2.10a, Movie S3). In contrast, *Clec1b*$^{-/-}$ DCs maintained a rounded morphology following stimulation with either ligand (Figures 2.10b, c), indicating that protrusion activity triggered by PDPN or rhodocytin was CLEC-2-dependent. Compared with untreated DCs, which maintained a more rounded morphology and displayed small and short-lived pseudopods (Figures 2.10a-c, Movie S3), CLEC-2 ligand-induced protrusions extended greater distances (Figure 2.10d) from the cell body, were more abundant (Figure 5e), and persisted for longer periods of time (Figure 2.10f). Thus, CLEC-2 activation triggers dramatic changes in the morphodynamic behavior of DCs, driving the generation and stabilization of cell protrusions.

The PDPN-CLEC-2 interaction is necessary and sufficient to induce DC protrusions

To further dissect the roles of CLEC-2 and PDPN in DC migration along stromal cell scaffolds, we engineered a 3D model of the lymph node stromal network by seeding primary lymph node FRCs into a deformable matrix. In 3D, FRCs maintained high expression of PDPN and remodeled the matrix to form an extensively branched large (50-300 mm in length) reticular structure, reminiscent of the collagen network of the lymph node paracortex (Figure 2.11a, b). Highly motile leukocytes, such as DCs and B cells that were co-seeded into the networks, interacted with the FRC scaffold (Figures 2.11a, b and data not shown). Time-lapse imaging revealed that upon contact with FRCs, DCs extended protrusions and then spread along the stromal cell surface (Figure 2.11c). Where DCs reached a branch in the FRC scaffold, protrusions were often simultaneously induced along both potential tracks before one was retracted (Movie

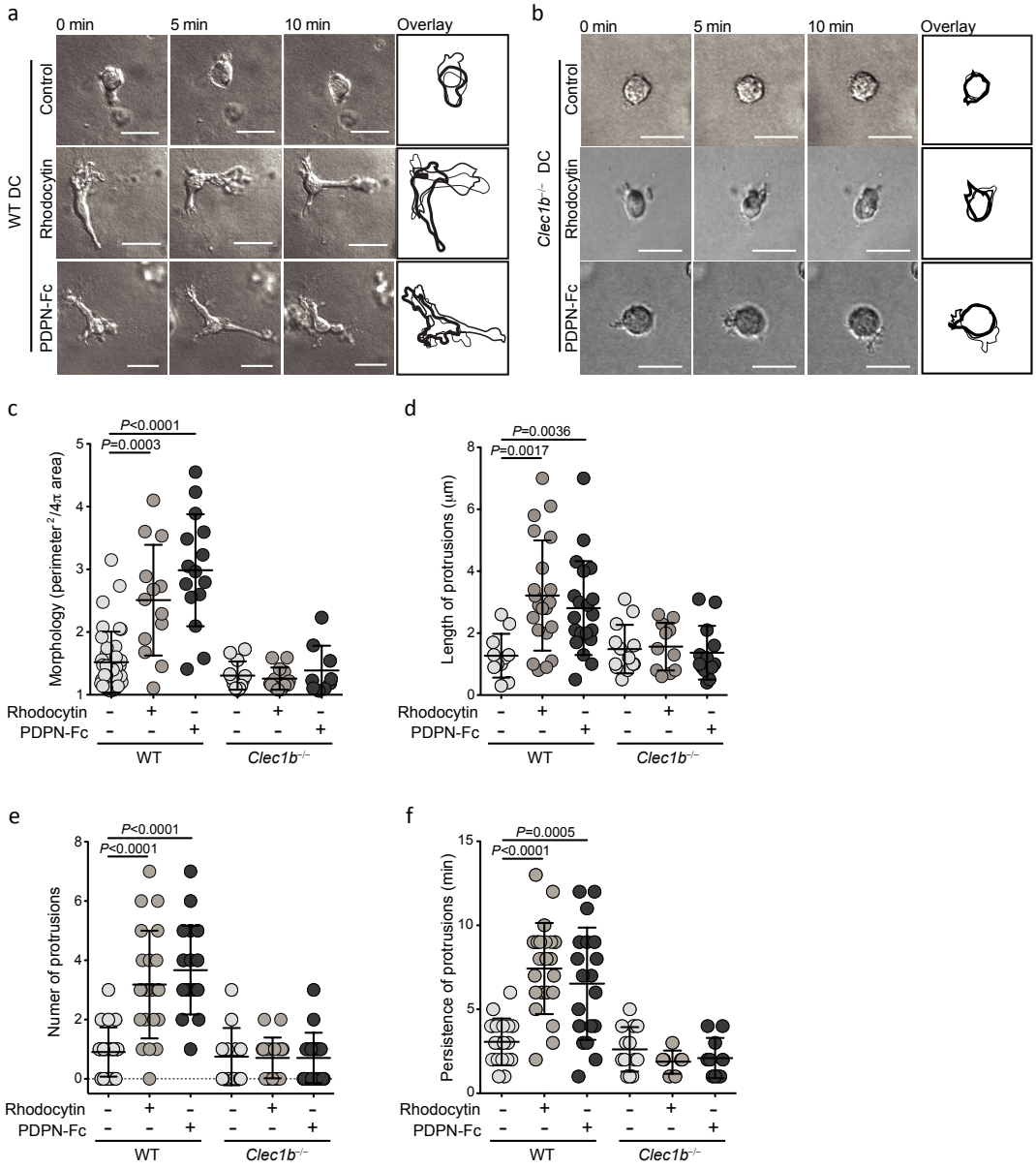

Figure 2.10. CLEC-2 activation induces protrusion formation in DCs. a, b, Time-lapse imaging of control-, PDPN-Fc-, and rhodocytin-treated WT (a) and *Clec1b*$^{-/-}$ (b) BMDCs at 0, 5, and 10 min after stimulation. Scale bars, 20 μm. *Far right*, overlays of still traces from each time point. c, Morphology index, d, Protrusion length (mm), e, Number of protrusions per cell, f, Protrusion persistence (min) for control, rPDPN-Fc, and rhodocytin-treated DCs from WT and *Clec1b*$^{-/-}$ FLCs as in a and b.

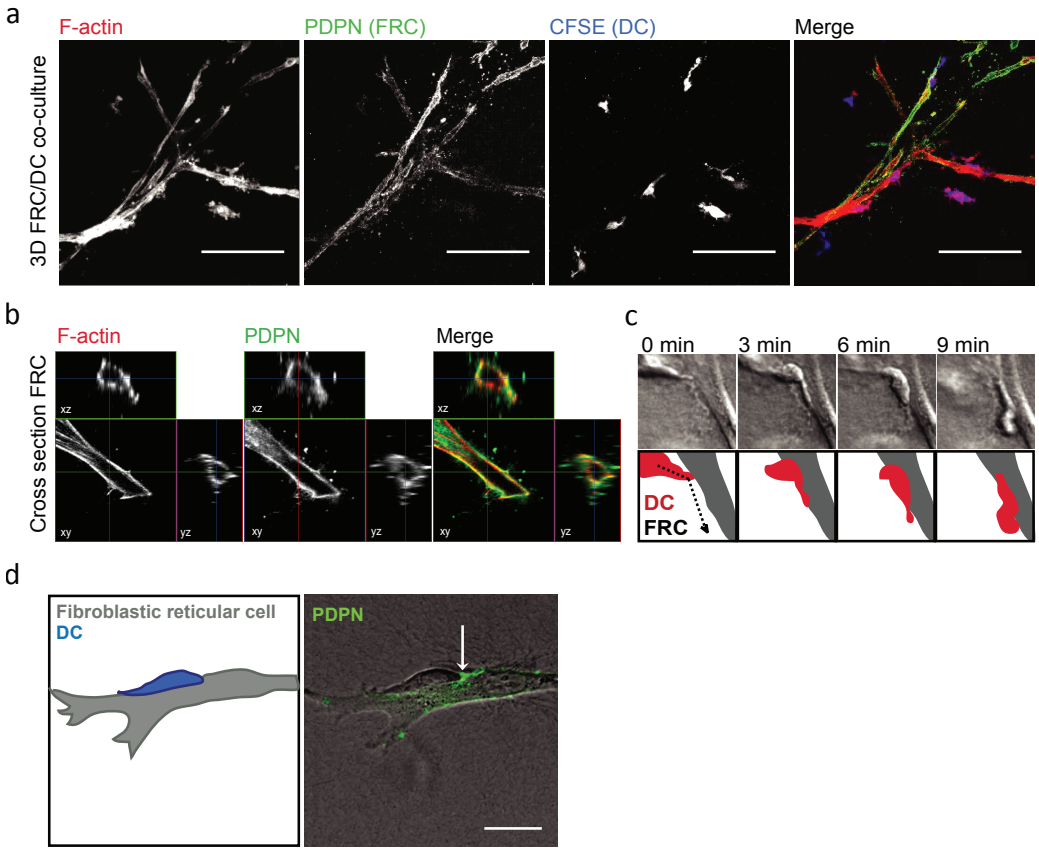

Figure 2.11. DCs make closely interact with PDPN^{+} FRCs in 3D gels. a, Z-projection of 3D FRC network with DCs. Scale bar, 100 mm. b, Representative cross-section of FRC in 3D culture showing PDPN localization at the plasma membrane. Scale bar, 5 μm. c, Time-lapse imaging (top) and schematic (bottom) of DC-FRC interaction at 1, 3, 6, and 9 min after contact. d, *Left,* schematic of DC (blue) and FRC (grey) in contact in 3D deformable matrix. *Right,* overlay of transmitted light image and immunofluorescence imaging of a FRC and DC in contact. Arrow indicates PDPN clustering at cell-cell interface. Scale bar, 20 μm.

S4). Notably, PDPN rapidly accumulated at sites of contact between DCs and FRCs (Figure 2.11d).

Once the DCs adhered to and spread along the FRCs, they began migrating while maintaining close contact with the FRCs. The DCs generally migrated relatively long distances on the FRC network: between 50 and 300 μm in any one direction over 60 minutes (Figure 2.12a, Movies S4 and S5). In contrast, DCs not in contact with the FRC network, or cultured alone, were relatively immotile (Figure 2.12aiii). Interestingly, we found that FRCs isolated from the spleen formed similar networks when seeded into a 3D matrix and supported DC migration (data not shown). We also evaluated whether any tensile cell scaffold could induce DC migration by creating matrices with NIH3T3 fibroblasts. When seeded into the NIH3T3 network, DCs made contact with the fibroblasts but did not migrate efficiently (Figure 2.12aiii), despite the fact that these cells formed a branched network reminiscent of the FRC scaffolds. Interestingly, NIH3T3 cells express 80% less PDPN than cultured FRCs (Figure 2.12b).

We next directly evaluated whether CLEC-2 activation by PDPN influenced DC migration along FRC scaffolds. To this end, we co-seeded 3D matrices with different combinations of DCs and FRCs lacking either CLEC-2 or PDPN and examined DC migration on the networks. When seeded in WT FRC matrices, *Clec1b*$^{-/-}$ DCs were profoundly impaired in migration on the FRC network compared with WT DCs (Figure 2.12c). In addition to impaired migration, *Clec1b*$^{-/-}$ DCs also failed to spread along the stromal cell surface, exhibiting a distinctly rounded morphology (Figure 2.12ci and Movie S6). These results suggest that DCs still make contact with the FRC network in the absence of CLEC-2 but lack the ability to spread and crawl on this surface.

We also examined the role of PDPN in DC migration along stromal scaffolds. Initially, we compared the motility of WT DCs in networks formed by NIH3T3 fibroblasts or FRCs. As described above, DCs did not migrate efficiently on the NIH3T3 fibroblasts compared with FRCs

Figure 2.12. CLEC-2-PDPN interaction is required for DC migration along the FRC network. a, i, Transmitted light image of WT DCs interacting with WT FRCs in 3D network. Scale bar, 50 µm. ii, Diagram showing tracks of migrating DCs over 1 hour time course. iii, Quantification of DC migration along primary FRCs or NIH3T3 fibroblasts in 3D network. Each point represents the path of one DC collated from >3 independent experiments. b, Histogram of PDPN levels on FRCs and NIH3T3 cells. Grey indicates isotype control. c, i, Transmitted light image of *Clec1b*$^{-/-}$ DCs interacting with WT FRCs in 3D network. Scale bar, 50 µm. ii, Diagram showing tracks of migrating DCs over 1 hour time course. iii, Quantification of WT and *Clec1b*$^{-/-}$ DC migration along WT FRCs in 3D network. Each point represents the path of one DC. d, i, Transmitted light image of WT DCs interacting with *Pdpn*$^{-/-}$ FRCs in 3D network. Scale bar, 50 µm. ii, Diagram showing tracks of migrating DCs over 1 hour time course. iii, Quantification of WT DCs along FRCs with control siRNA, PDPN-targeted siRNAs, or *Pdpn*$^{-/-}$ FRCs in the 3D network. Each point represents the path of one DC. e, f, Representative histogram of PDPN staining in WT FRCs and *Pdpn*$^{-/-}$ FRCs (e) or FRCs transfected with siRNA against *Pdpn* (f).

Figure 2.12 (continued)

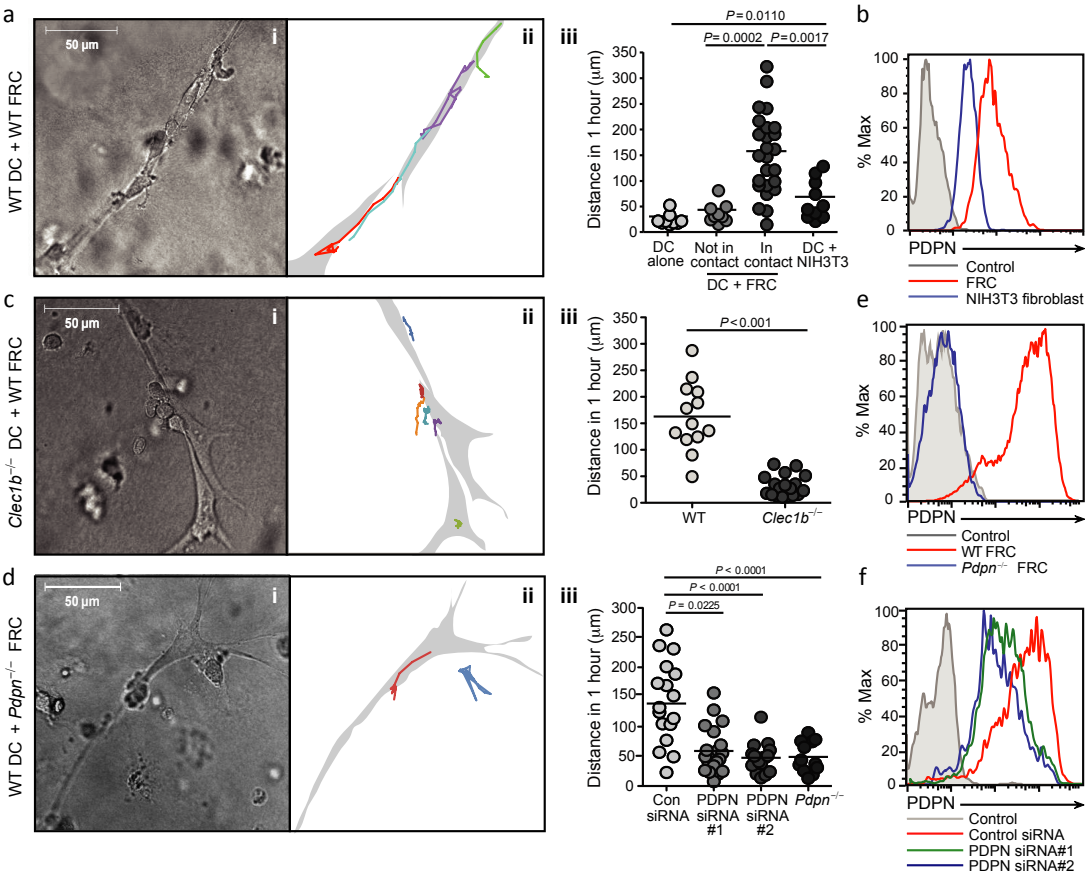

(Figure 2.12aiii), which led us to further examine the sufficiency of PDPN on stroma in this interaction. To this end, we seeded DCs into a 3D matrix with *Pdpn*$^{-/-}$ FRCs and found that DC migration was severely diminished on these networks compared with those formed by WT FRCs (Figure 2.12d, e and Movie S7). Similarly, WT DCs were markedly less efficient at spreading and migrating on FRCs in which PDPN surface levels were reduced following transfection with PDPN-targeting short interfering RNAs (siRNAs) compared with control siRNA-transfected FRCs (Figure 2.12diii, f). Thus, our findings suggest that PDPN is required for DCs to spread and migrate efficiently along the FRC surface.

To determine whether CLEC-2-PDPN interactions were able to support DC motility independently of known motility cues, we confirmed that chemokines and other adhesion molecules were not involved in our in vitro co-culture system. Accordingly, we found that DC migration in the *in vitro* 3D network occurred independently of CCR7 and its ligands CCL19 and CCL21, as FRCs rapidly downregulated their expression of both CCL19 and CCL21 when cultured ex-vivo, and *Ccr7*$^{-/-}$ DCs migrated as well as WT DCs along the scaffold (Figures 2.13a-c). We also tested the requirement of integrins by utilizing FRCs cultured from *Icam1*$^{-/-}$ mice, and found, in agreement with published studies, that DCs did not require engagement of this integrin for migration along stromal networks (Figures 2.13d-f).

To know whether CLEC-2 activation was sufficient to induce protrusion formation, we utilized A375 cells, a human melanoma cell line lacking CLEC-2 expression, that migrates in an amoeboid manner and exhibits a rounded morphology[25]. Control A375 cells that were seeded into the 3D matrix maintained their rounded morphology and did not form protrusions whether they were in contact with FRCs or not (Figures 2.14). In contrast, A375 cells expressing GFP-CLEC-2 formed long protrusions only when in contact with FRCs (Figures 2.14).

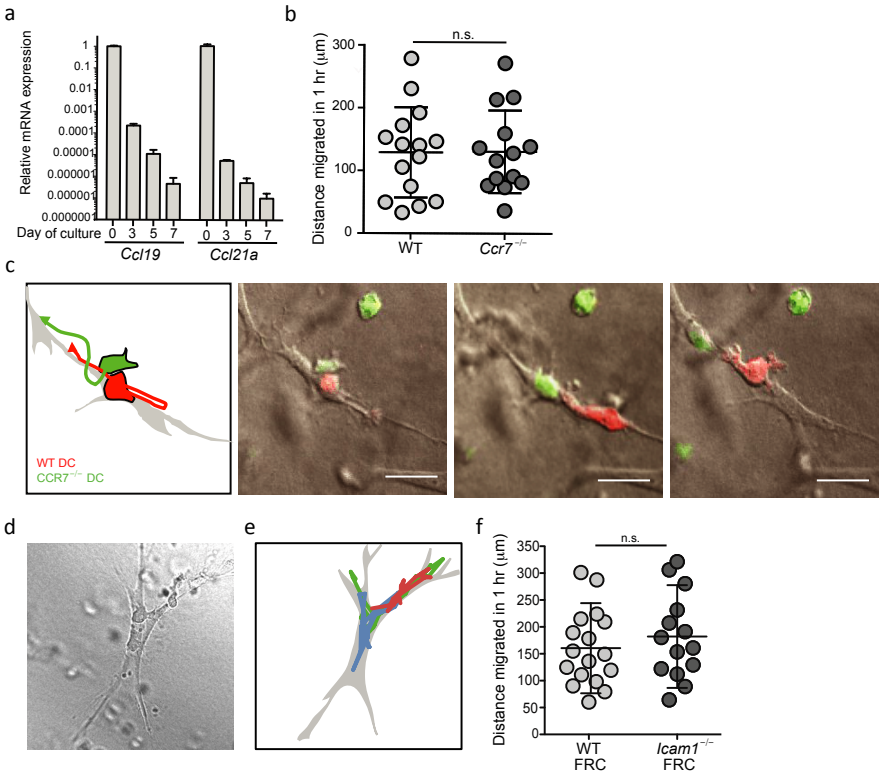

Figure 2.13. **DCs migrate along the FRC network independently of CCR7 and ICAM signaling.** a, Quantitative PCR analysis of CCL19 and CCL21 mRNA in primary FRCs during 7 days of *in vitro* culture. b, Quantification of distance migrated by WT and *Ccr7*$^{-/-}$ DCs in 1 hr. Each point represents one DC. *P* value calculated using Mann Whitney U test. c, *Left,* schematic showing tracks of WT [red] and *Ccr7*$^{-/-}$ [green] DCs moving on a fibroblastic reticular cell. *Right,* Stills from time-lapse imaging showing WT [red] and *Ccr7*$^{-/-}$ [green] DCs migrating along FRCs in 3D deformable matrix. Scale bar, 20 μm. d, Transmitted light image shows WT DCs interacting with *Icam1*$^{-/-}$ FRCs. Scale bar, 50 μm. e, Diagram shows tracks following migration of DCs during 1 hr time course. f, Quantification of DC migration along WT and *Icam1*$^{-/-}$ fibroblastic reticular cell scaffolds in 3D network. Each point represents the path of one DC. *P* value calculated using Mann Whitney U test.

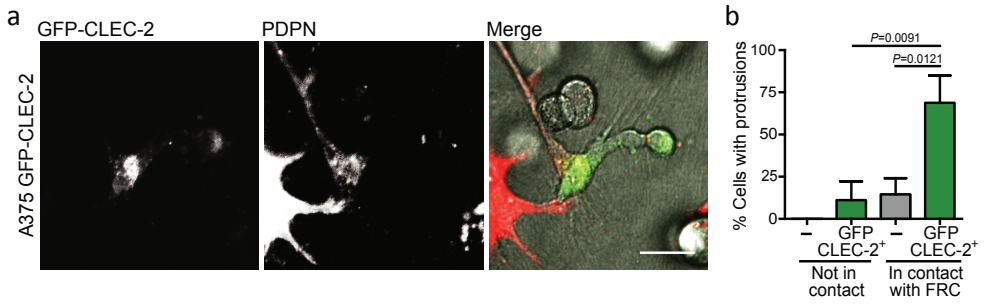

Figure 2.14. CLEC-2 is sufficient to induce protrusions. a, Immunofluorescence showing A375 GFP-CLEC-2 transfectants in contact with FRCs in the 3D network. Scale bar, 20 μm. b, Quantification of cells with protrusions.

These results demonstrate that over-expression of CLEC-2 by a cell type that normally lacks it is sufficient to incite the formation of protrusions in response to contacting PDPN-rich FRCs. Therefore, PDPN activation of CLEC-2 is necessary and sufficient to induce dynamic protrusions and spreading to support migration of DCs and potentially any CLEC-2-expressing cell type along PDPN-replete stromal scaffolds.

CLEC-2 signaling coordinately reduces actomyosin contractility and promotes actin polymerization

To elucidate the mechanism by which CLEC-2 activation promotes cell motility, we investigated how engagement by its ligands affects the actin cytoskeleton. CLEC-2 activation by either rPDPN-Fc or rhodocytin led to a marked accumulation of F-actin in the tips of newly extended protrusions, suggesting that actin polymerization drives their formation (Figure 2.15a). CLEC-2 signaling has been shown to activate a cascade of tyrosine kinase signaling involving Vav[19]. Given that Vav family members can also function as exchange factors for Rho family GTPases[26], master regulators of the actin cytoskeleton[27], we investigated whether the

Figure 2.15. CLEC-2 signaling coordinately reduces actomyosin contractility and promotes actin polymerization. a, F-actin and DAPI staining of control-, rhodocytin-, and rPDPN-Fc-treated DCs. Scale bar, 20 μm. b, Morphology index of WT and *Vav1*$^{-/-}$*Vav2*$^{-/-}$*Vav3*$^{-/-}$ DCs. Data are collated from 3 individual experiments, and each data point represents the morphology of an individual DC. c, Immunofluorescence of A375 cells transfected with GFP-CLEC-2 and treated with rhodocytin in two-dimensional culture. DAPI, F-actin, and GFP fluorescence are shown. Scale bar, 20 μm. d, Quantification of area comprised by cells plated in two-dimensions following rhodocytin stimulation relative to untransfected A375 cells. e, Protein blots showing levels of GFP-CLEC-2 and total and activated Rac1 and RhoA in A375 clones expressing either low or high levels of GFP-CLEC-2 or A375 control cells following treatment with rPDPN-Fc or rhodocytin. f, Quantification of Rac1-GTP as in e (*n*=3). g, Quantification of RhoA-GTP as in e (*n*=3). h, Immunofluorescence of FRCs and DCs in 3D network showing DAPI, CD11c, and pMLC (19) staining. Scale bar, 20 μm. i, Quantification of pMLC fluorescence intensity in 3D network relative to untreated DCs or DCs not in contact with FRCs.

Figure 2.15 (continued)

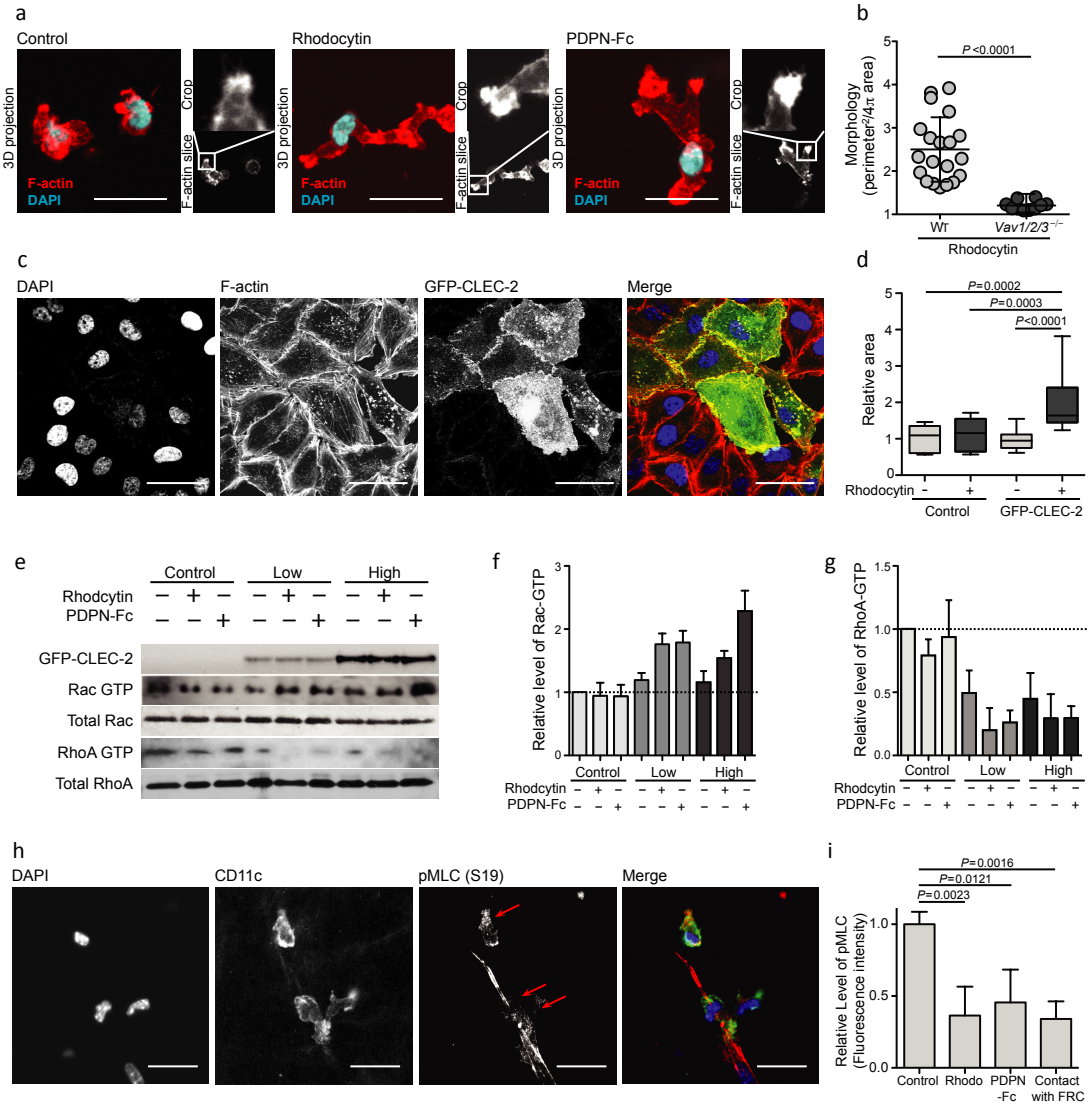

morphologic changes in DCs upon CLEC-2 activation were dependent on Vav. While WT DCs exhibited extensive protrusions upon stimulation with rhodocytin, *Vav1*$^{-/-}$*Vav2*$^{-/-}$*Vav3*$^{-/-}$ DCs maintained a rounded morphology upon CLEC-2 activation (Figure 2.15b). Indeed, the morphology of the *Vav1*$^{-/-}$*Vav2*$^{-/-}$*Vav3*$^{-/-}$ DCs was highly reminiscent of the *Clec1b*$^{-/-}$ DCs shown in Figures 2.10b (data not shown). These data indicate that the cytoskeletal rearrangements and actin-rich protrusions formed in DCs upon CLEC-2 activation are driven by a similar cascade of tyrosine kinase signaling, dependent on Vav, as has been described in CLEC-2-induced platelet aggregation[14].

The small G-protein Rac1 is known to promote the nuclearization and polymerization of actin filaments, and its activation is classically characterized by the spreading of lamellipodia and induction of membrane ruffles[27,28]. Furthermore, rhodocytin activation of CLEC-2 in platelets has been shown to activate Rac1[14]. To examine whether the cytoskeletal changes that we observed following CLEC-2 activation by PDPN were indicative of Rac1 activation, GFP-CLEC-2^{+} A375 cells were treated with CLEC-2 ligands and examined in 2D culture. A375 cells expressing GFP-CLEC-2 spread rapidly upon exposure to rhodocytin and within 5 minutes had spread to cover nearly twice the surface area of neighboring untransfected cells (Figures 2.15c, d). To directly ascertain whether CLEC-2 signaling triggers actin polymerization via Rac1, the levels of GTP-bound Rac1 relative to total Rac1 were measured by protein blot following exposure of GFP-CLEC-2 A375 transfectants to either rPDPN-Fc or rhodocytin. These experiments demonstrated that Rac1 activity was indeed increased as a result of CLEC-2 activation (Figures 2.15e, f). Together, these results suggest that CLEC-2 signaling, initiated by ligand engagement, triggers actin polymerization and protrusion formation via Rac1.

Next, we sought to understand how CLEC-2 activation promotes spreading along the stromal cell surface. RhoA is known to induce myosin light chain (MLC) phosphorylation and

increase actomyosin contractility through its interaction with Rho kinases[29]. We wondered whether CLEC-2 signaling altered RhoA activity to reduce actin contractility and thereby permit a DC or other CLEC-2-expressing cell to spread along the stromal cell surface. To this end, we quantified the amounts of GTP-bound RhoA relative to total RhoA in GFP-CLEC-2^{+} A375 cells that were treated with either rPDPN-Fc or rhodocytin. CLEC-2 activation with either ligand caused a striking reduction in GTP-bound RhoA compared with untreated cells (Figures 2.15e, g), suggesting that the downstream signaling that controls contractility of the acto-myosin cytoskeleton would also be reduced as a result of CLEC-2 activation. We directly tested whether this signaling pathway downstream of CLEC-2 might elicit a reduction in contractility of the actin cytoskeleton in DCs. MLCII is a key subunit of the conventional myosin motor, and phosphorylation of MLC at serine 19 (S19) promotes its activity[30]. The phosphorylation of MLC is highly dependent on the activity of RhoA effector kinases, and the global levels of pMLC (S19) in a cell can be used as a measure of the overall MLCII activity and contractility of the actin cytoskeleton[30]. Thus, we examined pMLC in DCs crawling along stromal cell scaffolds, where CLEC-2 will be activated by engagement of PDPN. Immunofluorescence analysis of 3D DC-FRC co-cultures revealed that DCs in contact with the FRC network exhibited markedly reduced levels of pMLC compared with DCs that were not in contact with FRCs (Figures 2.15h, i). Similar measurements were taken in DCs cultured alone in a 3D matrix and treated with CLEC-2 ligands. A significant reduction in the levels of pMLC (S19) in DCs was also observed following CLEC-2 activation by either rhodocytin or rPDPN-Fc (Figure 2.15i). Collectively, these findings suggest that CLEC-2 engagement by PDPN leads to a coordinate set of events: 1) the upregulation of Rac1 activity and stimulation of actin polymerization to drive protrusion formation and 2) the downregulation of RhoA activity and a decrease in pMLC to reduce cell contractility. Together,

these coordinated events would allow cells to spread along a stromal cell scaffold, extend actin-rich protrusions, and migrate.

Discussion

Here we describe a role for CLEC-2 signaling in DC motility. The CLEC-2 ligand PDPN is highly expressed by LECs and FRCs lining structures that DCs encounter during migration from tissues to lymph nodes. CLEC-2 is expressed by skin and lymph node DCs, but surface levels of this protein appear to be tightly regulated. Engagement of CLEC-2 by PDPN coordinately reduces actomyosin contractility and promotes actin polymerization in DCs, thereby allowing them to spread along stromal cell scaffolds, extend protrusions, and migrate. The CLEC-2-PDPN interaction promotes DC migration to lymph nodes at all stages of this journey: from leaving peripheral tissues and entering lymphatic vessels, to crossing the subcapsular sinus, and finally to migrating through lymph node parenchyma to the T cell zone. T cell activation in lymph nodes was markedly reduced despite the fact that some *Clec1b*$^{-/-}$ DCs completed the passage from skin to lymph node as measured by FACS analysis. This could suggest a preferentially important role for CLEC-2 in a DC subset that efficiently cross-presents antigen such as the CD103^{+} dermal DC. Alternatively, this could suggest that CLEC-2 deficiency not only reduces DC migration but also prevents DCs from properly interacting with the FRC network and T cells. Consistent with this latter possibility, we found that *Clec1b*$^{-/-}$ DCs were severely impaired in spreading and crawling on the FRC network in 3D.

Analysis of the downstream signaling components revealed that CLEC-2 activation in DCs, as in platelets, required the adaptor protein and exchange factor Vav, and led to alterations of actin dynamics via activation of Rac1. Our study shows that CLEC-2 activation by PDPN induces F-actin-rich protrusions conducive to cell migration. Additionally, we find that RhoA activity is coordinately decreased upon CLEC-2 activation. Rac and Rho have been shown to be

antagonistic in a variety of contexts[31,32], and this exclusivity may act to spatially separate Rho and Rac. One potential antagonistic mechanism is the ability of Rac to induce the translocation of p190RhoGAP to locally downregulate Rho activity[32]. An opposing mechanism is also reported whereby Rho activity leads to the activation of FilGAP to inactivate Rac[31].

Based on the signaling events following contact between *Clec1b*$^+$ DCs and *Pdpn*$^+$ stromal cells, we propose the following model. Initially CLEC-2 and PDPN interact and cluster on the respective cell membranes. CLEC-2 oligomerization then induces tyrosine phosphorylation events via Syk and PLCγ and Vav. Vav promotes the activity of Rac1, which indirectly and coordinately reduces RhoA activity. These events are spatially restricted to domains on the DC surface that are in direct contact with PDPN. Therefore, specifically at the contacts between DCs and FRCs, the activity of RhoA effectors, such as ROCK (Rho-associated protein kinase), are reduced, leading to reduced phosphorylation of MLC[30] and reduced contractility of the actomyosin cytoskeleton. We suggest that this mechanism can explain the ability of DCs to spread along the underlying stromal cell scaffold. The increase in Rac1 activity then promotes actin polymerization and the induction of protrusions reaching along the stromal cell. As the DC reaches forward, CLEC-2 signaling would need to be tempered to allow RhoA effector activity to contract the cell rear and allow the cell body to follow the protrusion[27]. We have noted that CLEC-2 oligomers are rapidly internalized following ligand binding, which may allow temporal and spatial restriction of CLEC-2 signaling.

The utilization of our 3D co-culture system provided critical insights into leukocyte interactions with FRCs and molecular mechanisms promoting DC migration in this stromal niche. For example, by using this system in which primary FRCs downregulate chemokine expression, we discovered that PDPN-driven activation of CLEC-2 was necessary and also sufficient to induce bona fide DC migration in the absence of additional motility cues such as CCL19 and CCL21. DC

migration in this system was confined to FRC surfaces but was not directional. DCs migrated back and forth along FRC scaffolds, suggesting that PDPN activation of CLEC-2 would not be sufficient to guide DCs in one particular direction. Rather, simultaneous signals from chemokine gradients and fluid flow *in vivo* would confer directionality on DC motility. Coordination of these different signaling processes would thereby endow DCs with the capacity to migrate through complex stromal niches from their sentry posts in parenchymal tissues to tissue-draining lymph nodes where T cell responses commence.

CLEC-2 activation may affect the motility of other leukocytes that express this CLR. Neutrophils have been reported to express CLEC-2[17] and as such their migration to infected tissues or to tertiary lymphoid structures may also be affected upon CLEC-2 engagement of PDPN. B cells, which also express CLEC-2[18] and data not shown), may utilize this pathway to migrate along PDPN-rich FRCs en route to follicles in secondary lymphoid organs. Indeed, we found that like DCs, B cells migrate along FRCs in the 3D culture system[33], and may use CLEC-2 to move within lymph nodes.

Beyond LECs and lymph node FRCs, PDPN is expressed by splenic FRCs[34] and stromal cells in bone marrow and thymus (our unpublished data). PDPN is also upregulated in tissue fibroblasts during inflammation, and PDPN-rich stroma is often observed in tumors[12], perhaps supporting the function of tumor-infiltrating leukocytes. Activation of CLEC-2 by PDPN may therefore be a widely applicable mechanism promoting leukocyte motility along stromal networks of all PDPN-rich lymphoid organs and inflamed tissues, irrespective of which chemokine cues are present. Thus, targeting CLEC-2 to specifically harness leukocyte migration may have significant therapeutic potential for treating inflammatory and autoimmune diseases.

Methods

Mice

C57BL/6 mice 6-10 weeks of age were purchased from Jackson Laboratories. *Pdpn*$^{-/-}$ mice on some genetic backgrounds die at birth but some survive on the C57BL/6 background; thus, we used *Pdpn*$^{-/-}$ mice on the C57BL/6 background as described previously[35]. *Clec1b*$^{-/-}$ mice were generated as previously described[10]. *Vav1*$^{-/-}$*Vav2*$^{-/-}$*Vav3*$^{-/-}$ mice were generated as previously described[26]. Animals were maintained under pathogen free conditions in the Animal Facility of the Dana-Farber Cancer Institute in accordance with US National Institutes of Health guidelines.

Generation of fetal liver chimeras

To generate CLEC-2 FLCs, *Clec1b*$^{+}$ and *Clec1b*$^{-/-}$ embryos were collected from females at day E14.5-E18.5 and were processed into a single cell suspension. Recipient B6.SJL-Ptprc^{a}Pep3^{b}/BoyJ mice (Jackson Laboratories, USA) were irradiated at 2x550 Rad, and 10^6 fetal liver cells were subsequently injected retro-orbitally. The mice received antibiotics (Baytril) for 3 weeks after irradiation and were used in experiments 6-7 weeks after the cell transfer. At this point, total lymph node DCs were >95% reconstituted by flow cytometric analysis and no *Clec1b*$^{-/-}$ mRNA transcript was detected in freshly isolated DCs from the *Clec1b*$^{-/-}$ FLCs (data not shown and Figure 2.4A). Furthermore, total cellularity and lymph node DC numbers did not differ significantly between WT and *Clec1b*$^{-/-}$ FLCs (data not shown).

Ubiquitin-GFP (Ub-GFP) BM chimeric mice (WT BM>Ub-GFP host) were generated as follows: BM was prepared from C57BL/6 mice and T, NK, and B cells were depleted via MACS separation using the following biotinylated antibodies: NK1.1 (PK136), CD19 (6D5) and CD3ε (145-2C11) (Biolegend). Recipient Ub-GFP mice (Jackson Laboratories, USA) were irradiated at 2x650 Gy. 24 hours later, 10^6 T, B, and NK cell-depleted BM cells were injected i.v. Recipient mice

received antibiotic (Baytril) for the first 4 weeks after irradiation and were used for experiments 8 weeks after receiving BM cells.

Isolation and culture of primary cells

FRCs were isolated and expanded as previously described[33]. For BMDCs, bone marrow was taken from the tibias and femurs of 5-week-old C57BL/6, *Ccr7*$^{-/-}$, *Vav1*$^{-/-}$*Vav2*$^{-/-}$*Vav3*$^{-/-}$, and *Clec1b*$^{-/-}$ mice and cultured in RPMI containing 10% FBS and 3% GM-CSF (derived from supernatant of J558L culture) for 5-6 days. Unstimulated BMDCs were used in functional experiments unless specified otherwise. For experiments in which matured BMDCs were used, the cultures were treated with 10 ng/ml LPS for 24 hours.

3D culture system

DCs were seeded either alone or at a 5:1 ratio with FRCs into a collagen/matrigel matrix[25] (1.8 mg/ml Matrigel (BD Biosciences) and 3.2 mg/ml collagen type 1 (BD Biosciences)) on glass-bottomed cell culture plates (MatTek). Gels were incubated at 37°C with 10% CO_2 in aMEM containing 10% FCS during imaging. For experiments involving CLEC-2 activation in 3D culture, CLEC-2 ligands (rhodocytin, 200 nM and PDPN-Fc, 0.04 μg/ml) were added to the gel as all components were mixed.

Quantification of cell morphology and cell migration in vitro

Using ImageJ software, the area and perimeter of cells were determined by manually drawing around the cell shape using phase contrast images. Ratios were calculated as follows: perimeter^2/4πarea. Elongation factor was calculated using ImageJ 'fit ellipse' function. The ratio of major/minor axis was plotted to measure cell elongation on FRCs. ImageJ was also used to

determine the cell centroid and its translocation over time to calculate distance migrated along. The motion analysis (Figure 2.1) shows three time points overlaid in red, green and blue. Static cells and collagen matrix are shown in white, motile cells are visualized by the separation of the red, green and blue channels.

Analysis of DC movement in tissues

DC entry to lymphatic vessels was carried out as previously described[6]. Briefly, ears of C57BL/6 mice were split and the cartilage-free half was incubated with directly conjugated Lyve-1-488 antibody (eBioscience) in PBS containing 1% BSA for 1 hour on ice. The stained ears were incubated with either WT or *Clec1b*$^{-/-}$ LPS-matured BMDCs labeled with 5 μM Far-red cell tracker dye (Invitrogen) for 2 hours at 37°C with 5% CO_2. Non-infiltrating DCs were then gently washed away and ears were fixed in 1% PFA for 4 hours. Ear sheets were imaged using an inverted Zeiss 510 confocal microscope.

For DC migration in lymph nodes, lymph nodes were dissected from Ubiquitin-GFP chimeric mice (WT BM>Ub-GFP host) and embedded in 4% low-melting temperature agarose at 36°C. Blocks were then cooled on ice. Vibratome sections of lymph nodes 300 μm thick were cut and incubated with RPMI containing 10% FCS for 30 min at 37°C. WT and *Clec1b*$^{-/-}$ BMDCs were labeled with cell tracking dyes, washed with PBS, then incubated with the lymph node slices for 90 minutes at 37°C. After this time, lymph node slices were gently washed with RPMI containing 10% FCS, laid into MatTek dishes and imaged using an inverted Zeiss 510 confocal microscope for 2 hours at 37°C with 5% CO_2. Z-stacks of 30 μm were projected using ImageJ z-project. Time-lapse sequences were analyzed using the ImageJ manual tracking plugin to measure cell velocity and to track individual cells.

Endocytosis assays

BMDCs from WT or *Clec1b*$^{-/-}$ FLCs were incubated with 2 μm fluorescent latex beads (Polysciences inc.) in media at 37°C. Beads were added at a concentration of <5 beads per DC. Free beads were washed away and DCs were fixed with 4% PFA, washed with PBS, and bead enumeration was assessed by FACS.

Generation of PDPN-Fc recombinant protein

PDPN extracellular domains were PCR amplified from mouse cDNA using the following primers: F: GTGATATCTGGGAGCGTTTGGTTCTG, R: GGCAGATCTTGGCAAGCCATCTTTC. PCR product was ligated into pFUSE-rFc2 (IL2ss) (InvivoGen) containing a rabbit Fc domain (CH2, CH3, and hinge region) and electroporated into COS-7 cells (ATCC). 24 hours after electroporation, the culture medium was replaced with complete DMEM (Gibco) supplemented with ultra low Ig-containing serum (Gemini Bio-Products) and 200 μg/ml zeocin for selection (Invivogen). Cells were single cell sorted after 2 weeks of selection. Single cell clones were expanded for large-scale protein production. Supernatant was harvested and purified over a protein G column (GE Healthcare). Proteins were eluted with 0.1 M glycine, pH 2.5, followed by neutralization using 1M Tris, pH 9.0. The proteins were buffer exchanged against PBS.

Transfection of GFP-CLEC-2.

Clec1b cDNA was cloned into eGFPC1 (Clontech) from the I.M.A.G.E clone (ATCC, 574821 pT7T3D-Pac). GFP-CLEC-2 fusion was transiently transfected into the human melanoma cell line A375 using Effectene (Qiagen) according to manufacturer's instructions. Twenty four hours after transfection, A375 cells were seeded into a 3D deformable matrix at 3:1 ratio with primary FRCs, or plated onto glass-bottomed MatTek dishes for stimulation with CLEC-2 ligand. Single cell

clones with high or low expression were generated by single cell sorting transiently transfected A375 GFP-CLEC-2 following 2 weeks of selection with 0.2 μg/ml G418.

siRNA knockdown of PDPN

siRNA complexes were as follows: Con siRNA (all stars control (Qiagen)), PDPN#1 (GCUGCAUCUUUCUGGAUAATT), and PDPN#2 (CGCAGACAACAGAUAAGAATT). FRCs were transfected with siRNA using oligofectamine (Invitrogen) according to the manufacturers instructions. Efficiency of knockdown was determined by FACS 72 hours after transfection. PDPN surface expression was measured by FACS.

Analysis of Clec1b and Pdpn mRNA expression

DCs were sorted from lymph nodes of WT mice by FACS and from WT and *Clec1b*$^{-/-}$ FLCs by MACS with CD11c-biotin beads (Miltenyi, USA). mRNA was extracted from DCs using the RNeasy mini kit (Qiagen) and cDNA template was transcribed using MLV-RT (Invitrogen) according to the manufacturer's instructions. *Clec1b* mRNA expression was determined by qPCR using the following primers: F: AACATCAAGCCCCGGAAACAA, R: GCCACGAGTCCAACAACCA and by RT-PCR using the following primers: F: CAATAGGTCCTGGATGGTCTTC, R: TTACACTGGCTTACCGTGACAG and compared to expression of GADPH or β-actin, respectively. LNSCs were sorted as previously described[33] and PDPN expression levels were determined by microarray (MCBI GEO Database accession number GSE15907).

FITC painting of ear skin

The ears of mice were painted on both sides with 15 μl FITC solution (5 mg/ml Fluorescein isothiocyanate (Sigma) in 1:1 mix dibutylphalate and acetone). Draining cervical

lymph nodes were collected after 24 and 72 hours, digested with collagenase P (Roche 11249002001), dispase (GIBCO 17105-041) and DNase (Roche 10104159001) and analyzed by FACS for the presence of $FITC^+$ migratory DCs.

FACS and antibodies

Cells were analyzed using either a FACSCalibur (BD biosciences) or LSR II (BD biosciences). Monoclonal antibodies: α-MHC class II (BD Pharmingen), α-CD40 (Biolegend IC10), α-CD11c (BD Biosciences HL3), α-CD103 (BD Biosciences M290), α-CD326 (Biolegend G8.8), α-CD19 (Biolegend 6D5), α-CD3ε (Biolegend 145-2C11), α-CD8α (Biolegend 53-6.7), α-Vα2 (Caltag laboratories RM5005), α-CD44 (Biolegend IM7), α-PDPN (hybridoma clone 8.1.1), α-CD45 (Biolegend 30-F11), and α-CD31 (Biolegend MEC13.3). Primary rabbit anti-pMLC (S19) and anti-rabbit-Alexa 555 were purchased from Cell Signaling Technology. Isotype control antibodies were obtained from Biolegend and BD Pharmingen.

Chemotaxis assay

Chemotaxis of BMDCs from WT and Clec1b-/- FLCs was measured by migration through a polycarbonate filter of 5 μm pore size in 24-well transwell chambers (Corning Costar). 600 μL media alone as control or containing CCL21 (50 – 500 μM) was added to the lower chamber; 1 x 10^5 DCs were added to the upper chamber and were incubated for 8 hours at 37°C with 5% CO_2. A 300 μL aliquot of the media from the lower chamber was counted by FACS to assess the percentage of migrating cells.

In vivo and in vitro T cell stimulation assays

For in vivo analysis, WT or *Clec1b*$^{-/-}$ DCs were loaded with 2.5 mg/ml OVA peptide

(SIINFEKL) for 2 hours at 37°C. DCs were then pre-incubated with rPDPN-Fc or an isotype control antibody. $5x10^5$ DCs were injected into the footpad in 10 ml PBS containing 10 ng/ml LPS. OT-1 splenocytes were labeled with CFSE by resuspending cells in RPMI at $10x10^6$ cells/ml plus 2.5 mM CFSE, incubated at 37˚C for 10 min, washed three times, and then counted. 24 hours after DC injection, the mice were intravenously injected with $1.5x10^6$ CFSE-labeled OT-1 T cells in 200 ml PBS. Axillary (distal) and popliteal (draining) lymph nodes were removed 48 hours later and T cell proliferation was evaluated by measuring CFSE dilution among OT-1 T cells (identified by TCR clonotype) using FACS. Division index was calculated as the average number of divisions among cells that had divided at least one time. For in vitro analysis, a single cell suspension of red blood cell-depleted splenocytes was prepared from OT-1xRag1$^{-/-}$ mice. The OT-1 splenocytes were then labeled with CFSE by resuspending cells in RPMI at $10x10^6$ cells/ml plus 2.5 μM CFSE and incubating at 37˚C for 10 min. Cells were washed twice in cold RPMI containing 10% FCS and counted. BMDCs from WT and *Clec1b*$^{-/-}$ FLCs were loaded with 2.5 μg/ml OVA peptide (SIINFEKL, AnaSpec) and then co-cultured with CFSE-labeled OT-1 T cells in culture media (RPMI; 10% FCS, 1% penicillin/streptomycin) for 48 hours. T cell proliferation was assessed by measuring CFSE dilution among OT-1 T cells (identified by TCR clonotype) by FACS. Division index was calculated as above.

Analysis of RhoA and Rac1 activation

A375 single cell clones expressing either low or high levels of GFP-CLEC-2 were treated with CLEC-2 ligands (Rhodocytin, 200 nM and PDPN-Fc, 0.4 μg/ml) for 5 min then washed with PBS and lysed on ice. Cell lysates were incubated for 5 hour with GST-Rhotekin-RBD or GST-PAK1-PBD bound to glutathione agarose. Beads were then washed, and bound proteins were

eluted by boiling the beads in LDS sample buffer. Levels of RhoA-GTP and Rac1-GTP were evaluated by western blot and compared to total RhoA and total Rac-1 in whole cell lysates.

Analysis of pMLC

3D matrices seeded with DCs and FRCs or DCs alone were fixed after 18 hours with 4% PFA for 2 hours at 4˚C, permeabilized with 0.25% Triton in PBS for 30 min at room temperature, then blocked with 3% BSA 0.01% Tween-20 in PBS for 2 hours at room temperature. Primary rabbit anti-pMLC (S19) (Cell Signaling Technology) was added in blocking buffer at a 1:100 dilution for 3 hours at room temperature. Cultures were washed 3x in blocking buffer for 10 min each. Anti-rabbit Alexa 555 was then diluted 1:300 in blocking buffer and incubated for 2 hours at room temperature. A CD11c-FITC conjugated antibody was used at 1:50 to visualize DCs. Images were captured on a Zeiss LSM 510 confocal microscope. ImageJ software was utilized to quantify the intensity of pMLC staining in DCs.

Immunofluorescence staining of tissues and cells

For staining of the 3D deformable matrices, cultures were washed with PBS then fixed with 4% PFA for 1 hour, permeabilized with 0.2% Triton in PBS for 20 minutes and blocked with 3% BSA for 2 hours before staining. PDPN was visualized using clone 8.1.1 conjugated to Alexa-647 (Biolegend). F-actin and cell nuclei were visualized using TRITC-phalloidin and DAPI, respectively (Invitrogen). For whole mount staining of ear skin, ears were split and ventral halves were used for staining. Ears were fixed in 1% PFA for 3 hours, permeabilized with 0.1% Triton for 30 min and blocked in 1% BSA for 3 hours before staining. Monoclonal antibodies (8.1.1 conjugated to Alexa-647) and Lyve-1 (eBioscience FITC-conjugated) were used. F-actin was visualized with TRITC-phalloidin.

Imaging

Confocal imaging was conducted using a Zeiss LSM510 Meta microscope with the 20x objective. Time-lapse microscopy was also conducted using a Zeiss LSM510 Meta microscope with the transmitted light detector. Multi-photon intravital was conducted as previously described (Gonzalez et al., 2010). BMDCs were treated with 10 ng/ml LPS for 18 hours, labeled with 5 μM CFSE (Invitrogen), and then injected into recipient mice. Mice received 2.5 x 10^5 labeled DCs injected into the footpad in 10 μl PBS 18 hours before multi-photon intravital imaging was conducted.

Statistical analysis

Statistical tests in this manuscript were performed using Prism software (Graphpad). Data sets were first subjected to an F test to establish whether data to be compared exhibited comparable standard deviation. Following this, the appropriate tests were performed as indicated in each figure legend. In general, comparison of multiple groups was performed using a Kruskal-Wallis analysis of variance and if significant followed by Dunn's post-test between individual data sets. Comparisons of two data sets were most commonly performed using a Mann-Whitney U test.

References

1. Turley, S. J., Fletcher, A. L. & Elpek, K. G. The stromal and haematopoietic antigen-presenting cells that reside in secondary lymphoid organs. *Nature Publishing Group* **10,** 813–825 (2010).

2. Randolph, G. J., Angeli, V. & Swartz, M. A. Dendritic-cell trafficking to lymph nodes through lymphatic vessels. *Nat Rev Immunol* **5,** 617–628 (2005).

3. Förster, R. *et al.* CCR7 coordinates the primary immune response by establishing functional microenvironments in secondary lymphoid organs. *Cell* **99,** 23–33 (1999).

4. Schumann, K. *et al.* Immobilized chemokine fields and soluble chemokine gradients cooperatively shape migration patterns of dendritic cells. *Immunity* **32,** 703–713 (2010).

5. Link, A. *et al.* Fibroblastic reticular cells in lymph nodes regulate the homeostasis of naive T cells. *Nat Immunol* **8,** 1255–1265 (2007).

6. Lämmermann, T. *et al.* Rapid leukocyte migration by integrin-independent flowing and squeezing. *Nature* **453,** 51–55 (2008).

7. Frittoli, E. *et al.* The signaling adaptor Eps8 is an essential actin capping protein for dendritic cell migration. *Immunity* **35,** 388–399 (2011).

8. Link, A. *et al.* Association of T-Zone Reticular Networks and Conduits with Ectopic Lymphoid Tissues in Mice and Humans. *The American Journal of Pathology* **178,** 1662–1675 (2011).

9. Peduto, L. *et al.* Inflammation Recapitulates the Ontogeny of Lymphoid Stromal Cells. *The Journal of Immunology* **182,** 5789–5799 (2009).

10. Bertozzi, C. C. *et al.* Platelets regulate lymphatic vascular development through CLEC-2-SLP-76 signaling. *Blood* **116,** 661–670 (2010).

11. Schacht, V. *et al.* T1alpha/podoplanin deficiency disrupts normal lymphatic vasculature formation and causes lymphedema. *EMBO J.* **22,** 3546–3556 (2003).

12. Wicki, A. & Christofori, G. The potential role of podoplanin in tumour invasion. *Br J Cancer* **96,** 1–5 (2006).

13. Chaipan, C. *et al.* Incorporation of podoplanin into HIV released from HEK-293T cells, but not PBMC, is required for efficient binding to the attachment factor CLEC-2. *Retrovirology* **7,** 47 (2010).

14. Watson, S. P., Herbert, J. M. J. & Pollitt, A. Y. GPVI and CLEC-2 in hemostasis and vascular integrity. *J. Thromb. Haemost.* **8,** 1456–1467 (2010).

15. Colonna, M., Samaridis, J. & Angman, L. Molecular characterization of two novel C-type lectin-like receptors, one of which is selectively expressed in human dendritic cells. *Eur. J. Immunol.* **30,** 697–704 (2000).

16. Suzuki-Inoue, K. *et al.* Essential in Vivo Roles of the C-type Lectin Receptor CLEC-2: EMBRYONIC/NEONATAL LETHALITY OF CLEC-2-DEFICIENT MICE BY BLOOD/LYMPHATIC MISCONNECTIONS AND IMPAIRED THROMBUS FORMATION OF CLEC-2-DEFICIENT PLATELETS. *Journal of Biological Chemistry* **285,** 24494–24507 (2010).

17. Kerrigan, A. M. *et al.* CLEC-2 is a phagocytic activation receptor expressed on murine peripheral blood neutrophils. *J. Immunol.* **182,** 4150–4157 (2009).

18. Mourão-Sá, D. *et al.* CLEC-2 signaling via Syk in myeloid cells can regulate inflammatory responses. *Eur. J. Immunol.* **41,** 3040–3053 (2011).

19. Pearce, A. C. *et al.* Vav1 and vav3 have critical but redundant roles in mediating platelet activation by collagen. *Journal of Biological Chemistry* **279,** 53955–53962 (2004).

20. Bajénoff, M. *et al.* Highways, byways and breadcrumbs: directing lymphocyte traffic in the lymph node. *Trends Immunol.* **28,** 346–352 (2007).

21. Stoitzner, P., Pfaller, K., Stössel, H. & Romani, N. A close-up view of migrating Langerhans cells in the skin. *J. Invest. Dermatol.* **118,** 117–125 (2002).

22. Baluk, P. *et al.* Functionally specialized junctions between endothelial cells of lymphatic vessels. *J. Exp. Med.* **204,** 2349–2362 (2007).

23. Farr, A. G. *et al.* Characterization and cloning of a novel glycoprotein expressed by stromal cells in T-dependent areas of peripheral lymphoid tissues. *J. Exp. Med.* **176,** 1477–1482 (1992).

24. Hooper, S., Marshall, J. F. & Sahai, E. Tumor cell migration in three dimensions. *Meth. Enzymol.* **406,** 625–643 (2006).

25. Pinner, S. & Sahai, E. Imaging amoeboid cancer cell motility in vivo. *J Microsc* **231,** 441–445 (2008).

26. Graham, D. B. *et al.* ITAM signaling by Vav family Rho guanine nucleotide exchange factors regulates interstitial transit rates of neutrophils in vivo. *PLoS ONE* **4,** e4652 (2009).

27. Nobes, C. D. & Hall, A. Rho, rac, and cdc42 GTPases regulate the assembly of multimolecular focal complexes associated with actin stress fibers, lamellipodia, and filopodia. *Cell* **81,** 53–62 (1995).

28. Olson, M. F. & Sahai, E. The actin cytoskeleton in cancer cell motility. *Clin Exp Metastasis* **26,** 273–287 (2008).

29. Parri, M. & Chiarugi, P. Rac and Rho GTPases in cancer cell motility control. *Cell Commun Signal* **8,** 23 (2010).

30. Wyckoff, J. B., Pinner, S. E., Gschmeissner, S., Condeelis, J. S. & Sahai, E. ROCK- and Myosin-Dependent Matrix Deformation Enables Protease-Independent Tumor-Cell Invasion In Vivo. *Current Biology* **16,** 1515–1523 (2006).

31. Ohta, Y., Hartwig, J. H. & Stossel, T. P. FilGAP, a Rho- and ROCK-regulated GAP for Rac binds filamin A to control actin remodelling. *Nature Cell Biology* **8,** 803–814 (2006).

32. Wildenberg, G. A. *et al.* p120-catenin and p190RhoGAP regulate cell-cell adhesion by coordinating antagonism between Rac and Rho. *Cell* **127,** 1027–1039 (2006).

33. Fletcher, A. L. *et al.* Reproducible isolation of lymph node stromal cells reveals site-dependent differences in fibroblastic reticular cells. *Front Immunol* **2,** 35 (2011).

34. Bekiaris, V. *et al.* Role of CD30 in B/T segregation in the spleen. *The Journal of Immunology* **179,** 7535–7543 (2007).

35. Peters, A. *et al.* Th17 Cells Induce Ectopic Lymphoid Follicles in Central Nervous System Tissue Inflammation. *Immunity* **35,** 986–996 (2011).

Chapter 3

Podoplanin controls fibroblastic reticular cell contractility and lymph node architecture

Attributions

The following individuals contributed to the work detailed in this chapter: Jillian L. Astarita, Jianxin Fu, Max C. Darnell, Matthew C. Woodruff, Kai Song, Lucas Onder, Michael C. Carroll, Burkhard Ludewig, David J. Mooney, Lijun Xia, and Shannon J. Turley.

J.L.A designed and performed experiments and analyzed the results. J.F., K.S., and L.X. supplied key reagents and mice. M.C.D performed the YAP and lymph node stiffness experiments. M.C.W. analyzed conduit function. L.O. and B.L. provided mice. L.X., D.J.M., M.C.C., and B.L. provided critical comments on experiments. S.J.T. supervised the study and provided crucial comments on experiments.

Introduction

Lymph nodes are highly organized structures that serve as rendezvous points for innate antigen presenting cells and adaptive T and B lymphocytes. The maintenance of lymph node structure and compartmentalization are critical for both the generation of effective immune responses and control of unwanted immune activation[1,2]. Lymph nodes are unique organs in their ability to increase many times in size during an immune response and then contract back again once the response has resolved. The vast proliferation of lymphocytes clearly contributes to this swelling. However, while the vasculature of the node increases and is remodeled[3-7] during swelling, other changes in the underlying stromal cells that support the structural integrity of the organ have not been elucidated.

Lymph node stromal cells are non-hematopoietic cells that form the underlying backbone of lymph nodes[8,9]. Fibroblastic reticular cells (FRCs) constitute the major non-hematopoietic stromal cell present in LNs[9-11]. They secrete and remodel extracellular matrix (ECM) components to create a dense, reticular network in the paracortex upon which T cells and dendritic cells (DCs) crawl[12]. FRCs ensheath these reticular fibers to form conduits, small vessel-like structures through which afferent lymph and small molecules flow deep into the LN parenchyma from the subcapsular sinus[11,13,14]. It is well established that FRCs are highly contractile cells[10,11], but a specific function and underlying mechanism for this contractility have not been elucidated. Given the organization of the network formed by these stromal cells, it is reasonable to speculate that the contractile nature of FRCs plays a role in governing the homeostasis of the reticular scaffold, LN expansion during immune responses, and integrity of high endothelial venules.

Podoplanin (PDPN, also known as gp38, Aggrus, T1α) is a heavily glycosylated transmembrane protein that is highly expressed by FRCs, lymphatic endothelial cells (LECs) and

several other cell types outside lymphoid organs[15-17]. It is critical for several processes in fetal development, including blood-lymph separation and lung organogenesis[18-20], and its overexpression in several cancer types is correlated with increased invasion and metastasis[21]. However, the intrinsic function of PDPN in healthy, postnatal animals has remained enigmatic. PDPN is the endogenous ligand for the c-type lectin receptor CLEC-2[22], which is expressed by platelets. The functions of CLEC-2 in platelet activation have been well studied[23] and a recent report detailing a new role for CLEC-2 in maintaining HEV vascular integrity[24]. However, it is unknown whether CLEC-2 engagement of PDPN results in any signaling into the PDPN-expressing cell.

While PDPN has been extensively used as a marker for LECs and FRCs, no specific function for this molecule has been described. Thus, in light of previous studies illuminating a cytoskeletal function for PDPN in cancer cells[25,26], we examined whether PDPN played a role in regulating the FRC cytoskeleton and actomyosin contractility. Furthermore, given that both FRCs and LECs would be constantly exposed to CLEC-2^{+} platelets and DCs, we tested whether CLEC-2 engagement of PDPN resulted in any downstream signaling into the stromal cells. We found that PDPN is a master regulator of FRC contractility and that disruption of this function resulted in increased lymph node swelling and an inability to control T cell proliferation during an immune response.

Results

PDPN is a master regulator of FRC elongation and contractility

To investigate the role of PDPN in lymph node FRCs, we cultured primary FRCs from WT or *Pdpn*$^{-/-}$ mice. While *Pdpn*$^{-/-}$ mice generally die soon after birth due to blood-lymph mixing and edema, when crossed onto certain backgrounds, about 20% of the mice survive and are viable

and fertile[18]. Indeed, upon ex vivo expansion, *Pdpn*$^{-/-}$ FRCs expressed normal levels of common FRC markers including PDGFRα, PDGFRβ, cadherin 11, CD44, and α-smooth muscle actin (Figure 3.1).

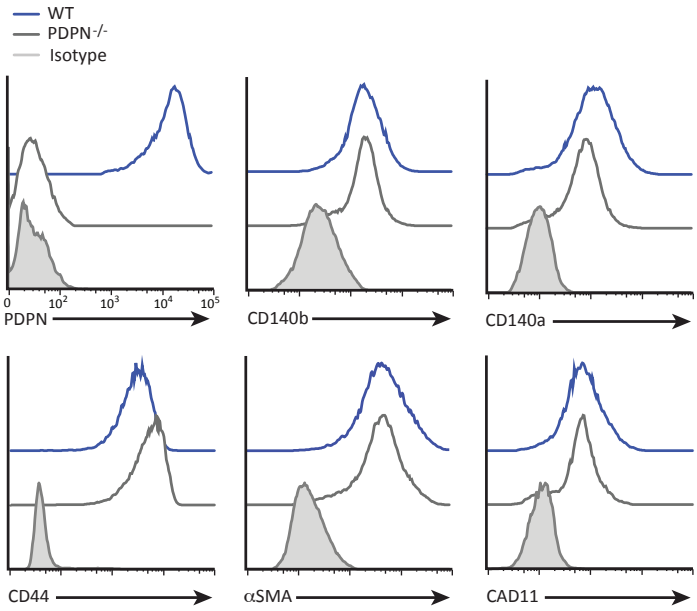

Figure 3.1. Normal expression of FRC surface markers on PDPN$^{-/-}$ FRCs. Purified FRCs were stained for PDPN, CD140b (PDGFRβ), CD140a (PDGFRα), CD44, α-smooth muscle actin (αSMA), and cadherin 11 (CAD11). Histograms are representative of three independent experiments.

Previous studies have demonstrated that PDPN is involved in adhesion and spreading[25], so we first examined whether *Pdpn*$^{-/-}$ FRCs had a defect in adhering to and spreading on collagen. Indeed, *Pdpn*$^{-/-}$ FRCs were significantly impaired in these processes at early time points (Figure 3.2a, b). Given that FRCs interact with collagen in a three-dimensional (3D) tissue environment in the lymph node, we seeded FRCs into collagen-based 3D deformable matrices that simulate this niche and examined their cytoskeletal architecture. PDPN-deficient FRCs were

strikingly elongated upon culture in these matrices (Figure 3.2c, d). Membrane protrusions rich in filamentous actin were less abundant in *Pdpn*$^{-/-}$ FRCs compared with wild-type (WT) FRCs; however, each protrusion extending from the cell body of *Pdpn*$^{-/-}$ FRCs was markedly longer than those of WT FRCs (Figure 3.2e, f). Finally, as in 2D, PDPN-deficient FRCs covered a smaller area in 3D compared with WT FRCs (Figure 3.2g). Thus, this phenotype reflects the defect in spreading and adhesion observed in 2D short-term cultures: *Pdpn*$^{-/-}$ FRCs are less able to adhere and spread on collagen, leading to fewer contact points being made with the substrate and FRCs adopting a longer or "stretched" appearance that actually covers a smaller area.

Given that adhesion and spreading are related to the ability of a fibroblast to contract, we next examined whether a lack of PDPN affected FRC contractility using multiple approaches. First, FRCs were treated with Y27632, an inhibitor of Rho-associated protein kinase (ROCK), a master regulator of contractility. Y27632-treated FRCs exhibited extensive cell elongation similar to PDPN deficiency; however, Y27632-treated FRCs were exhibited more protrusions than *Pdpn*$^{-/-}$ FRCs, indicating that PDPN may signal through additional pathways (Figure 3.3a-c). Next, as another measure of contractility, WT and PDPN-deficient FRCs were seeded into 3D collagen gels and allowed to contract the gels for 24 hours. WT FRCs rapidly contracted the gels, whereas PDPN-deficient FRCs were unable to significant contract the gels, even after several days of culture (Figure 3.3d and data not shown). Finally, as another measure of contractility, FRCs were plated on coverslips and stained for YAP, a transcription factor that has recently been shown to be critical for the contractility and tumor-supporting functions of cancer-associated fibroblasts[27]. In agreement with the gel contraction data, *Pdpn*$^{-/-}$ FRCs had significantly less nuclear (active) YAP (Figure 3.3e). Taken together, these results suggest that PDPN regulates fundamental aspects of FRC adhesion, elongation, and contraction.

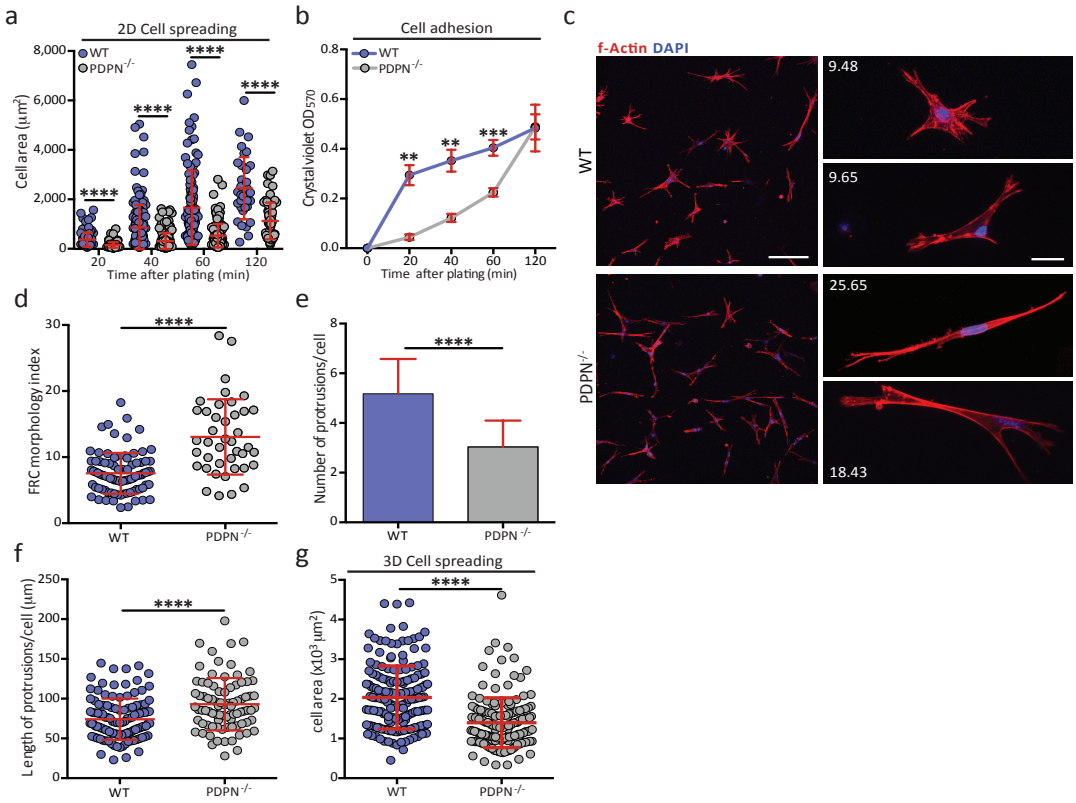

Figure 3.2. PDPN controls FRC spreading, elongation, and actomyosin contractility. a, Graphs depict the area covered by FRCs as they spread on collagen at different time points after plating. b, Graph representing the absorbance of crystal violet, which was used to stain FRCs adhering to collagen-coated wells at different time points after plating. c, Confocal images of WT and PDPN$^{-/-}$ FRCs seeded into 3D gels. Scale bar represents 100 μm in low magnification images (left) and 20 μm in high magnification images (right). Numbers indicate the morphology index value for the cell pictured. d, Quantification of FRC elongation (morphology index = perimeter^2/4πarea). e, f, Graphs depicting the number of protrusions per cell (e) and the lengths of individual protrusions (f) of FRCs in 3D gels. g, Quantification of the area covered by FRCs as they spread in collagen-based matrices. Data points represent cells from three independent experiments (mean±s.d., n>50 cells per experiment). Statistical analyses were conducted with a Student's t-test; **p<0.01; ****p<0.0001; n.s., not significant.

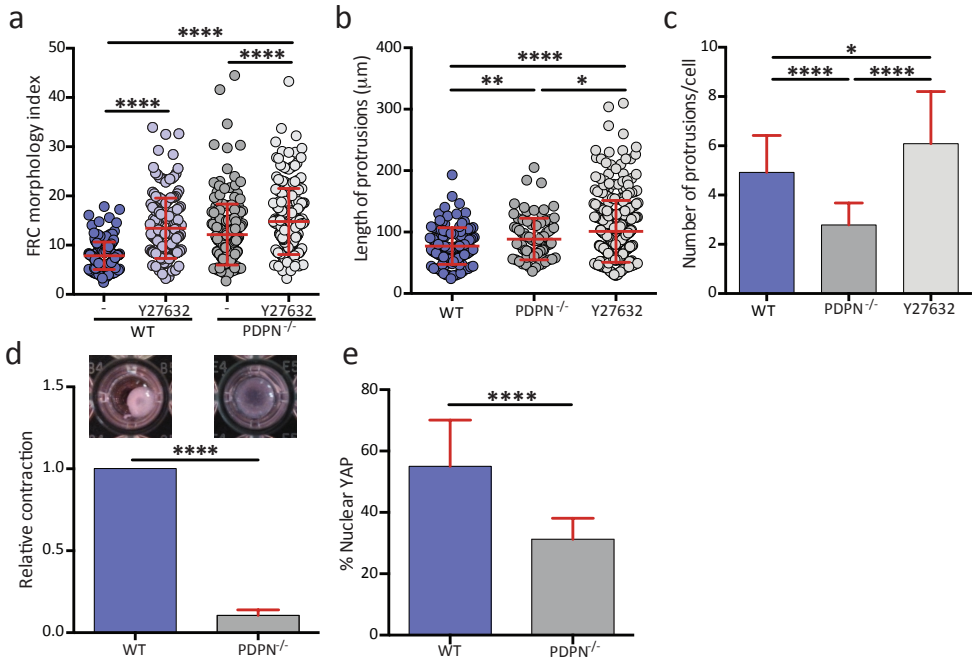

Figure 3.3. PDPN regulates FRC contractility. a, Morphology index of FRCs that were seeded into gels and left untreated or were treated with Y27632 for 12 hours. b, c, Graphs depicting the number of protrusions per cell (b) and the lengths of individual protrusions (c) of FRCs in 3D gels. Data points represent cells from three independent experiments (mean±s.d., n>50 cells per experiment). d, Relative amount that WT and PDPN$^{-/-}$ FRCs contracted collagen gels. Contraction was set relative to WT FRCs. Data are representative of five independent experiments (mean±s.d). e, Graph representing the percentage of cells with active, nuclear-localized YAP. Data are representative of three independent experiments (n>10 cells per experiment). Statistical analyses were conducted with a Student's t-test; *p<0.05; **p<0.01; ****p<0.0001.

PDPN cytoplasmic domain controls FRC elongation but is dispensable for contraction

The only known proximal signaling mechanism by which PDPN exerts direct effects on the cytoskeleton is by binding to and activating ezrin, radixin, and moesin (ERM) family proteins[25,26]. Given that a cluster of basic residues in the cytoplasmic tail of PDPN was identified as the ERM binding site[25], we generated knock-in mice in which PDPN lacking the cytoplasmic tail globally replaced full-length PDPN (hereafter referred to as Δcyto) (Figure 3.4), and the cytoskeletal architecture of Δcyto FRCs was examined. Deletion of the nine amino acid cytoplasmic tail was sufficient to recapitulate the elongated phenotype, with fewer, longer membrane protrusions, observed in the *Pdpn*$^{-/-}$ FRCs (Figure 3.5a-d). However, in the gel contraction assay, Δcyto FRCs were able to contract the gels nearly as well as WT FRCs (Figure 3.5e). In addition, the levels of active YAP in these cells were comparable to those in WT FRCs (Figure 3.5f). These results suggest that the extracellular or transmembrane domains of PDPN are largely responsible for actomyosin contraction in FRCs, perhaps through interactions with other transmembrane proteins.

Ezrin and myosin light chain are downstream mediators of PDPN function

We next examined the signaling downstream of PDPN in more detail. First, we stained FRCs for phosphorylated ezrin to determine whether it was rearranged upon deletion of PDPN. We did not observe any striking reorganization of this molecule, but the levels of the phosphorylated protein were diminished in the *Pdpn*$^{-/-}$ FRCs compared with the WT and Δcyto FRCs (Figure 3.6a). This finding was confirmed by western blotting for phosphorylated ERM proteins in WT, *Pdpn*$^{-/-}$, and Δcyto FRCs, which indicated that the levels were reduced about 50% in *Pdpn*$^{-/-}$ FRCs (Figure 3.6b, c). The degree to which pERM levels are reduced in *Pdpn*$^{-/-}$ FRCs is especially striking given that ERMs bind to multiple transmembrane proteins in addition to PDPN

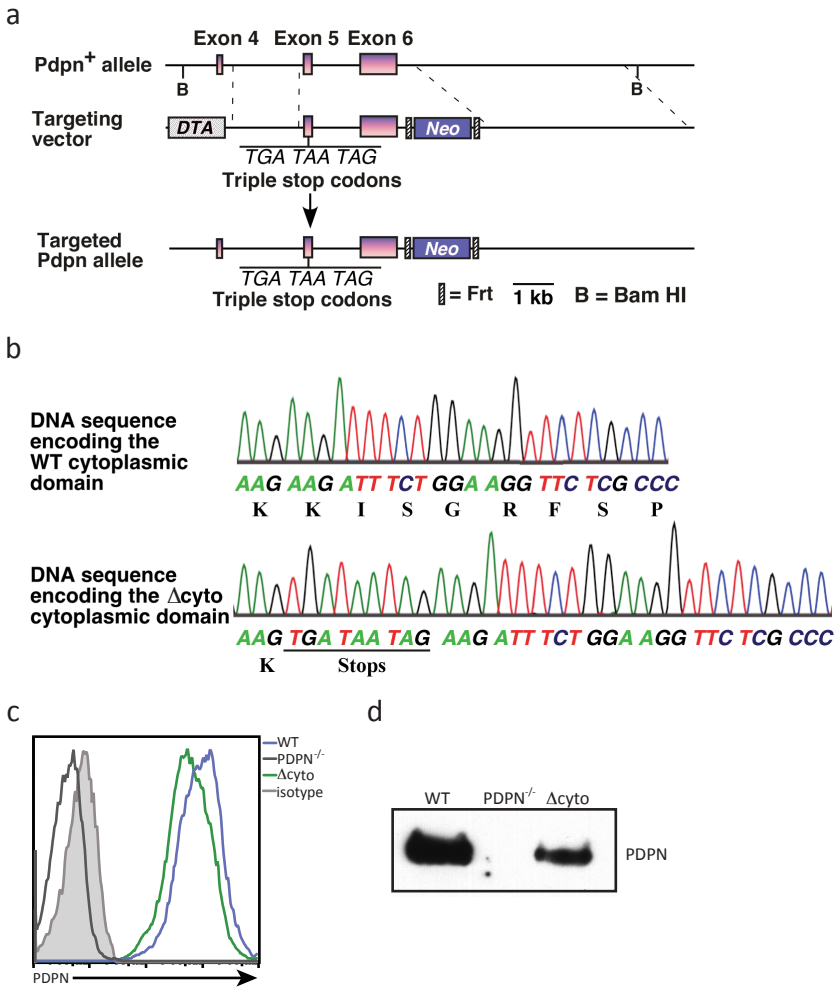

Figure 3.4. Generation of Δcyto mice. a, Schematic indicating the gene targeting strategy for the generation of the Δcyto mice. See methods for full details. b, Sequences of PCR fragments amplified from DNA from tail biopsies of WT and Δcyto pups indicating stop codons introduced after the transmembrane domain. c, Representative histogram indicating surface levels of PDPN on WT, PDPN$^{-/-}$, and Δcyto FRCs. d, Western blot showing total levels of PDPN in WT, PDPN$^{-/-}$, and Δcyto FRCs.

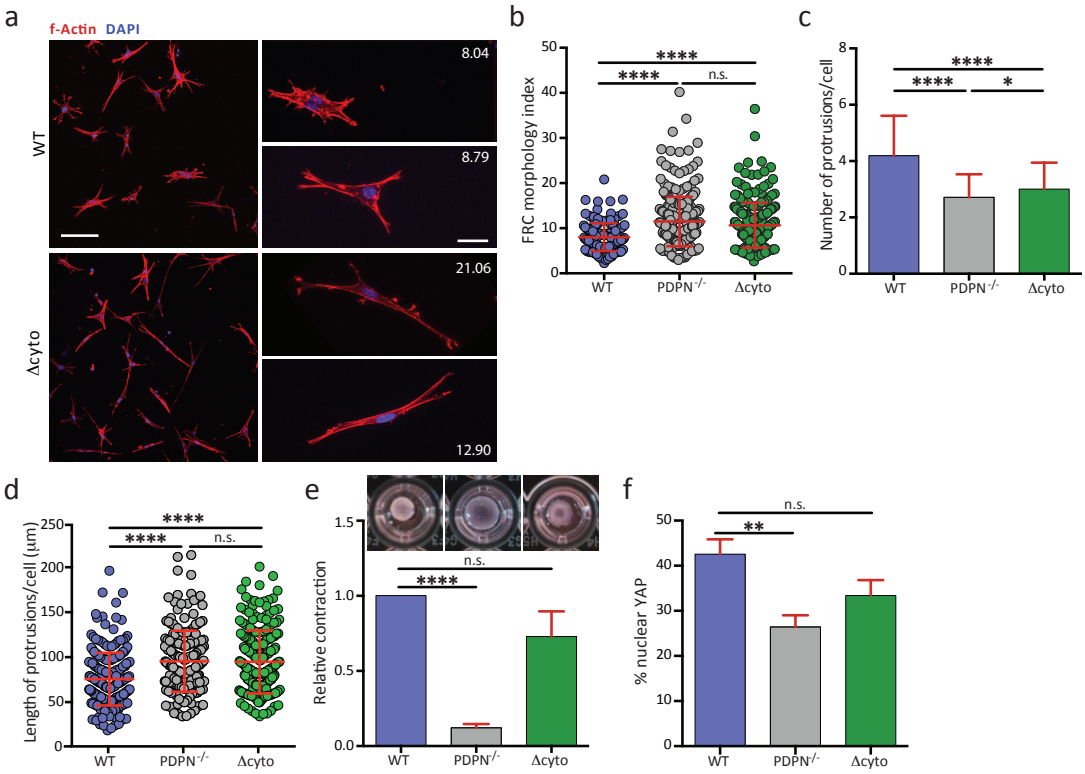

Figure 3.5. The PDPN cytoplasmic tail controls FRC elongation but is dispensable for contraction. a, Confocal images of WT and Δcyto FRCs seeded into 3D gels. Scale bar represents 100 μm in low magnification images (left) and 20 μm in high magnification images (right). Numbers indicate the morphology index value for that cell. b, Quantification of FRC morphology index. c, d, Graphs depicting the number of protrusions per cell (c) and the lengths of individual protrusions (d) for the FRCs. Data points represent individual cells from three independent experiments (mean±s.d., n>50 cells per experiment). e, Relative amount that WT, PDPN$^{-/-}$, and Δcyto FRCs contracted collagen gels. Contraction was set relative to WT FRCs. Data are representative of three independent experiments (mean±s.d.). f, Graph indicating percentage of active nuclear YAP in FRCs. Statistical analyses were conducted with a Student's t-test; *p<0.05; ****p<0.0001; n.s., not significant.

and suggests that PDPN contributes to a global regulation of ERM activation. This idea is further supported by the fact that phosphorylated ERM levels were normal in the Δcyto FRCs. While this result was somewhat surprising given that the cytoplasmic tail was previously reported to be required for activation of ERMs, those studies were conducted in epithelial cells using an overexpression system and elongation was not specifically examined. Thus, it is plausible that PDPN utilizes different signaling pathways in fibroblasts, or that the activation of ERMs is more dependent on other integral membrane proteins besides PDPN.

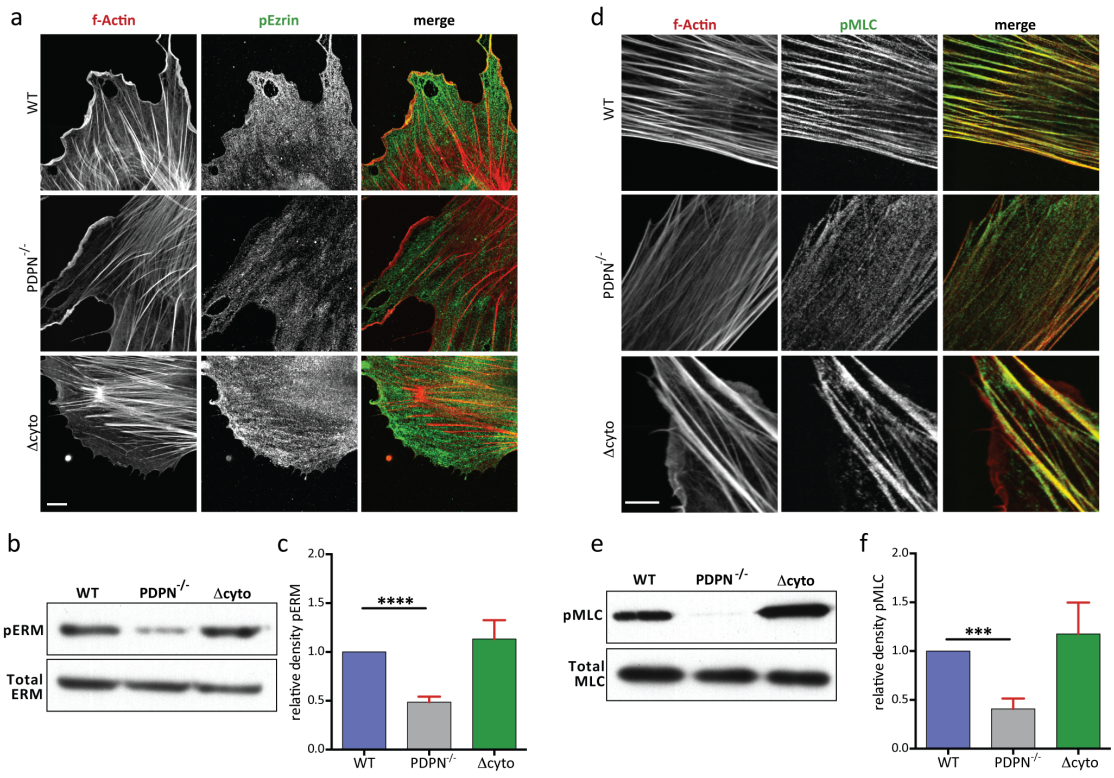

Figure 3.6. PDPN signals through ERM proteins and pMLC to mediate its effects. a, Representative images depicted pEzrin staining in WT, PDPN$^{-/-}$, and Δcyto FRCs. Scale bar, 10 μm. b, Representative western blot of the levels of total and activated ERM proteins in FRCs. c, Quantification of the relative levels of activated ERM proteins.

Figure 3.6 (continued). d, Representative images of pMLC staining in WT, *Pdpn*$^{-/-}$, and Δcyto FRCs. Scale bar, 10 μm. e, Western blot of pMLC levels in these FRCs. f, Quantification of relative pMLC levels from western blots, set relative to WT FRCs. Data are representative of 5 independent experiments. ***p<0.001; ****p<0.0001.

Due to the impaired contraction upon deletion of PDPN, we next examined the subcellular localization of phosphorylated myosin light chain (pMLC), a key regulator of contractility. In WT and Δcyto FRCs, pMLC strongly co-localized with the prominent actin filaments (Fig 3.6d). In contrast, and consistent with the functional contraction data, in *Pdpn*$^{-/-}$ FRCs, the pMLC molecules were not associated with actin filaments. Instead, they were more evenly distributed throughout the cell. Again, this finding was confirmed by western blot, which indicated that the pMLC levels were largely diminished in *Pdpn*$^{-/-}$ FRCs, whereas WT and Δcyto FRCs had similar levels of pMLC (Figure 3.6e, f).

Taken together, these data suggest that PDPN functions as a master regulator of the FRC actin cytoskeleton, orchestrating spreading, adhesion, and contractility. The fact that deletion of PDPN leads to a dramatic global decrease in pERMs and pMLC and that it causes a form of elongation that is distinct from simply blocking ROCK activity demonstrates that PDPN has global effects on several pathways controlling contraction. Furthermore, it is noteworthy that the cytoplasmic domain of PDPN is essential for controlling FRC elongation but not for maintaining contractility or normal levels of pERM and pMLC. These different requirements imply that the extracellular or transmembrane domains of PDPN are also critical for its functions. Perhaps these domains play a role in mediating the interactions between PDPN and several previously reported binding partners, such as CD44[28], CD9[29], or galectin-8[30].

PDPN controls normal FRC proliferation and survival

It is well known that fibroblasts are exquisitely sensitive to the stiffness of the substrates they adhere to and that they are capable of quickly responding to these external cues. For example, the extent to which fibroblasts can contract collagen gels has dramatic effects on their survival and signaling through the P13K-Akt axis[31,32]. Thus, we examined whether the PDPN-mediated decreased contractility of *Pdpn*$^{-/-}$ FRCs had any effect on their proliferation or survival. Upon culturing these cells, it was noted that while the numbers of WT FRCs and Δcyto FRCs did not increase substantially, the *Pdpn* $^{-/-}$ FRCs increased up to four-fold in number (Figure 3.7a). To determine whether this increase in cell numbers was due to increased survival or proliferation, we labeled the FRCs with CFSE and performed FACS to measure the mean fluorescent intensity of this dye over time. By day two, it was apparent that the PDPN$^{-/-}$ FRCs proliferated significantly more than WT FRCs (Figure 3.7b, c). In addition, AnnexinV staining indicated that *Pdpn*$^{-/-}$ FRCs also survived significantly better than either WT or Δcyto FRCs (Figure 3.7d, e). Overall, these data demonstrate that PDPN signaling is involved in regulating the growth and survival of FRCs. This effect may be secondary to the role of PDPN in maintaining contractility, as it has been previously reported that increased contractility of fibroblasts causes a downregulation of Akt signaling and increased death[31].

In vivo PDPN blockade causes lymph node expansion and FRC proliferation

Given the striking effects that PDPN deficiency had on the FRC cytoskeleton and actomyosin contractility on a cellular level, we next examined the effect of blocking PDPN on the FRC network *in vivo*. Due to the blood-lymph mixing phenotype and reduced viability found in global *Pdpn*$^{-/-}$ mice, we utilized a PDPN blocking antibody, clone 8.1.1, that recapitulates both the elongation and impaired contraction observed in *Pdpn*$^{-/-}$ FRCs (Figure 3.8a, b).

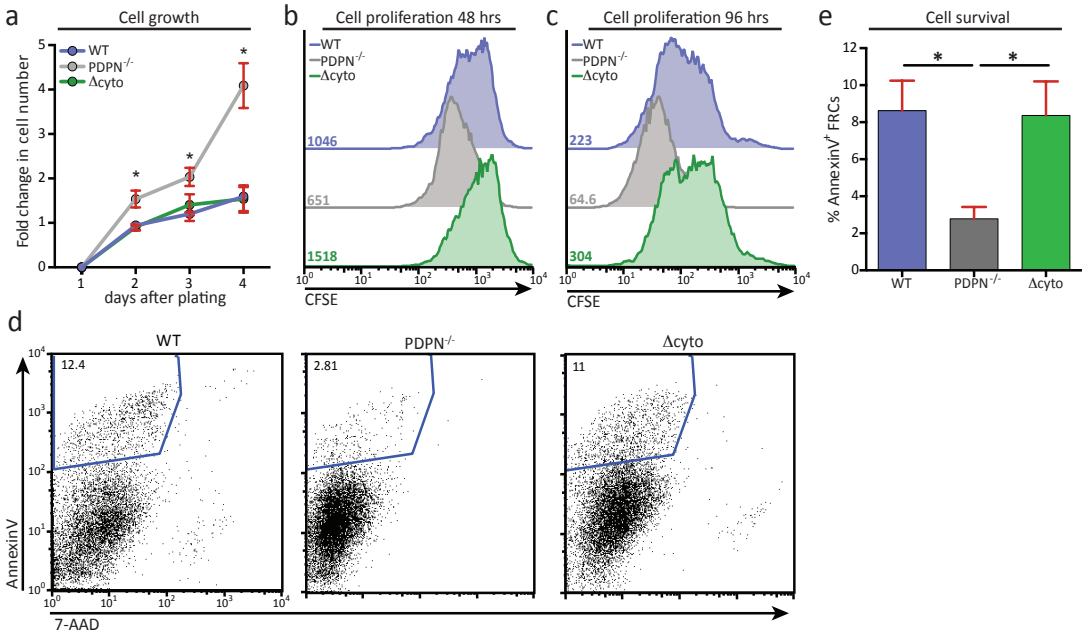

Figure 3.7. PDPN maintains normal FRC proliferation and survival. a, Graph indicating the relative amounts of cells present over four days of culture as measured by ATP content. Data are representative of three independent experiments (mean±s.d.). b, c, Representative histograms indicating CFSE staining of WT, *Pdpn*$^{-/-}$, and Δcyto FRCs after two (b) or four (c) days of culture. Numbers indicate the MFI for each condition. d, Representative FACS plots of AnnexinV and 7-AAD staining for apoptotic cells. Numbers in each gate indicate percentage of AnnexinV^{+} FRCs. e, Quantification of the percentage of AnnexinV^{+} FRCs. Statistical analyses were conducted with a Student's t-test; *p<0.05.

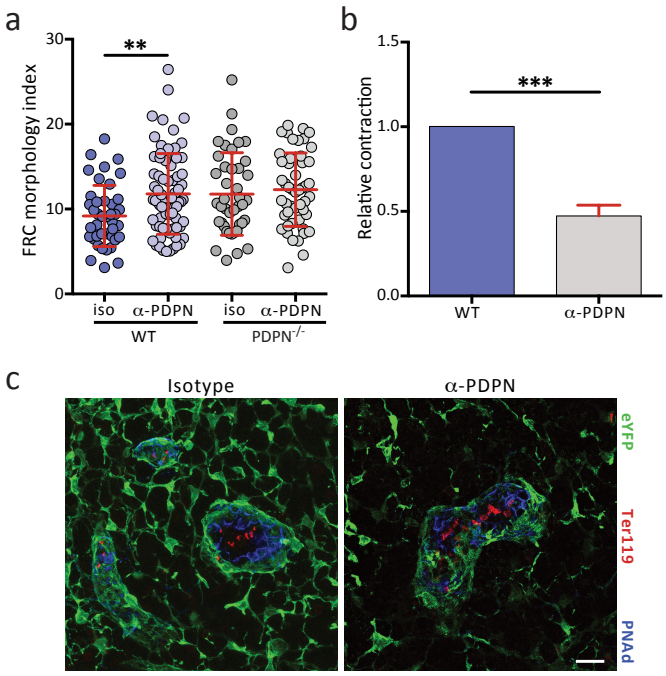

Figure 3.8. The α-PDPN antibody clone 8.1.1 recapitulates genetic deletion of PDPN. a, Graph depicting the FRC morphology index of WT and *Pdpn*$^{-/-}$ FRCs treated with the α-PDPN antibody for 12 hours. Representative of three independent experiments with >50 cells per experiment. b, Relative amount that untreated or α-PDPN-treated FRCs were able to contract collagen gels. The values are set relative to untreated FRCs and are representative of three independent experiments. Statistical analyses were conducted with a Student's t-test; ** $p<0.01$; *** $p<0.001$. c, Representative images of HEVs in lymph nodes from isotype- or α-PDPN-treated mice. Ter119 staining indicates red blood cells, which are confined within the HEV. eYFP staining indicates the FRCs.

We administered 8.1.1 i.v. into WT mice or *Ccl19*-Cre;*Rosa26*-eYFP mice (in which eYFP expression is restricted to FRCs[33]) and examined the lymph nodes by FACS and fluorescence microscopy, respectively, 48 and 96 hours later. We did not observe any gross abnormalities, such as the bleeding that has been reported in some transgenic mice[24,34], inflammatory infiltrates, or major disorganization of lymphocytes (Figure 3.8c and data not shown). The skin-draining lymph nodes were significantly enlarged at both time points, and while there was a slight increase in cellularity at 48 hours, there was no difference at 96 hours (Figure 3.9a, b). This increase in size without a great increase in cell numbers lead us to hypothesize that perhaps the lymph nodes would be more deformable if they did not have the inner pressure of expanded lymphocytes. Indeed, upon measuring lymph node stiffness, lymph nodes from antibody-treated mice were significantly less stiff than those from isotype-treated mice (Figure 3.9c).

Given the increased proliferation observed in ex vivo-expanded *Pdpn*$^{-/-}$ FRCs, in situ FRC proliferation was measured by BrdU labeling. Two days after antibody administration, the number of BrdU^{+} (proliferating) FRCs in LNs increased significantly; accordingly, at 96 hours, the numbers of LN FRCs were significantly increased over control-treated mice (Figure 3.9d, e). Additionally, the FRCs in antibody-treated mice were significantly larger, as measured by side and forward scatter (Figure 3.9f, g). Taken together with our *in vitro* data, these results suggest that PDPN blockade initiated a decrease in FRC contractility, leading to rapid relaxation of the FRC network and LN expansion. Then, either due to a direct signal from PDPN or a secondary signal due to the lack of contraction, LN FRCs began to proliferate and accrue in number, which allowed them to accommodate the increase in organ size.

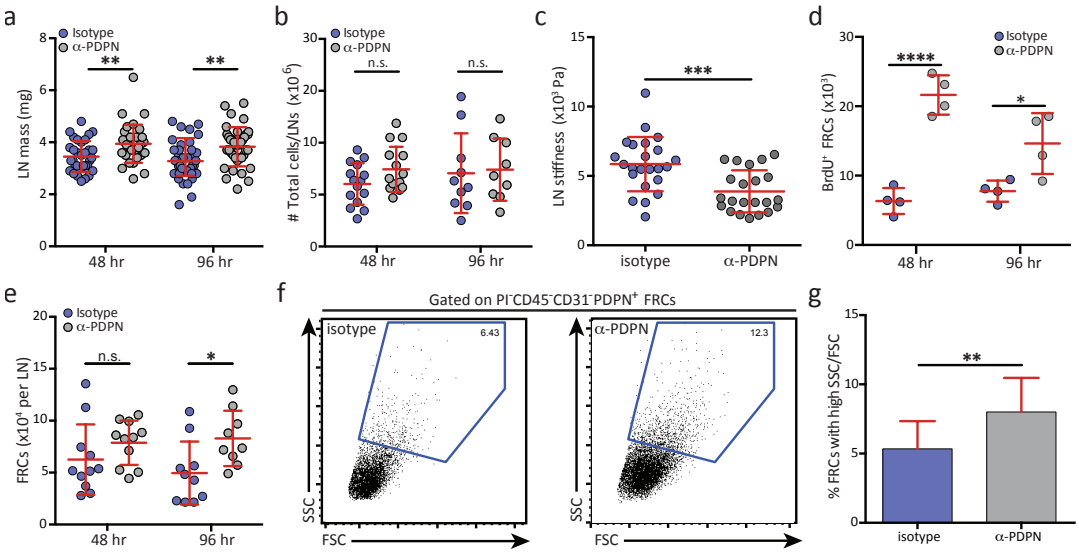

Figure 3.9. *In vivo* blockade of PDPN results in enlarged LNs and FRC proliferation and enlargement. a, Graph indicating LN mass from mice at 48 and 96 hours after i.v. injection of an isotype control or α-PDPN antibody. b, Total LN cellularity from isotype control or α-PDPN-treated mice. c, Graph indicating the stiffness of lymph nodes from control or α-PDPN-treated mice. d, The number of $BrdU^+$ proliferating FRCs in LNs from mice treated with an isotype control or α-PDPN antibody. e, Total numbers of FRCs ($PI^-CD45^-CD31^-PDPN^+$ cells) in LNs from mice treated with the isotype control or α-PDPN antibody. Data represent three independent experiments (each point is representative of one LN; mean±s.d., n>four mice per experiment). f, Representative FACS plots of the forward scatter (FSC) and side scatter (SSC) of FRCs (gated on $PI^-CD45^-CD31^-PDPN^+$ FRCs from total lymph node cells). g, Quantification of the percentage of FRCs with a high FSC/SSC. Data are representative of at least four independent experiments. Statistical analyses were conducted with a Student's t-test; *p<0.05; **p<0.01; ***p<0.001; ***p<0.0001; n.s., not significant.

In vivo PDPN blockade causes an expansion of the FRC network and disruption of high endothelial venules

We next examined how PDPN blockade affected the FRC network. First, the conduit network was examined at by injecting FITC into the hind footpads of isotype- or antibody-treated mice, and the popliteal LNs were collected 48 hours later. As FITC is smaller than the 70 kDa exclusion limit for entrance into the conduit system, the extensive collagen network underlying the subcapsular sinus could be visualized. No obvious abnormalities were noted in either the paracortical or cortical regions beneath the SCS in α-PDPN-treated mice (Figure 3.10). This suggests that the antibody did not totally disrupt fluid flow in the lymph nodes.

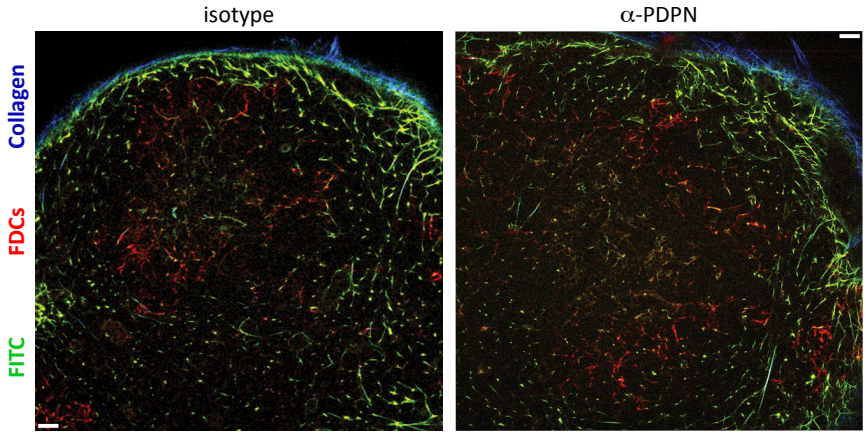

Figure 3.10. PDPN blockade does not affect conduit function. The footpads of isotype- or α-PDPN-treated mice were injected with FITC four hours before sacrifice, and the LNs were cleared and imaged. The scale bar indicates 30 μm.

We next examined the FRC reticular network. At 48 hours after antibody administration, when lymph nodes are enlarged but FRC numbers have yet to increase, the FRC network was significantly less dense and more space was evident between the FRC cell bodies and between the ERTR7^{+} fibers that FRCs secrete and remodel (Figure 3.11). Confocal microscopy combined

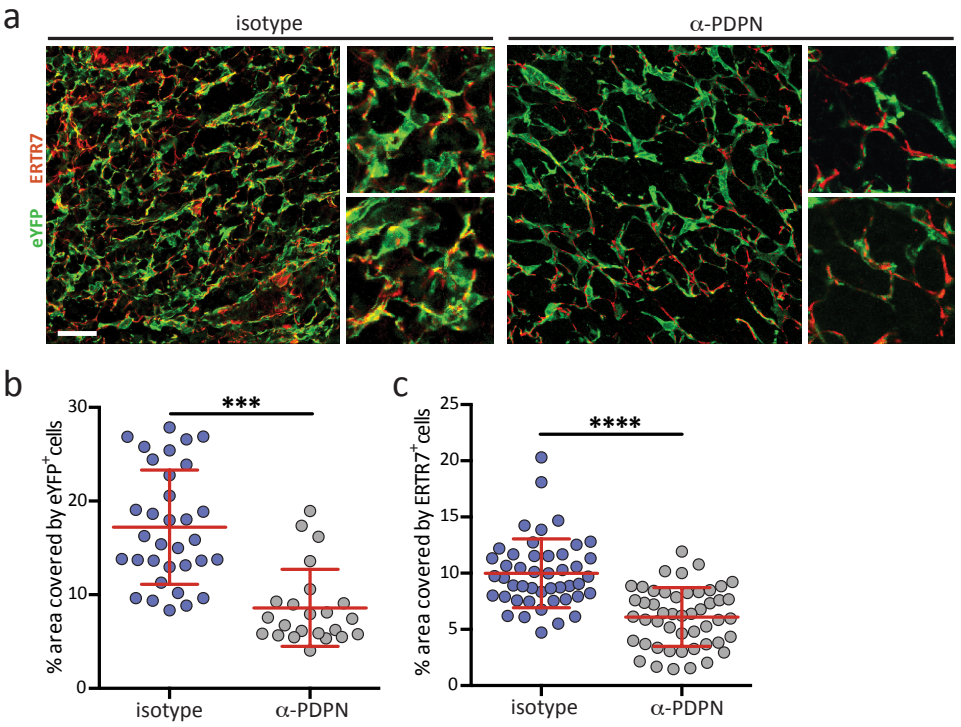

Figure 3.11. Blockade of PDPN decreases the area covered by FRCs and ERTR7 fibers. a, Z-stack projections of confocal images of the FRC network from LNs of isotype- or antibody-treated CCL19-cre;Rosa26-eYFP mice. b, c, Quantification of the percentage area covered by the FRCs (b) and ERTR7 (c). Statistical analyses were conducted with a Student's t-test; ***p<0.001; ****p<0.0001.

with 3D reconstruction and isosurface rendering revealed that there was less surface area and volume covered by the FRCs themselves and the ERTR7$^+$ fibers following administration of the PDPN blocking antibody (Figure 3.12). These differences were not present at 96 hours, once the FRC numbers had increased (data not shown). It is noteworthy that these differences were larger for the eYFP signal than for the ERTR7 signal, which may indicate that FRCs respond to PDPN blockade rapidly, whereas their accompanying ECM components are less malleable and

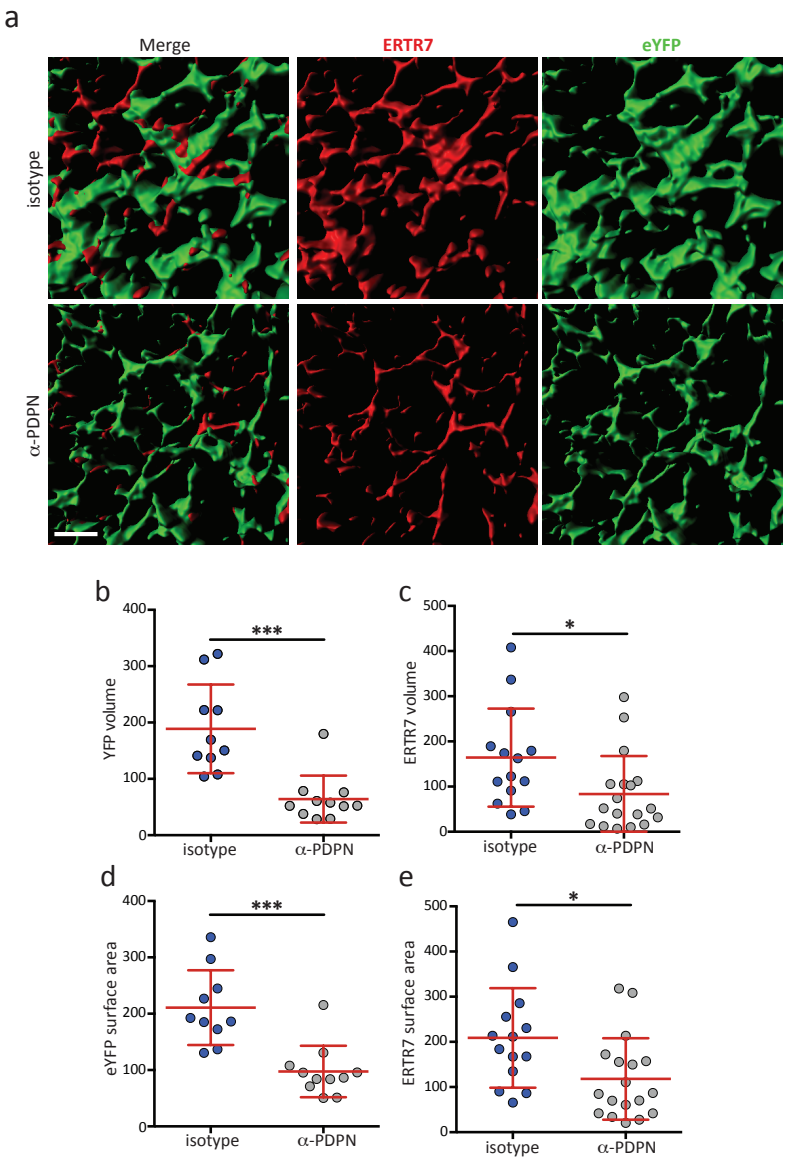

Figure 3.12. Blockade of PDPN decreases the surface area and volume covered by FRCs and ERTR7 fibers. a, 3D confocal images were analyzed in Imaris and isosurfaces were generated. Scale bar represents 20 μm. b, c, The total volume covered by eYFP (b) and ERTR7 (c) signals. d, e, The total surface area covered by eYFP (d) and ERTR7 (e) signals. Data representative three independent experiments (mean±s.d., at least three fields of view from the LNs of four mice per experiment). Statistical analyses were conducted with a Student's t-test; *p<0.05; ***p<0.001.

take longer to turn over.

The Δcyto mice provided an opportunity to dissect whether the elongation or impaired contraction were the main drivers of these in vivo effects, given that the cells were elongated but able to contract normally. The lymph node size, cellularity, and FRC numbers were all comparable between Δcyto and WT mice (Figure 3.13a-c). Furthermore, we did not observe any disrupted HEVs (data not shown), and accordingly, the numbers of B and T cells were not altered (Figure 3.13d, e). We next studied the FRC network to determine whether it was altered. In agreement with the normal lymph node size and FRC number, the area and volume covered by the $eYFP^+$ cells and $ERTR7^+$ fibers were comparable to those in WT mice (Figure 3.13f-j).

Finally, we examined the role of FRC PDPN in HEV function because a recent study demonstrated that the interaction between PDPN on FRCs and CLEC-2 on platelets is critical for HEV integrity[24]. In agreement with these findings, we observed significantly more disrupted HEVs in lymph nodes from the 8.1.1-treated mice compared with control-treated mice (Figure 3.14a, b). FRCs are normally tightly wrapped around the $PNAd^+$ endothelial cells but upon PDPN blockade, the FRCs became less closely associated with the vessels. We also observed a significant increase in T and B cells in the 8.1.1-treated LNs at this time point (Figure 3.14c, d), which may be due to increase blood flow through these HEVs. Disruption of HEVs and increased lymphocyte trafficking have been previously reported during the expansion of LN vasculature that occurs during immune responses[5].

These findings indicate that PDPN expression on FRCs has the intrinsic ability to maintain normal FRC spreading, contractility, proliferation, and homeostasis of the dense FRC network. A lack of PDPN, whether by genetic deletion or antibody blockade, results in elongated FRCs with diminished contractile function. In vivo, these effects translate to an inability of the FRCs to maintain lymph node size, the reticular network, and HEV integrity.

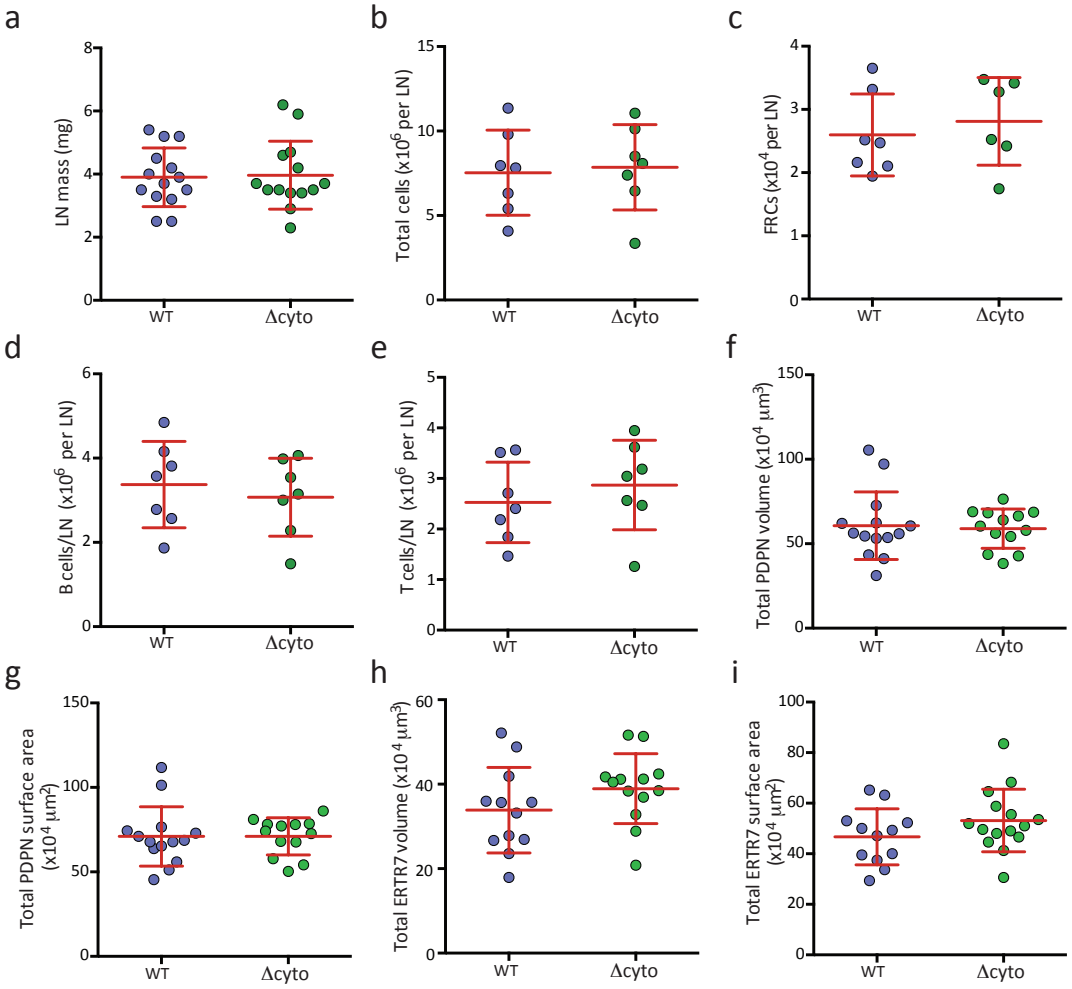

Figure 3.13. Lymph node size, FRC numbers, and the reticular network are unchanged in Δcyto mice. a, Graph indicating LN mass from WT and Δcyto mice. b, Total LN cellularity from WT and Δcyto mice. c, Total numbers of FRCs ($PI^-CD45^-CD31^-PDPN^+$ cells) in LNs from WT and Δcyto mice. d, e, The numbers of B (d) and T (e) cells in lymph nodes from WT and Δcyto mice. Data represent three independent experiments (each point is representative of one LN; mean±s.d., n>four mice per experiment). f, g, The total volume (f) and surface area (g) covered by FRCs (PDPN staining). h, i, The total volume (h) and surface area (i) covered by $ERTR7^+$ fibers. Data are representative of two independent experiments.

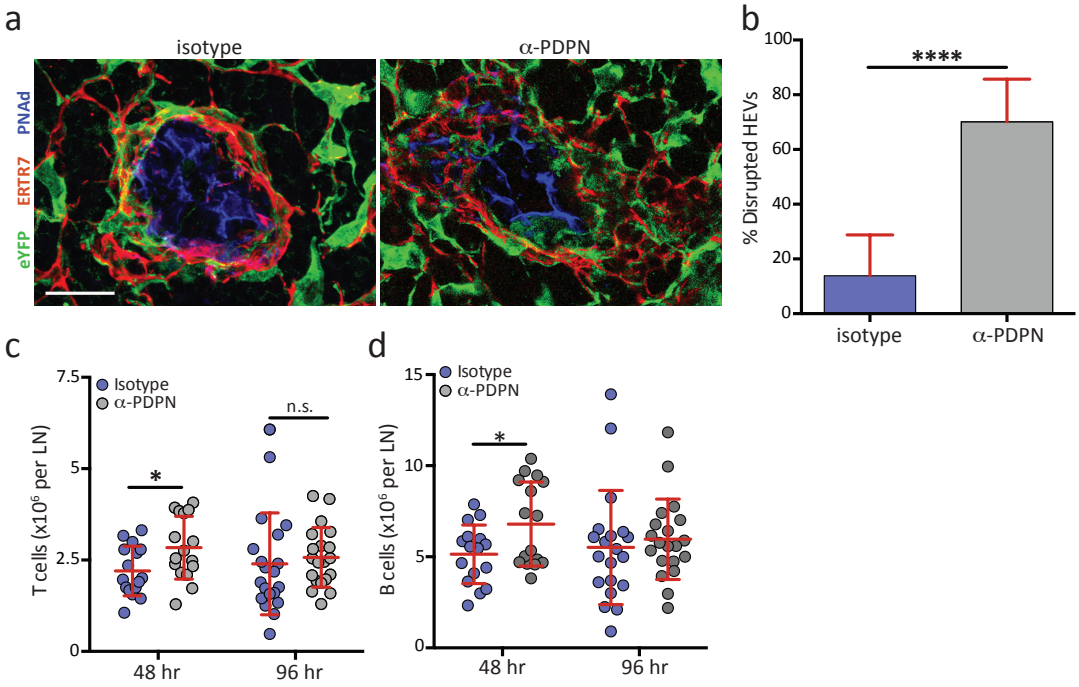

Figure 3.14. PDPN blockade disrupts HEV structure and increases B and T cell numbers. a, Representative images of HEVs in LNs from mice treated with either the isotype control or α-PDPN antibody. Data are representative of three independent experiments (mean±s.d., at least three fields of view from the LNs of four mice were analyzed per experiment). Scale bar represents 20 μm. b, Quantification of the percentage of disrupted HEVs in LNs of treated mice (n=12 fields from two mice over three independent experiments). c, d, T (c) and B (d) cell numbers present in LNs from mice treated with the isotype or α-PDPN antibody (n=four mice from three independent experiments). Statistical analyses were conducted with a Student's t-test; *p<0.05; ****p<0.0001; n.s., not significant.

Inhibition of PDPN causes a dysregulation of T cell responses to inflammation

Given the changes observed in lymph node homeostasis and the FRC network, we next examined how a lack of PDPN function and FRC contractility would affect an immune response. We hypothesized that blocking PDPN would exacerbate immune responses by causing greater LN swelling and FRC proliferation. To this end, WT mice were treated with the α-PDPN antibody two days before receiving purified CFSE-labeled OTI T cells i.v. Then, four hours later, LPS and ovalbumin were also given i.v. After another 48 and 96 hours, lymph nodes were collected from the mice, and lymph mass, FRC numbers, and OTI responses were measured. As predicted, lymph nodes from antibody-treated mice swelled to an even greater extent than those from isotype-treated mice. Furthermore, on day four after immunization, when control lymph nodes had already begun to contract, antibody-treated lymph nodes remained large (Figure 3.15a). As seen in steady state, these changes in lymph node mass were not accompanied by changes in total cellularity (Figure 3.15b).

In control mice, the number of FRCs was significantly increased just two days after immunization (Figure 3.15c), which is consistent with previous reports[35]. However, in the 8.1.1-treated LNs, FRC numbers increased even more and remained elevated at 96 hours after immunization, when FRCs in control mice had already begun to contract (Figure 3.15c). The signals regulating FRC proliferation during immune response have not been elucidated; our data indicates that it likely arises at least in part from a relaxation of FRCs as the lymph node swells, but there could also be other signals arising from direct sensing of inflammation or cytokines secreted by immune cells.

Finally, we examined the numbers of OTI cells in immunized LNs and found that while the numbers were comparable between control and treated animals at 48 hours, there were significantly more OTI cells present in 8.1.1-treated LNs 96 hours after immunization (Figure

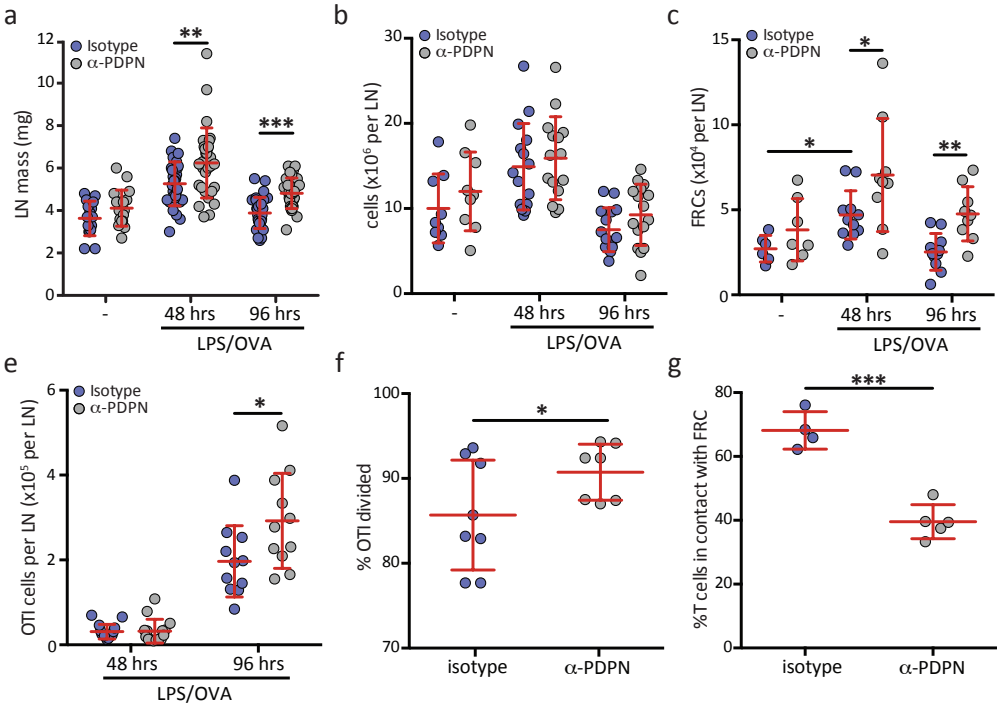

Figure 3.15. PDPN is required to control lymph node swelling and T cell proliferation following immunization. a, b, Graphs depicting the masses (a) and total cells (b) of lymph nodes from isotype- or α-PDPN-treated mice 48 and 96 hours after immunization with LPS and OVA. c, Total FRCs present in lymph nodes from isotype- or α-PDPN-treated mice 48 and 96 hours after immunization. d, Number of transferred OTI T cells in isotype- or α-PDPN-treated mice 48 and 96 hours after immunization. f, The percentage of OTI cells that had divided at least once at 48 hours after immunization. g, The percentage of T cells in contact with the eYFP^{+} FRC network in lymph nodes treated with the isotype control or α-PDPN antibody. Statistical analyses were conducted with a Student's t-test; *p<0.05; **p<0.01; ***p<0.001.

3.15e). The CFSE staining of these cells indicated that significantly more OTI cells had divided in α-PDPN-treated lymph nodes compared with control-treated lymph nodes immunization (Figure 3.15f). We previously reported that FRCs suppress T cell proliferation and that this requires cell-cell contact[36], and given that we observed greater spacing between FRCs upon PDPN blockade, we next examined whether there was a change in T cells touching FRCs in the antibody-treated mice. Indeed, significantly less T cells were in contact with the FRC network upon PDPN blockade compared with control mice (Figure 3.15g).

Overall, these findings indicate that PDPN-mediated control of FRC contractility is critical for the control of lymph node swelling and T cell responses to immunization. Without PDPN, lymph nodes swell more than in WT mice and do not contract normally as the response contracts. Perhaps more importantly, upon PDPN blockade, division of OTI cells was not as well controlled. This finding indicates that PDPN is required for proper FRC contact and subsequent suppression of activated T cells.

CLEC-2 engagement of PDPN recapitulates genetic deletion of PDPN

Although PDPN has striking effects on its own, data from this work and other studies[24,34] raised the possibility that the endogenous receptor for PDPN, CLEC-2, may induce PDPN signaling upon engagement. While these studies reported effects on the CLEC-2$^+$ DCs and platelets engaging with PDPN$^+$ FRCs, it is likely that the FRCs also receive a signal and respond to these close associations. To determine whether CLEC-2 engagement of PDPN has any effect on FRCs, WT FRCs were cultured in a 3D matrix and incubated with soluble CLEC-2-Fc or a control rabbit IgG. Within three hours, the FRCs became elongated, and by 12 hours, they closely resembled *Pdpn*$^{-/-}$ FRCs (Figure 3.16a, b). CLEC-2-Fc had no effect on the elongation of *Pdpn*$^{-/-}$ or Δcyto FRCs (Figure 3.16c), as expected because FRCs do not have Fc receptors[11]. To determine

Figure 3.16. CLEC-2 engagement of PDPN phenocopies a complete PDPN genetic deletion. a, Confocal images of control- and CLEC-2-Fc-treated WT FRCs in 3D Matrigels. Scale bar indicates 100 μm in low magnification images (left) and 20 μm in high magnification images (right). b, The morphology index for WT FRCs treated with CLEC-2-Fc for the indicated times. c, Graph depicting the morphology index for control- or CLEC-2-Fc-treated WT, $PDPN^{-/-}$, and Δcyto FRCs. d, Morphology index of FRCs co-cultured with WT or $CLEC\text{-}2^{-/-}$ bone marrow-derived dendritic cells that were either untreated or stimulated overnight with LPS. e, Morphology index of FRCs co-cultured with WT or $CLEC\text{-}2^{-/-}$ platelets. Data represent three independent experiments (mean±s.d.; n>60 cells for each condition). f, Images of PDPN staining in control- or CLEC-2-Fc-treated WT FRCs. Middle, example of PDPN clustering; Bottom, example of FRC-rich protrusions. Scale bar indicates 5 μm. g, Quantification of the percentage of FRCs exhibiting PDPN clustering or protrusions in response to CLEC-2-Fc treatment. h, Graph representing the morphology index of WT FRCs that were pre-treated with cytochalasin D prior to CLEC-2-Fc treatment. i, Relative contraction of CLEC-2-Fc-treated WT, $PDPN^{-/-}$, and Δcyto FRCs. Contraction was set relative to untreated FRCs. Data represent three independent experiments (mean±s.d.). j, Quantification of the percentage of control- or CLEC-2-Fc-treated WT FRCs with nuclear-localized YAP over time. Data are representative of three independent experiments (n>10 cells). k, Graph depicting the cell area of FRCs spreading on collagen in the presence or absence of CLEC-2-Fc. Data are representative of three independent experiments (mean±s.d., n>50 cells per experiment). Statistical analyses were conducted with a Student's t-test; *p<0.05; **p<0.01; ****p<0.0001; n.s., not significant.

Figure 3.16 (continued)

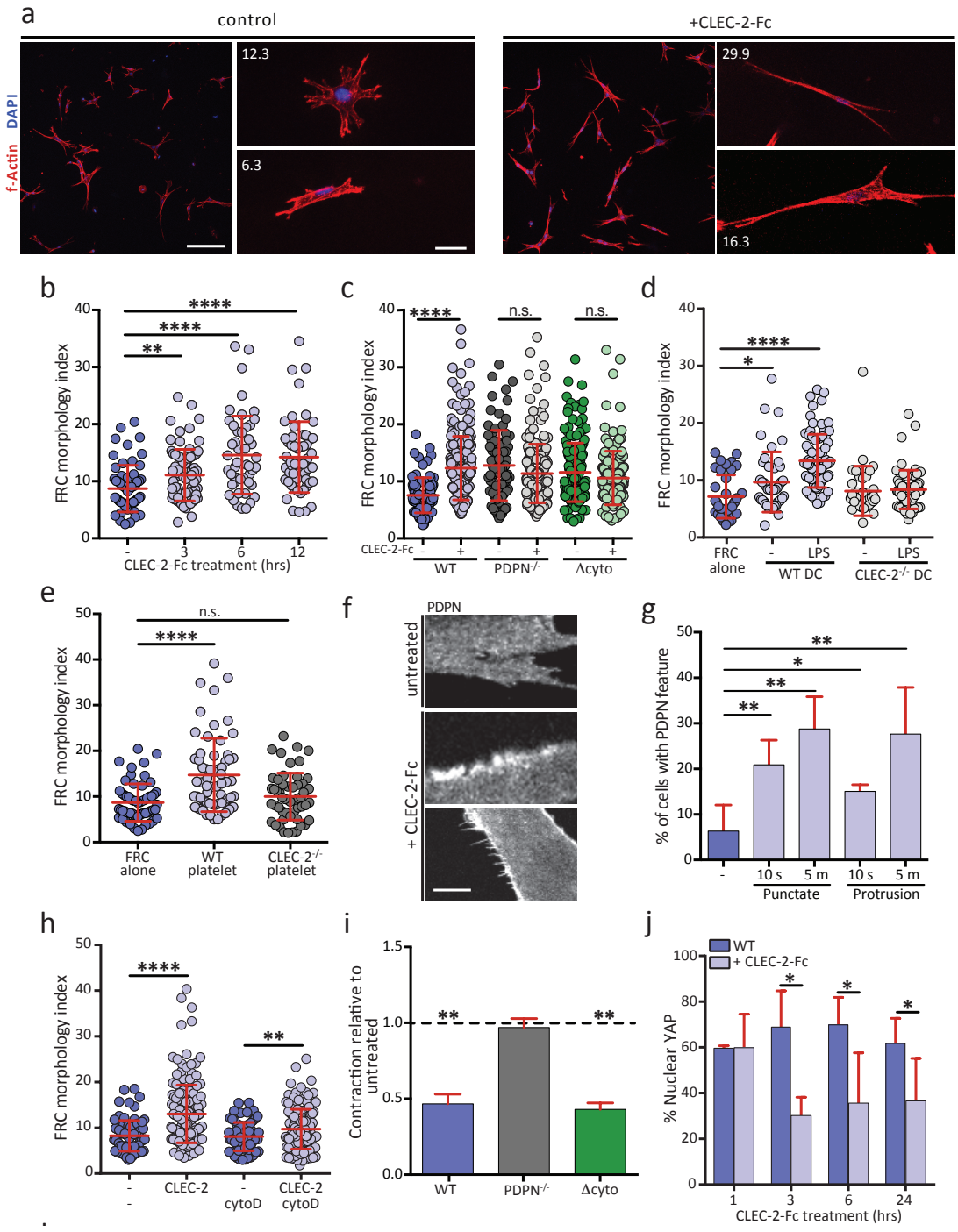

whether the same effect could be achieved with CLEC-2^{+} cells, we co-cultured WT FRCs with WT or *Clec-2*$^{-/-}$ platelets and with LPS-activated WT or *Clec-2*$^{-/-}$ bone marrow-derived DCs. LPS induces an increase in CLEC-2 ([37] and Figure 2.3). Notably, CLEC-2^{+} DCs and platelets induced elongation of the FRCs to a similar degree as soluble CLEC-2-Fc (Figure 3.16d, e).

Staining for PDPN indicated that CLEC-2-Fc treatment quickly induced both the clustering of PDPN and PDPN-rich membrane protrusions (Figure 316f, g). Thus, we examined whether this elongation was dependent on actin polymerization by pre-treating FRCs with cytochalasin D before adding CLEC-2-Fc. Cytochalasin D was used at low concentrations so as not to disrupt the cytoskeleton, but it did significantly reduce CLEC-2-Fc-elicited elongation in WT FRCs (Figure 3.16h).

Next, we examined whether CLEC-2-induced elongation was connected with a loss in contractility, as in PDPN-deficient FRCs. Upon CLEC-2 treatment of WT FRCs, the cells were significantly impaired in their ability to contract collagen gels and the amount of nuclear-localized YAP (Figure 3.16i, j). Additionally, CLEC-2 treatment of Δcyto FRCs also reduced their contractility (Figure 3.16i). This result further bolsters the idea that the extracellular domain of PDPN is critical for mediating contractility through lateral membrane interactions and that CLEC-2 inhibits PDPN by disrupting some of those interactions. Finally, treatment with CLEC-2-Fc impaired spreading of FRCs on collagen (Figure 3.16k). Overall, these data indicate that CLEC-2 engagement of PDPN phenocopies the complete deletion of PDPN, indicating that CLEC-2 inhibits the function of PDPN.

Finally, we tested whether CLEC-2 signaling resulted FRC relaxation and lymph node expansion in vivo. WT mice were administered CLEC-2-Fc or an isotype control i.v., and lymph nodes were collected one and four hours later. At one hour, lymph nodes had swelled and were significantly enlarged; however, by four hours, the lymph nodes had already contracted back to

baseline mass (Figure 3.17). Thus, as expected from our in vitro data, CLEC-2 delivers a quick but transient signal that causes a relaxation of the FRC network and lymph node expansion.

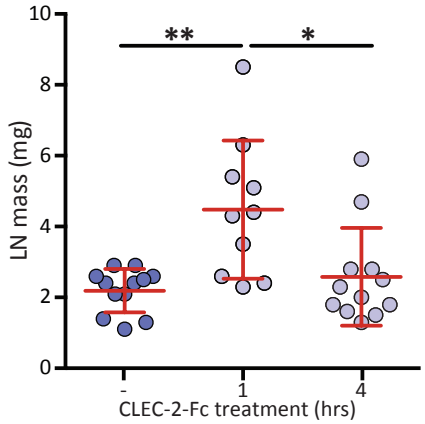

Figure 3.17. In vivo treatment with CLEC-2-Fc causes rapid lymph node swelling and contraction. Graph depicting the lymph node mass of wild-type mice treated with a rabbit isotype control (-) or with CLEC-2-Fc for one or four hours.

Discussion

FRCs are specialized fibroblasts that closely interact with lymphocytes and DCs[38,39]. Thus, they are uniquely positioned to play a role in orchestrating immune responses and have been shown to control T cell proliferation[36,40,41], support DC migration[12], and maintain vascular integrity[24,34]. Here, we expand upon a long-standing observation that FRCs are contractile by first identifying PDPN as a master regulator of contraction and, second, by elucidating a function for this contraction in regulating homeostasis of the FRC network, HEV integrity, and T cell responses. Genetic deletion of PDPN causes FRCs to become greatly elongated and inhibits their ability to contract extracellular matrix components. Interestingly, the cytoplasmic domain of

PDPN is required for maintaining normal FRC elongation, but works through an unknown signaling pathway. In contrast, the cytoplasmic domain is dispensable for FRC contractility, indicating that the extracellular and transmembrane domains of PDPN are responsible for conferring this ability.

Several reports from varied fields have detailed the molecular interactions that PDPN engages in through its extracellular and transmembrane domains. PDPN interacts with CD44 and galectin-8, both of which are involved in adhesion and spreading[28,30]. PDPN also interacts with CD9, a tetraspanin involved in regulating integrin signaling[29], and must be present in lipid rafts to signal properly[42]. These studies have largely been conducted in epithelial cells with overexpression studies. Thus, further work is necessary to determine which interactions are most important in FRCs. Furthermore, as the regulation of contraction is a newly identified function of PDPN, these interactions must be re-examined to determine which are involved in this specific function.

PDPN deletion also resulted in increased proliferation and survival in FRCs. This effect is likely secondary to the loss of PDPN-mediated contraction, but more work is needed to confirm this hypothesis. Cell contractility and sensing matrix stiffness are extremely important processes in all cells, especially fibroblasts, and are known to regulate differentiation, migration, and survival[43]. There is a balance between cell adhesion to a substrate of a given stiffness and the resulting amount of tension that forms within the cell due to actomyosin signaling downstream of integrins, which under normal physiological conditions results in a tensional homeostasis[44,45]. Disruption of this balance, whether by a change in matrix stiffness or a loss in the ability to contract within the cell, results in dysregulated proliferation. For example, integrin-dependent signaling through the PI3K/Akt/PKB axis regulated fibroblast survival and was dependent on fibroblast contraction of collagen gels[31,32]. Thus, the fact that *Pdpn*$^{-/-}$ FRCs cannot efficiently

adhere to substrates and contract causes uncontrolled growth and proliferation.

The effects of PDPN deletion that we observed in vitro translated to global changes in lymph node homeostasis and immune cell function when PDPN was blocked in vivo. The dense FRC network has been well-studied and is known to support the migration and survival of DCs and T cells and to deliver small molecules through the conduit system[10,12,14,38]. However, the roles played by FRC contractility or ECM remodeling has not been explored. Now, we demonstrate that disrupted PDPN contractility causes an enlargement of the whole lymph node and an expansion of the spacing between FRC fibers. It is possible that some of these changes are caused by changes to lymph flow, as the α-PDPN antibody would also bind to LECs. While PDPN functions in LECs are not well-defined, PDPN has been reported to control in vitro tube formation and downstream RhoA signaling[46]. Thus, it is possible that the PDPN blockade causes a relaxation in LECs, which could result in increased lymph flow and lymph node swelling.

It was recently demonstrated that FRCs proliferate in response to inflammatory signals[35], but a specific molecule governing this process was not identified. Our data reported here indicate that a relaxation of the FRCs likely also contributes to this proliferation. Intriguingly, it was noted there and elsewhere that PDPN levels increase on FRCs in response to a variety of inflammatory stimuli[35,47]. This increase in PDPN could, at least in part, be involved in restoring high levels of contractility to FRCs and contribute to lymph node contraction after resolution of the immune response. This process is critical to controlling immune responses, as indicated by the increased OTI cell proliferation and numbers upon PDPN blockade and continued lymph node swelling.

Finally, we detail a role for CLEC-2 engagement of PDPN in inhibiting normal PDPN signaling. Previous studies examining the function of PDPN-CLEC-2 interactions focused on signaling downstream of CLEC-2 upon engagement with the PDPN ligand. First, a recent study[24]

found that platelet CLEC-2 and FRC PDPN are required to maintain HEV integrity. Second, a study by Benezech, et al.[34] further elucidated a role for platelet CLEC-2 in the maintenance of adult LNs. Finally, in Chapter 2 of this dissertation, we described the effects that CLEC-2 engagement of PDPN has on DCs. Our data indicate that there is signaling on both sides of this interaction and that FRCs sense and respond to interactions with CLEC-2^+ cells. Furthermore, CLEC-2 delivers a fast, inhibitory signal to PDPN to briefly relax FRCs and allow for lymph node expansion.

Overall, our data indicate that during the earliest stages of an immune response, interactions between CLEC-2^+ DCs and platelets entering the LN could initiate a relaxation of the FRC network and in turn result in an expansion of FRCs to support the enlargement of LNs and proliferation of lymphocytes. Then, as the inflammatory signals cause an upregulation of PDPN, and the CLEC-2 signal is removed, FRCs would regain their contractility and this would promote a return to homeostasis in the reticular network.

Methods

Mice

C57BL/6 mice were purchased from Jackson Laboratory. *Ccl19-cre* mice were generated as previously described[33] and were crossed to *Rosa26-eYFP* mice (Jackson Laboratory) to generate mice where only FRCs express eYFP. To determine the cytoplasmic function of PDPN, we generated knock-in mice lacking the cytoplasmic tail of PDPN (Δcyto). To delete the cytoplasmic domain, we made a targeting construct that introduced three stop codons immediately after the sequence encoding its transmembrane domain. C57BL/6 embryonic stem (ES) cells were used for gene targeting. A neomycin cassette flanked by Frt sites was used for selection of positive ES clones. DTA was used for negative selection. Two positive ES clones were injected into C57BL/6J blastocytes, which were then implanted into pseudopregnant mice. Chimeras among the offspring were bred with C57BL/6J FLP mice (B6.Cg-Tg (ACTFLEe)9205Dym/J, Jackson Laboratories) to test germline transmission and to delete the Frt flanked neomycin cassette. Genotypes of mice were determined by conducting PCR on DNA isolated from tail biopsies. Four chimeras transmitted the PDPN knock-in mutation into their offspring. Breeding with the FLP mice also successfully deleted the Frt flanked neomycin cassette in the F1 generation. Mice were maintained under specific pathogen-free conditions as mandated by the National Institutes of Health guidelines. The mice were used between 4-7 weeks of age and were age and sex matched for all experiments. Animal studies were approved by the Research Animal Care committee of Dana-Farber Cancer Institute.

Stromal cell isolation

For cell culture or flow cytometry analysis, stromal cells were isolated from LNs as previously described[48]. Briefly, skin-draining and mesenteric LNs were incubated in digestion

media (RPMI containing 0.1 mg/ml DNase I (Invitrogen), 0.2 mg/ml Collagenase P (Roche) and 0.8 mg/ml Dispase (Roche)) and cell fractions were collected every 10-15 minutes over a period of 45 minutes. The single cell suspension was filtered and either plated in α-MEM containing 10% FBS and 1% penicillin-streptomycin or were stained with antibodies for fluorescent-activated cell sorting (FACS) analysis.

FRC isolation

After LN digestion and plating, the non-adherent hematopoietic cells were washed away and the remaining stromal cells were allowed to grow for 5-7 days. To purify FRCs from this mixed culture, cells were trypsinized and incubated with biotinylated anti-CD31 and anti-CD45 antibodies for 10 minutes. After washing, the cells were incubated with anti-biotin microbeads for 15 minutes. Then the cells were washed, run through an LS magnetic-activated cell sorting column (Miltenyi Biotech), and the flow-through containing FRCs was collected. FRCs used in experiments were greater than 85% pure.

3D Matrigel cultures and imaging

For 3D cultures, gels were prepared as previously described[49]. Briefly, 15,000 FRCs were mixed with 100 μL of the Matrigel mix (1.8 mg/ml reduced growth factor Matrigel (BD Biosciences) and 3.2 mg/ml type I collagen (BD biosciences)) and plated in glass-bottom 24 well plates (MatTek Corporation, Ashland, MA, USA). For treatment conditions, a final concentration of 10 μg/mL α-PDPN, 7 μg/mL CLEC-2-Fc, or appropriate controls was added to the cell suspensions 15 minutes before the addition of the Matrigel mix. Or, for short-term treatments, the cells were allowed to populate the gels for 24 hours and 250 nm cytochalasin D (Sigma), 10 μm Y27632 (Sigma) or 7 μg/mL CLEC-2-Fc were added directly to the media. To image the cells,

the media was removed and the gels were washed twice in PBS. Next, cells were fixed in 4% paraformaldehyde (PFA; Affymetrix, Santa Clara, CA, USA), washed, and permeabilised in 0.25% Triton-X. Cells were then stained with DAPI and rhodamine phalloidin (Invitrogen). Finally, the gels were washed with PBS and then imaged with a Leica SP5X laser-scanning confocal microscope. Z-stack projections were generated in ImageJ (imagej.nih.gov), and the area and perimeter of the cells were measured. The morphology index was calculated with the following equation: $\text{perimeter}^2/4*\pi*\text{area}$.

FRC spreading and adhesion

For spreading, 10 cm dishes were coated with type I collagen according to the manufacturer's instructions (BD Biosciences). FRCs were plated and imaged with a light microscope at the indicated times. Cell area was determined with ImageJ (NIH). For adhesion, 96 well plates were coated with collagen, and 2,000 FRCs per well were added. At the indicated times, the wells were washed three times with PBS to remove non-adherent cells and the adherent cells were fixed in 4% PFA then stained with crystal violet. After several washes to remove unbound crystal violet, the cells were lysed in 0.25% Triton-X and the absorbance of crystal violet was determined with a spectrophotometer at 570 nm.

Western blotting

Purified FRCs were plated in 10 cm dishes at a density of 300,000 cells per plate overnight. Cells were serum-starved for 5 hours and then were lysed in lysis buffer (25 mM Tris-HCl pH 7.4, 150 mM NaCl, 1 mM EDTA, 1% NP-40 and 5% glycerol; Thermo Scientific) containing protease and phosphatase inhibitor cocktails (Thermo Scientific). The lysate was incubated on ice for 10 minutes and then centrifuged for 10 minutes at 10,000xg. The soluble fraction was

collected and protein concentration was determined with the BCA protein assay kit (Thermo Scientific). Equal amounts of protein were loaded onto 4-12% Bis-Tris gels (Life Technologies) and then proteins were transferred to a nitrocellulose membrane. After blocking in 5% non-fat milk for 1 hr, the membranes were incubated with primary antibodies in 5% BSA overnight. The following primary antibodies were used: anti-ERM, anti-pERM, anti-MLC, and anti-pMLC (S19) (all from Cell Signaling Technology, Danvers, MA, USA). After three washes with TBS, the membranes were incubated with an anti-rabbit antibody conjugated to HRP (Cell Signaling Technology) for two hours at room temperature. Finally, the signal was visualized with the SuperSignal WestDura Chemiluminescent Substrate (Fisher).

Gel contraction assay

For contraction assays, 10,000 cells were mixed with 50 μL of the Matrigel mix described above and plated in 96 well culture dishes. Once the gels had polymerized, 100 μL of media was added to the wells, and gels were detached from wells of the plate with a sterile pipette tip. After 24 hours, images were taken of the wells and dimensions of gels were measured relative to well diameter in ImageJ (NIH). For experiments where CLEC-2-Fc or 8.1.1 were added, the cells were allowed to seed the gel overnight before the gels were detached from the well. Then CLEC-2-Fc or 8.1.1 were added every 4-8 hours and the contraction was measure 24 hours later.

Proliferation assays

To measure the numbers of FRCs present in cultures over four days, 2,000 WT, PDPN$^{-/-}$, and Δcyto FRCs were plated in triplicate at a density of 2,000 cells per well in a 96 well plate. On days one, two, three, and four, the number of viable cells was measured with the CellTiter-Glo Luminescent Cell Viability Assay (Promega), according to the manufacturer's instructions. Data

were normalized to the amount of cells present on day 1 for each condition. To determine the amount the cells proliferating, FRCs were labeled with 1 μM of Carboxyfluorescein succinimidyl ester (CFSE; Invitrogen) and then 30,000 FRCs per well were plated in 6 well plates. On days one, two, three, and four, the cells were trypsinized and analyzed by FACS to determine the mean fluorescent intensity of the CFSE dye.

YAP staining

WT or *Pdpn*$^{-/-}$ FRCs were plated on eight well chamber slides and allowed to adhere for 12 hours in order to minimize the role of differential cell spreading in the quantification of nuclear YAP. Where indicated, CLEC-2-Fc was added to the medium for 15 minutes prior to plating. After 12 hours, the media was changed and fresh media either containing CLEC-2-Fc or not was added. At each time point, cells were fixed for 15 minutes with 4% PFA and washed three times for five minutes in PBS. Immunostaining was performed with a rabbit anti-mouse anti-YAP/TAZ antibody (Cell Signaling) and visualized using a goat anti-rabbit secondary antibody conjugated to Alexa-555 (Cell Signaling) per the manufacturer's instructions. Nuclei were counterstained with DAPI. The percentage of nuclear YAP was quantified using MATLAB software by summing the fluorescence intensity within the region masked by the nucleus compared to the total fluorescence intensity on a per-cell basis.

In vivo experiments with the α-PDPN antibody

C57BL/6 mice between 4-6 weeks of age were injected i.v. into the tail vein with 100 μg of purified α-PDPN (clone 8.1.1, Biolegend) or the hamster IgG isotype control antibody (clone SHG-1, Biolegend). After 48 or 96 hours, the mice were sacrificed and the skin-draining LNs were collected for either FACS analysis or sectioning and imaging.

Immunizations

To investigate the role of PDPN during an immune response, BoyJ mice were first given the 8.1.1 antibody as described above. Two days later, CD45.2^{+} OTI cells were isolated from *Rag*$^{-/-}$ mice and were labeled with 1 μM CFSE (Invitrogen). Then, 1x10^{6} OTI cells were injected i.v. into each mouse. Four hours later, 500 μg of OVA and 30 μg of LPS were injected i.v. into each mouse. The mice were analyzed two and four days after administration of the OTI cells, LPS, and OVA. Axillary and brachial LNs were collected and digested for FACS analysis, while inguinal LNs were collected and fixed for imaging.

GTPase Pulldowns

For each condition, 1 X 10^{6} WT *Pdpn*$^{-/-}$, and Δcyto FRCs were plated in 10 cm dishes. The activation status of Rac-1 and RhoA were determined with active Rac-1 and RhoA pulldown kits (Thermo Scientific), following the manufacturer's instructions. Equal amounts of protein were run in gels and western blots were performed with anti-Rac1/2/3 (Cell Signaling) or anti-RhoA (Thermo Scientific) antibodies followed by an anti-rabbit-HRP secondary antibody (Cell Signaling).

Compression tests

Mice were treated with the hamster isotype control or anti-PDPN antibody 48 hours prior to collection of the lymph nodes. Cylindrical discs (1.3 mm^{2}) were punched from lymph nodes with a biopsy punch to ensure a consistent cross-sectional area. These samples were subjected to compression using an Instron mechanical tester at a strain rate of 0.5 mm/min, and the stiffness was calculated as the slope of the first 10% of the resulting stress/strain curve.

FACS analysis and antibodies

After the enzymatic LN digestion, cells were resuspended in FACS buffer (PBS containing 2% FBS and 2 mM EDTA) and were incubated for 15 minutes with the following antibodies: anti-PDPN (clone 8.1.1, Biolegend), anti-CD31 (clone MEC13.3, Biolegend), anti-CD45 (clone 30-F11, Biolegend), anti-B220 (clone RA3-6B2, eBioscience), anti-CD3e (clone 17A2, Biolegend), anti-CD4 (clone RM 4-5, eBioscience), anti-CD8 (clone 53-6.7, Biolegend). For the BrdU labeling, mice were injected i.p. with 2 mg of BrdU 24 hours before analysis. Cells were stained with the BrdU flow kit according to the manufacturer's instructions (BD Pharmingen). Cells were then analyzed on either a FACSCalibur or a FACSAria (both from BD Biosciences). FACS data were analyzed with FlowJo.

Immunofluorescence staining of cells and tissue sections

Cells were plated on collagen-coated coverslips and allowed to adhere overnight. Then they were washed with PBS, fixed in 4% PFA for 10 min, and permeabilized with 0.25% Triton-X before staining with anti-PDPN (clone 8.1.1, Biolegend). LNs were collected from mice and fixed in 4% PFA for 4 hours. Then they were incubated in 30% sucrose in PBS overnight. Finally, the LNs were frozen in optimal cutting temperature media (Fisher Scientific) on dry ice and then 20-80 μm sections were cut with a cryostat. Slides were stained immediately or stored at -80°C. Sections were fixed in 4% PFA for 10 min, then permeabilized with 0.25% Triton-X for three minutes, and then were blocked with 2% BSA in PBS for 30 min before incubation with antibodies. The sections were incubated with were anti-ERTR7 (AbCam), anti-GFP (Molecular Probes), and anti-PNAd-biotin (clone MECA-79, Biolegend) for 1 hour, then were washed three times with 2% BSA. The secondary antibodies anti-rat-Alexa-555, anti-rabbit-Alexa-488, and streptavidin-647 (all from Invitrogen) were then added for 30 minutes. After a final wash step,

the slides were imaged on either a Leica SP5X laser-scanning confocal microscope or a Zeiss 710 two photon laser-scanning confocal microscope. Images were analyzed with ImageJ. The percentage area covered was measured with CellProfiler[50] and the surface area and volume analyses were conducted with Imaris (Bitplane AG, Zurich, Switzerland).

Tracer injection and conduit imaging

WT mice were injected i.v. with the isotype control or α-PDPN antibody. Four-eight hours later, they were injected subcutaneously in the footpad with 10 μL saturated FITC solution (Sigma) in HBSS (~0.1 mg/mL). Popliteal LNs were collected four hours post injection and fixed in 4% PFA. LNs were optically cleared as previously described[51], and mounted as whole organ explants for multi-photon microscopy. Cortical and paracortical regions were identified by collagen density and presence or absence of an anti-CR1 follicular dendritic cell antibody (clone 8C12, made in-house) of which 3 μg was injected i.v. six hours prior to the start of the experiment.

Isolation of platelets and BMDCs from fetal liver chimeric mice

Clec-2$^{-/-}$ fetal liver chimeric (FLC) mice were generated as described in Chapter 2. Briefly, fetuses from pregnant *Clec-2*$^{+/-}$ mice were collected between days E14.5-18.5 and $1x10^6$ fetal liver cells were then injected retro-orbitally into lethally irradiated B6.SJL-Ptprc^{a}Pep3^b/BoyJ mice (Jackson Laboratories, USA). Mice were used 6-7 weeks later for experiments. BMDCs were generated by collecting bone marrow from the tibias and femurs of the FLCs and cultured in RPMI containing 10% FBS and 3% GM-CSF for 5-6 days. Platelets were isolated as previously described[52]. Briefly, approximately 500 μL whole blood was collected from the FLCs by retro-orbital bleeds into 3.8% sodium citrate. Red blood cells were lysed in ACK lysing buffer (Fisher).

Then the cells were resuspended and centrifuged at 300xg for 10 min with no break. The supernatant was collected and centrifuged again at 1,000xg to collect the platelet-rich fraction. BMDCs and platelets were seeded into 3D gels at a ratio of 5:1 to the FRCs.

Statistical analysis

Statistical analyses were conducted with Prism (GraphPad Software, Inc., La Jolla, CA, USA). Two-tailed Student's t-tests were used for all data except the YAP contraction experiments, where an ANOVA followed by a Tukey post-hoc analysis was used. Data were considered statistically significant when $p<0.05$.

References

1. Willard-Mack, C. L. Normal structure, function, and histology of lymph nodes. *Toxicol Pathol* **34,** 409–424 (2006).

2. Andrian, von, U. H. & Mempel, T. R. Homing and cellular traffic in lymph nodes. *Nat Rev Immunol* **3,** 867–878 (2003).

3. Herman, P. G., Yamamoto, I. & Mellins, H. Z. Blood microcirculation in the lymph node during the primary immune response. *J. Exp. Med.* **136,** 697–714 (1972).

4. Kumamoto, Y., Mattei, L. M., Sellers, S., Payne, G. W. & Iwasaki, A. CD4+ T cells support cytotoxic T lymphocyte priming by controlling lymph node input. *Proc. Natl. Acad. Sci. U.S.A.* **108,** 8749–8754 (2011).

5. Tzeng, T. C. *et al.* CD11chi Dendritic Cells Regulate the Re-establishment of Vascular Quiescence and Stabilization after Immune Stimulation of Lymph Nodes. *The Journal of Immunology* **184,** 4247–4257 (2010).

6. Chyou, S. *et al.* Fibroblast-type reticular stromal cells regulate the lymph node vasculature. *J. Immunol.* **181,** 3887–3896 (2008).

7. Chyou, S. *et al.* Coordinated Regulation of Lymph Node Vascular-Stromal Growth First by CD11c+ Cells and Then by T and B Cells. *The Journal of Immunology* **187,** 5558–5567 (2011).

8. Malhotra, D., Fletcher, A. L. & Turley, S. J. Stromal and hematopoietic cells in secondary lymphoid organs: partners in immunity. *Immunol. Rev.* **251,** 160–176 (2013).

9. Turley, S. J., Fletcher, A. L. & Elpek, K. G. The stromal and haematopoietic antigen-presenting cells that reside in secondary lymphoid organs. *Nature Publishing Group* **10,** 813–825 (2010).

10. Link, A. *et al.* Fibroblastic reticular cells in lymph nodes regulate the homeostasis of naive T cells. *Nat Immunol* **8,** 1255–1265 (2007).

11. Malhotra, D. *et al.* Transcriptional profiling of stroma from inflamed and resting lymph nodes defines immunological hallmarks. *Nat Immunol* **13,** 499–510 (2012).

12. Bajénoff, M. *et al.* Stromal Cell Networks Regulate Lymphocyte Entry, Migration, and Territoriality in Lymph Nodes. *Immunity* **25,** 989–1001 (2006).

13. Roozendaal, R. *et al.* Conduits Mediate Transport of Low-Molecular-Weight Antigen to Lymph Node Follicles. *Immunity* **30,** 264–276 (2009).

14. Sixt, M. *et al.* The conduit system transports soluble antigens from the afferent lymph to resident dendritic cells in the T cell area of the lymph node. *Immunity* **22,** 19–29 (2005).

15. Farr, A. G. *et al.* Characterization and cloning of a novel glycoprotein expressed by

stromal cells in T-dependent areas of peripheral lymphoid tissues. *J. Exp. Med.* **176,** 1477–1482 (1992).

16. Rishi, A. K. *et al.* Cloning, characterization, and development expression of a rat lung alveolar type I cell gene in embryonic endodermal and neural derivatives. *Developmental Biology* **167,** 294–306 (1995).

17. Breiteneder-Geleff, S. *et al.* Podoplanin, novel 43-kd membrane protein of glomerular epithelial cells, is down-regulated in puromycin nephrosis. *The American Journal of Pathology* **151,** 1141–1152 (1997).

18. Uhrin, P. *et al.* Novel function for blood platelets and podoplanin in developmental separation of blood and lymphatic circulation. *Blood* **115,** 3997–4005 (2010).

19. Ramirez, M. I. *et al.* T1α, a lung type I cell differentiation gene, is required for normal lung cell proliferation and alveolus formation at birth. *Developmental Biology* **256,** 62–73 (2003).

20. Schacht, V. *et al.* T1alpha/podoplanin deficiency disrupts normal lymphatic vasculature formation and causes lymphedema. *EMBO J.* **22,** 3546–3556 (2003).

21. Wicki, A. & Christofori, G. The potential role of podoplanin in tumour invasion. *Br J Cancer* **96,** 1–5 (2006).

22. Christou, C. M. *et al.* Renal cells activate the platelet receptor CLEC-2 through podoplanin. *Biochem. J.* **411,** 133–140 (2008).

23. Suzuki-Inoue, K., Inoue, O. & Ozaki, Y. Novel platelet activation receptor CLEC-2: from discovery to prospects. *J. Thromb. Haemost.* **9 Suppl 1,** 44–55 (2011).

24. Herzog, B. H. *et al.* Podoplanin maintains high endothelial venule integrity by interacting with platelet CLEC-2. *Nature* **502,** 105–109 (2014).

25. Martin-Villar, E. *et al.* Podoplanin binds ERM proteins to activate RhoA and promote epithelial-mesenchymal transition. *Journal of Cell Science* **119,** 4541–4553 (2006).

26. Wicki, A. *et al.* Tumor invasion in the absence of epithelial-mesenchymal transition: Podoplanin-mediated remodeling of the actin cytoskeleton. *Cancer Cell* **9,** 261–272 (2006).

27. Calvo, F. *et al.* Mechanotransduction and YAP-dependent matrix remodelling is required for the generation and maintenance of cancer-associated fibroblasts. *Nature Cell Biology* **15,** 637–646 (2013).

28. Martín-Villar, E. *et al.* Podoplanin associates with CD44 to promote directional cell migration. *Mol. Biol. Cell* **21,** 4387–4399 (2010).

29. Nakazawa, Y. *et al.* Tetraspanin family member CD9 inhibits Aggrus/podoplanin-induced platelet aggregation and suppresses pulmonary metastasis. *Blood* **112,** 1730–1739 (2008).

30. Cueni, L. N. & Detmar, M. Galectin-8 interacts with podoplanin and modulates lymphatic endothelial cell functions. *Experimental Cell Research* **315,** 1715–1723 (2009).

31. Xia, H., Nho, R. S., Kahm, J., Kleidon, J. & Henke, C. A. Focal Adhesion Kinase Is Upstream of Phosphatidylinositol 3-Kinase/Akt in Regulating Fibroblast Survival in Response to Contraction of Type I Collagen Matrices via a 1 Integrin Viability Signaling Pathway. *Journal of Biological Chemistry* **279,** 33024–33034 (2004).

32. Tian, B. beta 1 Integrin Regulates Fibroblast Viability during Collagen Matrix Contraction through a Phosphatidylinositol 3-Kinase/Akt/Protein Kinase B Signaling Pathway. *Journal of Biological Chemistry* **277,** 24667–24675 (2002).

33. Chai, Q. *et al.* Maturation of Lymph Node Fibroblastic Reticular Cells from Myofibroblastic Precursors Is Critical for Antiviral Immunity. *Immunity* 1–12 (2013). doi:10.1016/j.immuni.2013.03.012

34. Benezech, C. *et al.* CLEC-2 is required for development and maintenance of lymph nodes. *Blood* **123,** 3200–3207 (2014).

35. Yang, C. Y. *et al.* Trapping of naive lymphocytes triggers rapid growth and remodeling of the fibroblast network in reactive murine lymph nodes. *Proceedings of the National Academy of Sciences* **111,** E109–E118 (2014).

36. Lukacs-Kornek, V. *et al.* Regulated release of nitric oxide by nonhematopoietic stroma controls expansion of the activated T cell pool in lymph nodes. *Nat Immunol* **12,** 1096–1104 (2011).

37. Mourão-Sá, D. *et al.* CLEC-2 signaling via Syk in myeloid cells can regulate inflammatory responses. *Eur. J. Immunol.* **41,** 3040–3053 (2011).

38. Bajénoff, M., Glaichenhaus, N. & Germain, R. N. Fibroblastic reticular cells guide T lymphocyte entry into and migration within the splenic T cell zone. *J. Immunol.* **181,** 3947–3954 (2008).

39. Link, A. *et al.* Association of T-Zone Reticular Networks and Conduits with Ectopic Lymphoid Tissues in Mice and Humans. *The American Journal of Pathology* **178,** 1662–1675 (2011).

40. Khan, O. *et al.* Regulation of T cell priming by lymphoid stroma. *PLoS ONE* **6,** e26138 (2011).

41. Siegert, S. *et al.* Fibroblastic reticular cells from lymph nodes attenuate T cell expansion by producing nitric oxide. *PLoS ONE* **6,** e27618 (2011).

42. Fernández-Muñoz, B. *et al.* The transmembrane domain of podoplanin is required for its association with lipid rafts and the induction of epithelial-mesenchymal transition. *The International Journal of Biochemistry & Cell Biology* **43,** 886–896 (2011).

43. Wozniak, M. A. & Chen, C. S. Mechanotransduction in development: a growing role for contractility. *Nat Rev Mol Cell Biol* **10,** 34–43 (2009).

44. Provenzano, P. P. & Keely, P. J. Mechanical signaling through the cytoskeleton regulates cell proliferation by coordinated focal adhesion and Rho GTPase signaling. *Journal of Cell Science* **124,** 1195–1205 (2011).

45. Klein, E. A. *et al.* Cell-cycle control by physiological matrix elasticity and in vivo tissue stiffening. *Curr. Biol.* **19,** 1511–1518 (2009).

46. Navarro, A., Perez, R. E., Rezaiekhaligh, M. H., Mabry, S. M. & Ekekezie, I. I. Polarized migration of lymphatic endothelial cells is critically dependent on podoplanin regulation of Cdc42. *AJP: Lung Cellular and Molecular Physiology* **300,** L32–L42 (2010).

47. Peduto, L. *et al.* Inflammation Recapitulates the Ontogeny of Lymphoid Stromal Cells. *The Journal of Immunology* **182,** 5789–5799 (2009).

48. Fletcher, A. L. *et al.* Reproducible isolation of lymph node stromal cells reveals site-dependent differences in fibroblastic reticular cells. *Front Immunol* **2,** 35 (2011).

49. Pinner, S. & Sahai, E. PDK1 regulates cancer cell motility by antagonising inhibition of ROCK1 by RhoE. *Nature Cell Biology* **10,** 127–137 (2008).

50. Lamprecht, M., Sabatini, D. & Carpenter, A. CellProfiler™: free, versatile software for automated biological image analysis. *Biotech.* **42,** 71–75 (2007).

51. Ertürk, A. *et al.* Three-dimensional imaging of the unsectioned adult spinal cord to assess axon regeneration and glial responses after injury. *Nat. Med.* **18,** 166–171 (2012).

52. Kim, S. *et al.* RhoG protein regulates glycoprotein VI-Fc receptor γ-chain complex-mediated platelet activation and thrombus formation. *J. Biol. Chem.* **288,** 34230–34238 (2013).

Chapter 4

Conclusions and Broader Impacts

Attributions

Portions of this chapter were reproduced from the following publication (with permission from *Frontiers in Immunology*):

Astarita, J.L., Acton, S.E., Turley, S.J. Podoplanin: emerging functions in development, the immune system, and cancer. *Front Immunol* **3**, 283-293 (2012).

Conclusions

CLEC-2-PDPN interactions guide DC migration

In the first part of this dissertation, we discovered a new mechanism that mediates dendritic cell (DC) migration. Prior to this study, it was well known that chemokine gradients played a critical role in guiding DC migration from peripheral tissues to draining lymph nodes[1]. In addition, many studies had examined the molecular mechanisms underlying DC motility, such as extravasation and integrin-independent amoeboid movement[2,3]. However, we reasoned that there might be other interactions guiding DC migration for several reasons. First, it is difficult to envision how chemokine gradients could work efficiently over the vast distances required. Second, while the amoeboid migration of DCs is well documented, no specific molecules that initiate this process and cause DCs to move forward in such a manner had been identified. Finally, DCs must interact with stromal cells both in the lymphatics and once they arrive in the paracortex of the lymph node. Thus, it is likely that some of these cell-cell contacts provided important cues to incite DC motility.

We identified CLEC-2, a c-type lectin expressed by several immune cells, and podoplanin (PDPN), a glycoprotein expressed by lymphatic endothelial cells (LECs) and fibroblastic reticular cells (FRCs), as a potential interaction that could guide DC migration. Initially, we found that CLEC-2 signaling upon binding to PDPN or another ligand, rhodocytin, immediately caused the formation of actin-rich protrusions and DC motility. This signaling did not confer any directionality on its own; thus, the directional cues of chemokines would still be necessary to guide DCs towards the lymph node. Still, without CLEC-2, DCs were unable to enter into lymphatic draining the skin, were trapped in the subcapsular sinus upon reaching the lymph node, and finally were unable to effectively crawl deep within the T cell zone on FRCs. We

further demonstrated that this interaction required PDPN on FRCs by showing that WT DCs could not crawl on *Pdpn*$^{-/-}$ FRCs in an in vitro 3D network.

These findings indicate that DC-stroma interactions play an important role in DC migration at every step of the way. It was previously reported that DCs crawl along the FRC network in the T cell paracortex to facilitate interactions between antigen-bearing DCs and their cognate T cells[4-6]. Furthermore, DCs enter into the lymph node by extravasation through the floor of the subcapsular sinus and thus engage closely with LECs at that point[7]. However, these studies focused mostly on the DC migration and not on whether there were any specific interactions between the stromal cells and the DCs. Our findings indicate that there are likely many other cell surface molecules on stromal cells that could instruct DCs. For instance, in addition to CCL21 and CCL19, LECs and FRCs secrete many other chemokines and cytokines that support DC survival and differentiation, such as Flt3 and CXCL14[8]. FRCs and LECs also express TLR4 and thus are able to quickly sense and respond to inflammation. Thus, they may also provide maturation signals to DCs in the earliest stages of immune responses.

Another interesting possibility to consider is whether other immune cells use the CLEC-2-PDPN axis to guide their migration. Red pulp macrophages and CD11b^{+}CD103^{-}CX3CR1^{+} macrophages from the lamina propria of the small intestine express high levels of CLEC-2[9]. In the red pulp of the spleen, there are dense cords of composed of fibroblasts and reticular fibers where venous blood collects. These cords are full of dying red blood cells, which are phagocytosed by the macrophages that reside there[10]. These fibroblasts express PDPN[11] so the red pulp macrophages would be exposed to it.

The CD103^{-}CX3CR1^{+} macrophages that reside in the lamina propria are poor at antigen presentation but are adept at taking up soluble antigens in the lamina propria and may transfer them to DCs for presentation[12,13]. These macrophages are also important for patrolling the gut

and capturing microbiota restrict their entry into the mesenteric lymph nodes[14]. In this region of the gut, there is a dense network of PDPN$^+$ fibroblasts just below the epithelium. Thus, it is likely that both of these CLEC-2$^+$ macrophages would receive signals from CLEC-2 engagement of PDPN on fibroblasts.

These interactions could induce motility as in DCs, or, it is possible that CLEC-2 activation affects phagocytosis in these cells. Another c-type lectin family member, Dectin-1, has been implicated in phagocytosis and is thought to signal through ITAM motifs, similarly to Fc receptors[15]. Furthermore, it was recently reported that Syk signaling controls actin reorganization and Fcγ receptor mobility on the surface of macrophages, which affects their phaocytosis[16]. While we found that CLEC-2-deficient DCs were not impaired in antigen uptake, macrophages tend to phagocytose much larger particles[17] that may rely more on actin-rich protrusions to encompass them. CLEC-2 activation, in conjunction with TLR signaling, can induce IL-10 production in myeloid cells[18], which could be especially important for maintaining tolerance in the lamina propria macrophage population. Another function that has been identified for CLEC-2 is the phagocytic uptake of the human immunodeficiency virus (HIV). It appears that macrophages can recognize HIV particles that have budded from cells due to the incorporation of host cell PDPN in the virion[19]. While no other endogenous ligands for CLEC-2 have been identified in addition to PDPN, activation of CLEC-2 in conjunction with other specific phagocytic receptors could aid in actin reorganization and efficient uptake of pathogens.

Overall, our work opens up many new questions about DC migration during immune responses and myeloid-stromal cell interactions. It will be interesting to see what other molecular interactions between these cell types are uncovered in the future and what other aspects of myeloid cell biology they influence.

PDPN is a master regulator of fibroblastic reticular cell contractility

In the second part of this dissertation, we studied the effects of the CLEC-2-PDPN axis on the stromal cells. We discovered that CLEC-2 engagement of PDPN results in signaling downstream of PDPN to mediate vast changes in fibroblastic reticular cell (FRC) contraction and homeostasis. The effect of CLEC-2 binding mimics a complete lack of PDPN in FRCs. Specifically, in the absence of PDPN, FRCs are extremely elongated and unable to contract collagen gels. Presumably due to this lack in contractility, the *Pdpn*$^{-/-}$ FRCs proliferate more quickly and survive better compared with WT FRCs. These phenotypes are also observed in vivo: in steady state, blocking PDPN function results in enlarged lymph nodes, increased FRCs, and increasing spacing between FRC fibers in the reticular network. Importantly, disrupting PDPN function has important effects on immune responses. Upon PDPN blockade, lymph nodes swelled more and OTI cells proliferated more and were present in higher numbers compared with control-treated mice. Overall, we demonstrated that PDPN is a master regulatory of contractility in FRCs, and that FRC contraction in turn is necessary for several of its functions.

It has been known for decades that lymph nodes swell during time of inflammation or when the body is eradicating an infection. Still, no precise mechanism controlling lymph node swelling has been described. It is clear that a large amount of the swelling must be due to the great proliferation and expansion of lymphocytes in addition to the influx of migratory innate cells such as DCs. There are some studies detailing the remodeling of the vasculature that accompanies these great changes[20-22]. However, for an organ to be able to accommodate such a great size increase, and, especially, to return back to a normal size once the immune response has contracted, there must be other changes in the underlying extracellular matrix and fibroblastic cells that support the organ.

Indeed, it has been known for several years that FRCs are very contractile cells[23];

however, no specific function for FRC contractility has been described. Our work detailed here brings to light the importance of FRC contractility both for the integrity of the lymph node as a whole and for the homeostasis of the FRC network. We have demonstrated that blocking PDPN-induced contractility exacerbates immune responses and leads to prolonged swelling of the lymph node. This in turn leads to uncontrolled T cell responses. It would be interesting to perform the complementary experiment, whereby PDPN is overexpressed or cannot be bound by CLEC-2. Overexpression would be difficult, as FRCs already express very high levels of it. However, if FRCs expressed a form of PDPN with a mutated CLEC-2 binding region, then lymph nodes would likely not be able to swell properly and lymphocyte responses might be dampened.

In addition to linking FRC contractility to lymph node swelling, we have found that FRC contractility controls survival. Adhesion to and contraction of the underlying basement membrane and extracellular matrix is well known to affect multiple aspects of fibroblast biology[24,25]. Still, this is the first time that FRC contractility has specifically been linked to FRC survival and proliferation. And while our work makes it clear that FRCs receive a signal to relax from interactions with CLEC-2^+ DCs, it is likely that they receive additional signals to proliferate or stretch either directly from the inflammatory milieu or from activated T and B cells. FRCs express TLRs[8] and thus can directly sense bacterial or viral particles that may have entered lymph nodes through the conduits. It remains to be seen whether there are specific cell-cell interactions between T cells and FRCs; however, given their close association and that T cells preferentially “walk” along the FRC network, it seems likely that there would be some crosstalk. Previous work examining endothelial cell and FRC proliferation demonstrated that while FRCs still proliferate in mice lacking lymphocytes, they do not accumulate[26]. Thus, it would be interesting to examine PDPN signaling and FRC expansion in this scenario to determine exactly what role lymphocytes play in supporting FRC homeostasis.

Another function of FRCs that seems to require PDPN-mediated contraction is the adequate suppression of proliferating T cells. We believe this is in due in part of the increased spacing of the network that causes decreased contact between T cells and FRCs. Additionally, it has been reported that production of inducible nitric oxide, which is critical for suppressing T cell responses[27-29], requires normal contraction and activation of focal adhesion kinase in ventricular myocytes[30]. Thus, it is likely that the disruption in FRC contractility also directly affects their production of nitric oxide. Overall, these findings indicate that upon the initial influx of DCs and relaxation of FRCs, they would temporarily be less able to produce nitric oxide in response to proliferating lymphocytes. This would relieve T cell suppression at early stages. However, once FRCs began to proliferate and increased in number, they would not longer be so stretched and would begin to produce nitric oxide to keep T cell responses in check.

In addition to controlling T cells responses, a major role played by FRCs is the generation of the conduit network, which carries lymph and small, soluble antigens deep into the paracortex. While many of the molecular composition and functional size cutoffs have been identified[6,8,31], there is still relatively little known about how FRCs themselves may modulate conduit function. It is likely that FRCs could modulate the types of collagens they secrete to alter what types of antigens fit into the conduits. Interestingly, the secretion of extracellular matrix components and matrix metalloproteases can be controlled by fibroblast contractility[32-34]. Given that FRCs secrete a great variety of these molecules and that they are critical for conduit function, this would be an interesting area to investigate. It is likely that FRCs would secrete different groups of these proteins during times of lymph swelling, when they are stretched, and then again during times of lymph node contraction and quiescence.

Given the close association of FRCs around the conduit components, it was surprising that conduit functionality was not perturbed in mice treated with the α-PDPN blocking

antibody. We reasoned that FRC adhesion to and spreading along collagen fibers would be important for maintaining the integrity of the conduits. Additionally, it seemed that contractility would be important to maintain lymph flow and pressure in the conduits. However, a recent study from our lab found that complete ablation of FRCs did not result in the total disruption of conduits[35]. Upon FRC ablation, conduits were leaky, as indicated by the presence of thicker bands of fluorescent tracers. However, these tracers still flowed through in the conduits and did not immediately leak out to fill the whole the lymph node. This finding, although with the ones reported here, call for a closer look at the different roles played by the FRC cell body and the collagen fibers in determining the flow of small molecules in the conduits.

Another aspect that could affect fluid flow in conduits is global changes in lymph flow throughout the body. Lymph flow increases under a variety of inflammatory conditions, such as in certain cancers and rheumatoid arthritis[36-38]. Lymphatic endothelial cells (LECs), which line lymphatic vessels, play a role in regulating lymph flow[39,40]. They also line the subcapsular sinus and are present in the medulla of the lymph nodes, all of which puts them at a unique location to have an impact on lymph node swelling and contraction. Given that LECs express comparable levels of PDPN to FRCs, it is highly possible that PDPN signaling controls contractility or other functions in these cells. It remains to be examined whether inhibited PDPN function on LECs would affect lymph node and antigen delivery to lymph nodes.

Overall, the interactions between CLEC-2$^+$ DCs and PDPN$^+$ FRCs are a unique example of bidirectional signaling that is critical for multiple steps in an immune response. On one hand, CLEC-2 activation by PDPN binding causes signaling that incites actin polymerization and DC motility, which is required for DC entry into lymphatics and efficient arrival in the lymph node. On the other hand, CLEC-2 engagement of PDPN results in signaling downstream of PDPN that causes the FRCs to relax and allow for lymph node enlargement. These key steps in immunity

are ingeniously linked by this interaction. DCs are one of the first cell types to arrive in the lymph node following detection of an inflammatory stimulus. Furthermore, they are the cell type that activates T cells and causes them to begin proliferating. Thus, the FRCs will receive a signal to relax just before the extra space in the lymph node is necessary; this gives the FRCs enough time to also begin proliferating so that they can continue to support the enlarged lymph node. Finally, as the DCs have played their role, they will die off and the CLEC-2 signal will disappear. The activated lymphocytes will also emigrate from the lymph node to fight the inflammation in the periphery. Thus, PDPN will resume its normal signaling and FRCs will contract again to bring the lymph node back to its resting size.

Future Directions

There are still many unknowns about PDPN biology that remain to be answered, but there are three pressing questions in the field: (1) What signaling pathways does endogenously-expressed PDPN employ? It is possible that expression of PDPN in fibroblasts leads to similar downstream changes as those that have been described in transformed epithelial cells; however, it is possible that PDPN interacts with different molecules and signaling pathways in stromal cells than in malignant cancer cells. (2) What are the effects of CLEC-2 engagement of PDPN? This interaction has been almost exclusively studied with respect to signaling downstream of CLEC-2. While we have now answered this question with respect to lymph node FRCs, there are other environments where these two molecules would interact, such as in the tumor microenvironment. (3) What is the function of PDPN and CLEC-2 interactions in contexts outside of the lymph node? PDPN is expressed by a number of different cell types and is upregulated in a variety of inflammatory environments. Furthermore, in many of these instances, there are also CLEC-2^{+} cells present.

PDPN signaling and protein interactions

As described in the introduction, PDPN has many different reported binding partners. The intracellular tail of PDPN is very short – only nine amino acids – and has only been reported to bind directly to ezrin, radixin, and moesin (ERM) family proteins[41]. Two studies found that overexpression of PDPN in different epithelial tumor cell lines resulted in increased ERM phosphorylation[41,42]. However, our results indicated that the levels of phosphorylated ERMs were normal even in the absence of the cytoplasmic tail. This result, along with the fact that the Δcyto FRCs maintained normal contractility, indicates that interactions between the transmembrane and extracellular domains of PDPN are likely more important in driving its functions.

All of the studies describing protein interactions for PDPN have been conducted in endothelial cells or transformed epithelial cell lines with over expression constructs. FRCs express all of the reported binding partners, including CD44, the tetraspanin CD9, and galectin-8[8]. Thus, it is likely that PDPN also interacts with these proteins in FRCs, but that has yet to be explicitly demonstrated. Furthermore, the requirement of these interactions in promoting PDPN activity was evaluated based on the previously reported functions of PDPN, such as its ability to increase migration, invasion, and metastasis. Now that we have defined a new critical function for PDPN as a regulator of contractility in fibroblasts, the consequences of these interactions must be re-evaluated.

Another aspect of PDPN biology that has not been explored is whether PDPN on one fibroblast can bind to other PDPN molecules or other proteins on a neighboring cell to cause signaling. Cell-cell contacts control a variety of biological activities, such as secretion of extracellular matrix components, growth, and survival[43-45]. Given that the interaction between PDPN and CD44 is mediated by the extracellular domains of these proteins, it is possible that

they would interact across different cells. If this interaction is indeed necessary for PDPN-mediated control of contractility in fibroblasts, then signaling between cells could be another way that FRCs can sense the density of their network. If FRCs are not near enough cells to support full PDPN signaling, then they may relax until they contact more neighboring cells and get a signal to contract again.

CLEC-2 engagement of PDPN

This work is the first to demonstrate that PDPN signaling is altered by CLEC-2 binding. Previous studies considered PDPN only as a ligand for CLEC-2 and focused on the changes in CLEC-2 signaling upon binding to PDPN. Now that it is clear that there is signaling in both directions, further work is necessary to determine how CLEC-2 mediates these effects. One conclusion that can be drawn from the work presented here is that CLEC-2 likely disrupts some of the lateral membrane interactions PDPN would normally be engaged in, given that CLEC-2 is still able to signal and impair contraction in the Δcyto FRCs. Bringing together our results and what has been previously published[46-48], we envision that PDPN is normally present in lipid rafts and interacting with CD44 and CD9 in these microdomains. These interactions are mediated through the extracellular and transmembrane domains and allow for normal activation of ERM proteins and, further downstream, normal contractility. Upon CLEC-2 binding, CD44 and perhaps CD9 would be displaced, which would temporarily render PDPN unable to maintain contractile signaling into the cell.

The interaction between PDPN and CLEC-2 seems to be a fairly transient reaction. It was previously reported that the affinity of CLEC-2 binding PDPN was 24.5 μM[49], whereas a high affinity antibody can be in the nanomolar or even picomolar range[50]. We observed this transient activity level in our contraction experiments, as continual application of CLEC-2 was necessary to

inhibit contraction. Furthermore, in chapter 2, we demonstrated that within minutes of engaging soluble PDPN, CLEC-2 is internalized. However, PDPN remains on the surface of FRCs after interacting with CLEC-2 on expressed by DCs. Taken together, these data indicate that CLEC-2$^+$ DCs would provide a fast but reversible signal to PDPN$^+$ FRCs in the lymph node. This would allow for a transient relaxation of the FRC network that would continue only as long as CLEC-2$^+$ DCs were crawling along the network. Ultimately, normal contraction of FRCs would resume quickly after the removal of the CLEC-2 signal, which would occur as the immune response begins to wan and migratory DCs perish in the draining lymph node.

CLEC-2-PDPN interactions outside of the lymph node

PDPN is expressed by a variety of cell types in healthy, adult animals in addition to FRCs and LECs in lymph nodes, including type I alveolar epithelial cells[51,52], kidney podocytes[53], osteoblasts[54], myocardial cells[55], and skin fibroblasts[8]. The function of PDPN in these cell types has largely been described with respect to its requirements for normal development of these various organs. While these studies are certainly important, it is also critical to dissect the function of PDPN in these contexts and cells in healthy, adult animals. Until very recently, studies of this kind were limited by the lack of an inducible or conditional mouse model for PDPN deletion. However, now both an inducible model of PDPN deletion and a conditional PDPN-floxed mouse have been generated[56]. These tools are crucial in further dissecting the function of PDPN in adult animals. In the case of skin fibroblasts and the cardiac myofibroblasts, PDPN may control contractility as it does in FRCs. However, it could have different functions in kidney podocytes and lung epithelial cells. The role of PDPN would also depend greatly on whether CLEC-2$^+$ cells were present in the particular environment being studied.

The setting in which PDPN has been most extensively studied is cancer. Given that it is a specific marker of lymphatic vessels, and that increased lymphangiogenesis is often correlated with poor prognosis in cancer patients, the numbers of $PDPN^+$ vessels in a tumor is often used as a diagnostic marker[53,57,58]. Additionally, PDPN is upregulated on tumor cells themselves in several cancer types, including squamous cell carcinomas of the lung, head, and neck[42,59-61], malignant mesothelioma[62,63], and brain tumors[64,65]. PDPN is often expressed at the leading invasive edge of tumors and appears to play a role in EMT, invasion, and metastasis[41,42]. Interactions between CLEC-2 and PDPN in tumors also likely play a role in tumor progression and metastasis due to platelets interacting with tumor cells[66]. However, the exact mechanism of PDPN action in tumor cells is still unclear; in some cases, PDPN expression mediates the downregulation of E-cadherin and promotes EMT[41], while in others, PDPN expression enhances tumorigenesis and metastasis in the absence of EMT[42].

Interestingly, PDPN is also upregulated by cancer-associated fibroblasts (CAFs) in the stroma surrounding various tumors, including adenocarcinomas and colorectal cancers[67]. There is a wealth of data on the tumor-promoting effects of CAFs, which has been reviewed elsewhere[68,69], but only recently have specific functions for PDPN on CAFs been examined. Generally, the expression of PDPN on CAFs is associated with poor prognosis: for example, one study found that invasive adenocarcinomas in the lung had $PDPN^+$ fibroblasts, while all noninvasive cases were negative for PDPN staining[70]. Further studies from this group have examined the mechanism by which PDPN enhances the tumor-promoting effects of CAFs. They found that fibroblasts isolated from the vascular adventitia (VAFs) were better at promoting tumor growth than fibroblasts isolated from human lungs. One of the most differentially expressed genes in these cells was PDPN, and knockdown of PDPN in the VAFs abrogated their tumor-promoting effects[71]. Further studies indicated that this activity may be due in part to

increased RhoA activity in the PDPN$^+$ fibroblasts[72]. Recently, an elegant study reported that contractility and matrix remodeling in CAFs were essential to their maintenance and tumor-promoting functions[73]. While they did not examine PDPN expression, given our results and the fact that CAFs share many features with FRCs (our unpublished observations), it is highly likely that PDPN also plays a role in regulating CAF contractility.

While these studies illustrate that PDPN expression in CAFs is linked to poor prognosis for patients, it is important to keep in mind that the effect of PDPN$^+$ CAFs likely depends on the type of tumor cells and the tissue from which the CAFs originate. In fact, one study of colorectal CAFs found that PDPN expression was correlated with a better prognosis[74]. Knockdown of PDPN in CAFs resulted in enhanced cancer cell migration in a transwell assay. Furthermore, PDPN expression was seen in stroma surrounding the tumors in many areas except at the invasive front[74]. Thus, it was postulated that PDPN$^+$ stroma could act as a physical barrier to tumor cell invasion into surrounding tissues. In fact, this theory has been presented elsewhere and for other mucins[75]. The negative charge of the many sialic acids on these proteins acts to repel other molecules such as complement[76,77] and can affect cell adhesion[78]. Whether these properties play a role in PDPN function has not been definitively examined but it is an attractive hypothesis, given that PDPN is expressed on the apical surface of many cells that have contact with proteinase-rich fluids (i.e., lymph).

While it is clear that PDPN plays an important role in tumor progression and metastasis, more mechanistic studies are needed to fully elucidate the function of this molecule. Furthermore, a genetic dissection of PDPN function in malignant cells versus in the surrounding tumor stroma will significantly advance our understanding of this molecule in cancer.

PDPN$^+$ fibroblasts accumulate in a variety of inflammatory environments in addition to cancer. This phenomenon is often associated with the formation of ectopic lymphoid follicles,

which are structures that share similar organization to lymph nodes but arise in response to chronic inflammation in many diseases[79]. It is not entirely clear whether these structures are the result of activation or proliferation of local fibroblasts or the influx of precursors, but it seems to be the former. For instance, administration of CFA or infection with *Leishmania major* causes a massive increase in FRC-like cells, which appears to be due to increased proliferation tissue-resident fibroblasts[80]. Increased PDPN expression was also found in the brains of patients with multiple sclerosis[81] and in synovial fibroblasts during rheutamoid arthritis[82]. While it has already been demonstrated that the FRC-like cells in these ectopic lymphoid follicles support T and B cell homing, it would be interesting to dissect whether PDPN plays a role in attracting CLEC-2$^+$ myeloid cells to these areas as well.

PDPN as a therapeutic target

The presence of PDPN$^+$ fibroblasts and ectopic lymphoid follicles in inflammatory environments are generally associated with a worse disease course and poor outcomes. In ectopic lymphoid follicles, PDPN$^+$ fibroblasts likely support the influx of inflammation-inducing myeloid cells and provide a preferential niche for lymphocytes. Furthermore, in cancer, the extracellular matrix produced by PDPN$^+$ CAFs surrounds the collagen core and restricts access of both anti-tumor cytotoxic T cells and chemotherapeutic agents[83]. Thus, targeting PDPN in these contexts could have therapeutic potential. In the case of ectopic lymphoid follicles, an antibody that blocks CLEC-2 binding could inhibit the migration of myeloid cells and dampen the harmful levels of inflammatory cytokines present. The case of the CAFs, blocking PDPN-mediated contraction could be beneficial in relaxing the dense collagen corona and allowing for entry of cytotoxic T cells.

PDPN expression by tumor cells is associated with increased metastasis at least in part because PDPN attracts CLEC-2^{+} platelets. The tumor cells become surrounded by activated platelets, which forms protective cloak that aids in tumor cell entry into vessels and metastasis[84,85]. Thus, a podoplanin blocking antibody that inhibits CLEC-2 binding would also be beneficial here to inhibit metastasis. Blocking PDPN functions on cancer cells could provide additional benefits such as inhibiting tumor migration and invasion.

One major obstacle in utilizing PDPN as a therapeutic agent would be avoiding unintended consequences due to disrupting normal PDPN function on healthy lymphatics and FRCs in the lymph node. However, PDPN is a heavily glycosylated protein and may have different forms on different cell types similar to CD44[86,87], which would allow for specific targeting of PDPN on different cells. Interestingly, Kato and Kaneko[88] have recently generated a tumor-specific anti-PDPN antibody that does not bind to lymphatics. More studies are necessary to determine the cellular effects of binding of this antibody, but this study indicates that it is possible to specifically target tumor PDPN while sparing PDPN on normal cells.

Overall, PDPN plays a role in controlling the actin cytoskeleton, motility, and contraction in a variety of cell types. At the same time, it serves as a critical ligand for CLEC-2 that triggers signaling cascades leading to myeloid cell migration and platelet aggregation. As these functions play important roles in both cancer progression and inflammatory responses, PDPN represents an attractive target in modulating inflammation and metastasis.

References

1. Cyster, J. G. Chemokines and the homing of dendritic cells to the T cell areas of lymphoid organs. *J. Exp. Med.* **189,** 447–450 (1999).

2. Lämmermann, T. *et al.* Rapid leukocyte migration by integrin-independent flowing and squeezing. *Nature* **453,** 51–55 (2008).

3. Hynes, R. O. Integrins: bidirectional, allosteric signaling machines. *Cell* **110,** 673–687 (2002).

4. Bajénoff, M. *et al.* Stromal Cell Networks Regulate Lymphocyte Entry, Migration, and Territoriality in Lymph Nodes. *Immunity* **25,** 989–1001 (2006).

5. Katakai, T. *et al.* A novel reticular stromal structure in lymph node cortex: an immuno-platform for interactions among dendritic cells, T cells and B cells. *Int. Immunol.* **16,** 1133–1142 (2004).

6. Sixt, M. *et al.* The conduit system transports soluble antigens from the afferent lymph to resident dendritic cells in the T cell area of the lymph node. *Immunity* **22,** 19–29 (2005).

7. Braun, A. *et al.* Afferent lymph–derived T cells and DCs use different chemokine receptor CCR7–dependent routes for entry into the lymph node and intranodal migration. *Nat Immunol* **12,** 879–887 (2011).

8. Malhotra, D. *et al.* Transcriptional profiling of stroma from inflamed and resting lymph nodes defines immunological hallmarks. *Nat Immunol* **13,** 499–510 (2012).

9. Gautier, E. L. *et al.* Gene-expression profiles and transcriptional regulatory pathways that underlie the identity and diversity of mouse tissue macrophages. *Nat Immunol* **13,** 1118–1128 (2012).

10. Haan, den, J. M., Mebius, R. E. & Kraal, G. Stromal cells of the mouse spleen. *Front Immunol* **3,** 201 (2012).

11. Mueller, S. N. & Germain, R. N. Stromal cell contributions to the homeostasis and functionality of the immune system. *Nature Publishing Group* **9,** 618–629 (2009).

12. Shakhar, G. & Kolesnikov, M. Intestinal macrophages and DCs close the gap on tolerance. *Immunity* **40,** 171–173 (2014).

13. Mazzini, E., Massimiliano, L., Penna, G. & Rescigno, M. Oral tolerance can be established via gap junction transfer of fed antigens from $CX3CR1^{+}$ macrophages to $CD103^{+}$ dendritic cells. *Immunity* **40,** 248–261 (2014).

14. Diehl, G. E. *et al.* Microbiota restricts trafficking of bacteria to mesenteric lymph nodes by CX3CR1hi cells. *Nature* **494,** 116–120 (2014).

15. Herre, J. *et al.* Dectin-1 uses novel mechanisms for yeast phagocytosis in macrophages. *Blood* **104,** 4038–4045 (2004).

16. Jaumouillé, V. *et al.* Actin cytoskeleton reorganization by Syk regulates Fcγ receptor responsiveness by increasing its lateral mobility and clustering. *Developmental Cell* **29,** 534–546 (2014).

17. Gamvrellis, A. *et al.* Vaccines that facilitate antigen entry into dendritic cells. *Immunol. Cell Biol.* **82,** 506–516 (2004).

18. Mourão-Sá, D. *et al.* CLEC-2 signaling via Syk in myeloid cells can regulate inflammatory responses. *Eur. J. Immunol.* **41,** 3040–3053 (2011).

19. Chaipan, C. *et al.* Incorporation of podoplanin into HIV released from HEK-293T cells, but not PBMC, is required for efficient binding to the attachment factor CLEC-2. *Retrovirology* **7,** 47 (2010).

20. Herman, P. G., Yamamoto, I. & Mellins, H. Z. Blood microcirculation in the lymph node during the primary immune response. *J. Exp. Med.* **136,** 697–714 (1972).

21. Chyou, S. *et al.* Fibroblast-type reticular stromal cells regulate the lymph node vasculature. *J. Immunol.* **181,** 3887–3896 (2008).

22. Tzeng, T. C. *et al.* CD11chi Dendritic Cells Regulate the Re-establishment of Vascular Quiescence and Stabilization after Immune Stimulation of Lymph Nodes. *The Journal of Immunology* **184,** 4247–4257 (2010).

23. Link, A. *et al.* Fibroblastic reticular cells in lymph nodes regulate the homeostasis of naive T cells. *Nat Immunol* **8,** 1255–1265 (2007).

24. Paszek, M. J. *et al.* Tensional homeostasis and the malignant phenotype. *Cancer Cell* **8,** 241–254 (2005).

25. Provenzano, P. P. & Keely, P. J. Mechanical signaling through the cytoskeleton regulates cell proliferation by coordinated focal adhesion and Rho GTPase signaling. *Journal of Cell Science* **124,** 1195–1205 (2011).

26. Chyou, S. *et al.* Coordinated Regulation of Lymph Node Vascular-Stromal Growth First by CD11c+ Cells and Then by T and B Cells. *The Journal of Immunology* **187,** 5558–5567 (2011).

27. Lukacs-Kornek, V. *et al.* Regulated release of nitric oxide by nonhematopoietic stroma controls expansion of the activated T cell pool in lymph nodes. *Nat Immunol* **12,** 1096–1104 (2011).

28. Khan, O. *et al.* Regulation of T cell priming by lymphoid stroma. *PLoS ONE* **6,** e26138 (2011).

29. Siegert, S. *et al.* Fibroblastic reticular cells from lymph nodes attenuate T cell expansion by producing nitric oxide. *PLoS ONE* **6,** e27618 (2011).

30. Chu, M. *et al.* Contractile Activity Regulates Inducible Nitric Oxide Synthase Expression and NO(i) Production in Cardiomyocytes via a FAK-Dependent Signaling Pathway. *J Signal Transduct* **2012,** 473410–11 (2012).

31. Gretz, J. E., Norbury, C. C., Anderson, A. O., Proudfoot, A. E. & Shaw, S. Lymph-borne chemokines and other low molecular weight molecules reach high endothelial venules via specialized conduits while a functional barrier limits access to the lymphocyte microenvironments in lymph node cortex. *J. Exp. Med.* **192,** 1425–1440 (2000).

32. Shi, Z.-D., Wang, H. & Tarbell, J. M. Heparan sulfate proteoglycans mediate interstitial flow mechanotransduction regulating MMP-13 expression and cell motility via FAK-ERK in 3D collagen. *PLoS ONE* **6,** e15956 (2011).

33. Kook, S.-H., Jang, Y.-S. & Lee, J.-C. Involvement of JNK-AP-1 and ERK-NF-κB signaling in tension-stimulated expression of type I collagen and MMP-1 in human periodontal ligament fibroblasts. *J. Appl. Physiol.* **111,** 1575–1583 (2011).

34. Wang, P. *et al.* Mechanical stretch regulates the expression of matrix metalloproteinase in rheumatoid arthritis fibroblast-like synoviocytes. *Connect. Tissue Res.* **50,** 98–109 (2009).

35. Cremasco, V. *et al.* B cell homeostasis and follicle confines are governed by fibroblastic reticular cells. *Nat Immunol*

36. Mullins, R. J. & Hudgens, R. W. Increased skin lymph protein clearance after a 6-h arterial bradykinin infusion. *Am. J. Physiol.* **253,** H1462–9 (1987).

37. Staberg, B., Klemp, P., Aasted, M., Worm, A. M. & Lund, P. Lymphatic albumin clearance from psoriatic skin. *J. Am. Acad. Dermatol.* **9,** 857–861 (1983).

38. Harrell, M. I., Iritani, B. M. & Ruddell, A. Tumor-induced sentinel lymph node lymphangiogenesis and increased lymph flow precede melanoma metastasis. *The American Journal of Pathology* **170,** 774–786 (2007).

39. Podgrabinska, S. *et al.* Molecular characterization of lymphatic endothelial cells. *Proceedings of the National Academy of Sciences* **99,** 16069–16074 (2002).

40. Gogineni, A. *et al.* Inhibition of VEGF-C modulates distal lymphatic remodeling and secondary metastasis. *PLoS ONE* **8,** e68755 (2013).

41. Martin-Villar, E. *et al.* Podoplanin binds ERM proteins to activate RhoA and promote epithelial-mesenchymal transition. *Journal of Cell Science* **119,** 4541–4553 (2006).

42. Wicki, A. *et al.* Tumor invasion in the absence of epithelial-mesenchymal transition: Podoplanin-mediated remodeling of the actin cytoskeleton. *Cancer Cell* **9,** 261–272 (2006).

43. Hinz, B. & Gabbiani, G. Cell-matrix and cell-cell contacts of myofibroblasts: role in connective tissue remodeling. *Thromb. Haemost.* **90,** 993–1002 (2003).

44. Chen, C. S., Tan, J. & Tien, J. Mechanotransduction at cell-matrix and cell-cell contacts. *Annu Rev Biomed Eng* **6,** 275–302 (2004).

45. Sirén, V. *et al.* Cell-cell contact activation of fibroblasts increases the expression of matrix metalloproteinases. *Ann. Med.* **38,** 212–220 (2006).

46. Martín-Villar, E. *et al.* Podoplanin associates with CD44 to promote directional cell migration. *Mol. Biol. Cell* **21,** 4387–4399 (2010).

47. Fernández-Muñoz, B. *et al.* The transmembrane domain of podoplanin is required for its association with lipid rafts and the induction of epithelial-mesenchymal transition. *The International Journal of Biochemistry & Cell Biology* **43,** 886–896 (2011).

48. Nakazawa, Y. *et al.* Tetraspanin family member CD9 inhibits Aggrus/podoplanin-induced platelet aggregation and suppresses pulmonary metastasis. *Blood* **112,** 1730–1739 (2008).

49. Christou, C. M. *et al.* Renal cells activate the platelet receptor CLEC-2 through podoplanin. *Biochem. J.* **411,** 133–140 (2008).

50. Andersson, K., Björkelund, H. & Malmqvist, M. Antibody-antigen interactions: what is the required time to equilibrium? in *Nat Prec* (2010). at <<http://precedings.nature.com/documents/5218/version/1/files/npre20105218-1.pdf>>

51. Ramirez, M. I. *et al.* T1α, a lung type I cell differentiation gene, is required for normal lung cell proliferation and alveolus formation at birth. *Developmental Biology* **256,** 62–73 (2003).

52. Williams, M. C., Cao, Y., Hinds, A., Rishi, A. K. & Wetterwald, A. T1 alpha protein is developmentally regulated and expressed by alveolar type I cells, choroid plexus, and ciliary epithelia of adult rats. *Am. J. Respir. Cell Mol. Biol.* **14,** 577–585 (1996).

53. Breiteneder-Geleff, S. *et al.* Podoplanin, novel 43-kd membrane protein of glomerular epithelial cells, is down-regulated in puromycin nephrosis. *The American Journal of Pathology* **151,** 1141–1152 (1997).

54. Wetterwald, A. *et al.* Characterization and cloning of the E11 antigen, a marker expressed by rat osteoblasts and osteocytes. *Bone* **18,** 125–132 (1996).

55. Mahtab, E. A. F. *et al.* Cardiac malformations and myocardial abnormalities inpodoplanin knockout mouse embryos: Correlation with abnormal epicardial development. *Dev. Dyn.* **237,** 847–857 (2008).

56. Herzog, B. H. *et al.* Podoplanin maintains high endothelial venule integrity by interacting with platelet CLEC-2. *Nature* **502,** 105–109 (2014).

57. Swartz, M. A. & Lund, A. W. Lymphatic and interstitial flow in the tumour microenvironment: linking mechanobiology with immunity. 1–10 (2012). doi:10.1038/nrc3186

58. Ji, R.-C. Lymphatic endothelial cells, tumor lymphangiogenesis and metastasis: New insights into intratumoral and peritumoral lymphatics. *Cancer Metastasis Rev* **25,** 677–694 (2006).

59. Kato, Y. *et al.* Enhanced expression of Aggrus (T1alpha/podoplanin), a platelet-aggregation-inducing factor in lung squamous cell carcinoma. *Tumour Biol.* **26,** 195–200 (2005).

60. Martín-Villar, E. *et al.* Characterization of human PA2.26 antigen (T1alpha-2, podoplanin), a

small membrane mucin induced in oral squamous cell carcinomas. *Int. J. Cancer* **113,** 899–910 (2005).

61. Schacht, V. *et al.* Up-regulation of the lymphatic marker podoplanin, a mucin-type transmembrane glycoprotein, in human squamous cell carcinomas and germ cell tumors. *The American Journal of Pathology* **166,** 913–921 (2005).

62. Kimura, N. & Kimura, I. Podoplanin as a marker for mesothelioma. *Pathol. Int.* **55,** 83–86 (2005).

63. Ordóñez, N. G. D2-40 and podoplanin are highly specific and sensitive immunohistochemical markers of epithelioid malignant mesothelioma. *Hum. Pathol.* **36,** 372–380 (2005).

64. Mishima, K. *et al.* Increased expression of podoplanin in malignant astrocytic tumors as a novel molecular marker of malignant progression. *Acta Neuropathol.* **111,** 483–488 (2006).

65. Shibahara, J., Kashima, T., Kikuchi, Y., Kunita, A. & Fukayama, M. Podoplanin is expressed in subsets of tumors of the central nervous system. *Virchows Arch.* **448,** 493–499 (2006).

66. Lowe, K. L., Navarro-Nunez, L. & Watson, S. P. Platelet CLEC-2 and podoplanin in cancer metastasis. *Thromb. Res.* **129 Suppl 1,** S30–7 (2012).

67. Kitano, H. *et al.* Podoplanin expression in cancerous stroma induces lymphangiogenesis and predicts lymphatic spread and patient survival. *Arch. Pathol. Lab. Med.* **134,** 1520–1527 (2010).

68. Kalluri, R. & Zeisberg, M. Fibroblasts in cancer. *Nat Rev Cancer* **6,** 392–401 (2006).

69. Gaggioli, C. *et al.* Fibroblast-led collective invasion of carcinoma cells with differing roles for RhoGTPases in leading and following cells. *Nature Cell Biology* **9,** 1392–1400 (2007).

70. Kawase, A. *et al.* Podoplanin expression by cancer associated fibroblasts predicts poor prognosis of lung adenocarcinoma. *Int. J. Cancer* **123,** 1053–1059 (2008).

71. Hoshino, A. *et al.* Podoplanin-Positive Fibroblasts Enhance Lung Adenocarcinoma Tumor Formation: Podoplanin in Fibroblast Functions for Tumor Progression. *Cancer Research* **71,** 4769–4779 (2011).

72. Ito, S. *et al.* Tumor promoting effect of podoplanin-positive fibroblasts is mediated by enhanced RhoA activity. *BIOCHEMICAL AND BIOPHYSICAL RESEARCH COMMUNICATIONS* 1–6 (2012). doi:10.1016/j.bbrc.2012.04.158

73. Calvo, F. *et al.* Mechanotransduction and YAP-dependent matrix remodelling is required for the generation and maintenance of cancer-associated fibroblasts. *Nature Cell Biology* **15,** 637–646 (2013).

74. Yamanashi, T. *et al.* Podoplanin expression identified in stromal fibroblasts as a favorable prognostic marker in patients with colorectal carcinoma. *Oncology* **77,** 53–62 (2009).

75. Zimmer, G. *et al.* Cloning and characterization of gp36, a human mucin-type glycoprotein preferentially expressed in vascular endothelium. *Biochem. J.* **341 (Pt 2),** 277–284 (1999).

76. Michalek, M. T., Bremer, E. G. & Mold, C. Effect of gangliosides on activation of the alternative pathway of human complement. *The Journal of Immunology* **140,** 1581–1587 (1988).

77. Meri, S. & Pangburn, M. K. Discrimination between activators and nonactivators of the alternative pathway of complement: regulation via a sialic acid/polyanion binding site on factor H. *Proceedings of the National Academy of Sciences* **87,** 3982–3986 (1990).

78. Taylor, M. E. & Drickamer, K. Paradigms for glycan-binding receptors in cell adhesion. *Current Opinion in Cell Biology* **19,** 572–577 (2007).

79. Carragher, D. M., Rangel-Moreno, J. & Randall, T. D. Ectopic lymphoid tissues and local immunity. *Seminars in Immunology* **20,** 26–42 (2008).

80. Peduto, L. *et al.* Inflammation Recapitulates the Ontogeny of Lymphoid Stromal Cells. *The Journal of Immunology* **182,** 5789–5799 (2009).

81. Chaitanya, G. V. *et al.* Inflammation induces neuro-lymphatic protein expression in multiple sclerosis brain neurovasculature. *J Neuroinflammation* **10,** 125 (2013).

82. Ekwall, A.-K. H. *et al.* The tumour-associated glycoprotein podoplanin is expressed in fibroblast-like synoviocytes of the hyperplastic synovial lining layer in rheumatoid arthritis. *Arthritis Research & Therapy* **13,** R40 (2011).

83. Salmon, H. *et al.* Matrix architecture defines the preferential localization and migration of T cells into the stroma of human lung tumors. *J. Clin. Invest.* **122,** 899–910 (2012).

84. Philippe, C. *et al.* Protection from tumor necrosis factor-mediated cytolysis by platelets. *The American Journal of Pathology* **143,** 1713–1723 (1993).

85. Kunita, A. *et al.* The platelet aggregation-inducing factor aggrus/podoplanin promotes pulmonary metastasis. *The American Journal of Pathology* **170,** 1337–1347 (2007).

86. Screaton, G. R. *et al.* Genomic structure of DNA encoding the lymphocyte homing receptor CD44 reveals at least 12 alternatively spliced exons. *Proceedings of the National Academy of Sciences* **89,** 12160–12164 (1992).

87. Hathcock, K. S., Hirano, H., Murakami, S. & Hodes, R. J. CD44 expression on activated B cells. Differential capacity for CD44-dependent binding to hyaluronic acid. *The Journal of Immunology* **151,** 6712–6722 (1993).

88. Kato, Y. & Kaneko, M. K. A Cancer-specific Monoclonal Antibody Recognizes the Aberrantly Glycosylated Podoplanin. *Sci Rep* **4,** 5924 (2014).

Appendix I

Supplementary Information

Supplementary Movie 1

Multi-photon time-lapse imaging shows migratory DCs entering the popliteal lymph node as shown in Supplementary Figure 4b. CFSE-labeled DCs [green], second harmonic (collagen fibers) [red]. Frames are 30 sec apart and shown at 8 frames/sec.

Supplementary Movie 2

Confocal time-lapse imaging of DC motility in lymph node slices from WT BM -> Ub-GFP mice. The DCs were labeled with cell tracker dyes; WT DCs are shown in red and *Clec1b*$^{-/-}$ DCs are shown in green. Frames are 90 sec apart and shown at 8 frames/sec.

Supplementary Movie 3

Time-lapse imaging shows the behavior of DCs cultured in 3D deformable matrix and stimulated with CLEC-2 ligands. Control DCs are shown first followed by DCs treated with rhodocytin and PDPN-Fc. Frames are 90 sec apart and shown at 8 frames/sec. Scale bar, 20 μm.

Supplementary Movie 4

Time-lapse imaging shows DCs approaching branched FRCs in 3D matrix. Frames are 90 sec apart and shown at 8 frames/sec.

Supplementary Movie 5

Time-lapse imaging shows the migration of WT DCs along WT FRCs cultured in 3D matrix. Frames

are 2 min apart and shown at 8 frames/sec.

Supplementary Movie 6

Time-lapse imaging shows the interaction of *Clec1b*$^{-/-}$ DCs with WT FRCs cultured in 3D matrix. Frames are 2 min apart and shown at 8 frames/sec.

Supplementary Movie 7

Time-lapse imaging shows the interaction of WT DCs with *Pdpn*$^{-/-}$ FRCs cultured in 3D matrix. Frames are 2 min apart and shown at 8 frames/sec.